Modelling and Simulation of a Photovoltaic Fuel Cell Hybrid System

A Dissertation
in Candidacy for the Degree of
Doctor in Engineering (Dr.-Ing.)

Faculty of Electrical Engineering
University of Kassel

By
MSc. Eng. Abou El-Maaty Metwally Metwally Aly Abd El-Aal
From Ain Shams University/Egypt

Supervisors
Prof. Dr. Eng. Jürgen Schmid
Prof. Dr. Eng. Didier Mayer

Dissertation Day: April 15, 2005
Kassel, Germany

ACKNOWLEDGEMENTS

I would particularly like to thank my supervisor Prof. Dr.-Ing. Jürgen Schmid for his enthusiasm, encouragement, and guidance on fundamentally and theoretical important matters throughout the whole research work. My gratitude is also due to Prof. Dr. Didier Mayer who agreed to be my second supervisor for his strong support.

This research has been done at the Institute of Solar Energy supply Technology (ISET) associated with the University of Kassel. Thus, my thanks are due to the research staff and colleagues of ISET, especially the colleagues of the department of Energy Conversion and Control Engineering, for their useful help during the development phases of my research. My appreciation also goes to following colleagues: Mr Peter Caselitz (Head of the department), Jochen Bard, and Bahram Panahandeh for their help on various aspects of modelling and simulation, Jochen Giebhardt and Christian Langer for making sure my computer had all the necessary software installed. Also, I would also like to thank Ms Nandi Vergara Gómez, Ms Doris Schmidt, and Ms Claudia Erdt.

This thesis has been financed by a scholarship from my country, Arabic Republic of Egypt. I would like to thank my country for its support. Furthermore, my thanks aim Prof. Dr.-Ing. Mahmoud El-Bakry and my colleague Dr. Fathy Syam from Electronics Research Institute (Cairo, Egypt), who supported and helped me during writing of this work.

Finally, a special word of thanks to my family (mother, father, wife, and brothers), who helped me to make this work a reality.

Abou El-Maaty M. Abd El-Aal

ABSTRACT

A stand-alone power system is an autonomous system that supplies electricity to the user load without being connected to the electric grid. This kind of decentralized system is frequently located in remote and inaccessible areas. It is essential for about one third of the world population which are living in developed or isolated regions and have no access to an electricity utility grid. The most people live in remote and rural areas, with low population density, lacking even the basic infrastructure. The utility grid extension to these locations is not a cost effective option and sometimes technically not feasible.

The purpose of this thesis is the modelling and simulation of a stand-alone hybrid power system, referred to as "hydrogen Photovoltaic-Fuel Cell (PVFC) hybrid system". It couples a photovoltaic generator (PV), an alkaline water electrolyser, a storage gas tank, a proton exchange membrane fuel cell (PEMFC), and power conditioning units (PCU) to give different system topologies. The system is intended to be an environmentally friendly solution since it tries maximising the use of a renewable energy source. Electricity is produced by a PV generator to meet the requirements of a user load. Whenever there is enough solar radiation, the user load can be powered totally by the PV electricity. During periods of low solar radiation, auxiliary electricity is required. An alkaline high pressure water electrolyser is powered by the excess energy from the PV generator to produce hydrogen and oxygen at a pressure of maximum 30bar. Gases are stored without compression for short- (hourly or daily) and long- (seasonal) term. A proton exchange membrane (PEM) fuel cell is used to keep the system's reliability at the same level as for the conventional system while decreasing the environmental impact of the whole system. The PEM fuel cell consumes gases which are produced by an electrolyser to meet the user load demand when the PV generator energy is deficient, so that it works as an auxiliary generator. Power conditioning units are appropriate for the conversion and dispatch the energy between the components of the system. No batteries are used in this system since they represent the weakest when used in PV systems due to their need for sophisticated control and their short lifetime.

The model library, ISET Alternative Power Library (ISET-APL), is designed by the Institute of Solar Energy supply Technology (ISET) and used for the simulation of the hybrid system. The physical, analytical and/or empirical equations of each component are programmed and implemented separately in this library for the simulation software program Simplorer by C++ language. The model parameters are derived from manufacturer's performance data sheets or measurements obtained from literature. The identification and validation of the major hydrogen PVFC hybrid system component models are evaluated according to the measured data of the components, from the manufacturer's data sheet or from actual system operation. Then, the overall system is simulated, at intervals of one hour each, by using solar radiation as the primary energy input and hydrogen as energy storage for one year operation. A comparison between different topologies, such as DC or AC coupled systems, is carried out on the basis of energy

point of view at two locations with different geographical latitudes, in Kassel/Germany (Europe) and in Cairo/Egypt (North Africa).

The main conclusion in this work is that the simulation method of the system study under different conditions could successfully be used to give good visualization and comparison between those topologies for the overall performance of the system. The operational performance of the system is not only depending on component efficiency but also on system design and consumption behaviour. The worst case of this system is the low efficiency of the storage subsystem made of the electrolyser, the gas storage tank, and the fuel cell as it is around 25-34% at Cairo and 29-37% at Kassel. Therefore, the research for this system should be concentrated in the subsystem components development especially the fuel cell.

Key words: Stand-alone hybrid system, Photovoltaic, PEM fuel cell, electrolyser, and Power conditioning units.

Zusammenfassung

Autonome Systeme werden zur Versorgung von Verbrauchern und Lasten eingesetzt, die nicht mit dem elektrischen Stromnetz verbunden sind. Diese Systeme findet man daher oft in entlegenen oder schwer zugänglichen Gebieten. Die große Bedeutung autonomer Energieversorgungssysteme liegt darin, dass ein Drittel der Weltbevölkerung - vorwiegend in den Entwicklungs- und Schwellenländern – keinen Zugang zum Stromnetz hat. Den meisten Menschen, die in entlegenen ländlichen Gebieten mit geringer Bevölkerungsdichte leben, fehlt es an jeder Infrastruktur. Der Ausbau der öffentlichen Stromversorgung in solchen Regionen ist keine wirtschaftliche Lösung und mitunter technisch nicht realisierbar.

Das Ziel dieser Arbeit ist die Modellierung und Simulation eines autarken Hybridsystems auf der Basis von Photovoltaik (PV), Brennstoffzelle (PEM-BZ) und Wasserstoff. Darin sind gekoppelt ein Photovoltaikgenerator, ein alkalischer Wasserelektrolyseur, ein Gasspeicher, eine PEM Brennstoffzelle und die für die jeweilige Systemtopologie erforderliche Leistungselektronik. Das System soll eine umweltfreundliche Lösung darstellen und den größten möglichen Nutzen aus erneuerbaren Energien ziehen. Die notwendige elektrische Energie wird dabei von einem PV-Generator erzeugt. Bei ausreichender Solarstrahlung wird die Last vollständig vom PV-Generator versorgt. In Zeiten niedriger Einstrahlung wird eine zusätzliche Energieversorgung benötigt. Ein alkalischer Hochdruckelektrolyser wird mit Überschussenergie des PV-Generators betrieben und erzeugt Sauerstoff und Wasserstoff bei ma. 30 bar. Dies Gase werden ohne weitere Komprimierung für kurze (Stunden und Tage) oder lange (saisonale) Zeiträume gespeichert. Eine PEM-Brennstoffzelle wird eingesetzt um die Versorgungssicherheit auf dem üblichen Niveau konventioneller Anlagen zu halten und gleichzeitig die Umweltauswirkungen des Gesamtsystems zu verringern. Die PEM-Brennstoffzelle nutzt die vom Elektrolyseur erzeugten Gase um als Hilfsgenerator die Versorgung der Last sicherzustellen. Die Leistungselektronik dient zur Wandlung und Anpassung der Energieströme zwischen den Komponenten. Im untersuchten System kommt keine Bleibatterie zum Einsatz, da diese wegen der aufwendigen Betriebsführung und der kurzen Lebensdauer einen Schwachpunkt darstellt.

Für die Simulation des Hybridsystems wurde die von ISET entwickelte Modellbibliothek ISET-Alternative Power Library (ISET-APL) verwendet. Darin sind die physikalischen, analytischen oder empirischen Gleichungen jeder Komponente in der Sprache C++ programmiert und für den Einsatz im Simulator Simplorer implementiert. Die Modellparameter wurden für diese Arbeit von Datenblättern der Hersteller, aus der Literatur oder aus Messdaten des ISET abgeleitet. Die Auswahl und Validierung der wichtigsten Modelle der untersuchten Hybridsysteme erfolgte auf Grundlage von Messdaten des realisierten Systems oder von Datenblättern. Das Gesamtsystem wird simuliert mit der Solarstrahlung als primäre Energiezufuhr und Wasserstoffspeicherung in Stundenintervallen über einen Zeitraum von einem Jahr. Im Rahmen von

Energieflusssimulationen werden unterschiedliche Topologien, wie z.B. DC und AC gekoppelte Systeme an zwei klimatisch unterschiedlichen Standorten, namentlich Kassel und Kairo, untersucht.

In der vorliegenden Arbeit konnte gezeigt werden, dass mit Hilfe der Simulation das Betriebsverhalten der untersuchten Systeme unter verschiedenen Standortbedingungen visualisiert werden konnte. Darüber hinaus können unterschiedliche Topologien im Hinblick auf Ihren Gesamtwirkungsgrad verglichen werden. Das Betriebsverhalten ist dabei nicht nur von den Wirkungsgraden der Komponenten sondern auch von der Systemauslegung und dem Lastprofil abhängig. Das größte Verbesserungspotenzial liegt im Wirkungsgrad der Wasserstoffspeicherkette bestehend aus PEM-Brennstoffzelle, Elektrolyser und Wasserstoffspeicher mit Werten von 25-34% für den Standort Kairo und 29-37% am Standort Kassel. Daher sollten weitere Entwicklungen insbesondere auf die Komponentenentwicklung, vor allem der Brennstoffzelle konzentriert sein.

Stichworte: autonomes Hybridsystem, Photovoltaik, PEM-Brennstoffzelle, Elektrolyser, Wechselrichter.

TABLE OF CONTENTS

TABLE OF FIGURES

LIST OF TABLES

NOMENCLATURE

Substances

a-Si	Amorphous Silicon
CdTe	Cadmium Telluride
CO_2	Carbon dioxide
GaAs	Gallium Arsenide
H_2	Hydrogen
H_2O	Water
H_3PO_4	Concentrated Phosphoric acid
KOH	Potassium hydroxide
Li_2CO_3	Molten carbonate melts
MgH_2	Magnesium Hydride
O_2	Oxygen
Si	Silicon
ZrO_2	Yttrium-stabilized zirkondi-oxide

Abbreviations

AC	Alternating Current
AFC	Alkaline Fuel Cell
AM	Air Mass
APL	Alternative Power Library
ASM	Asynchronous Machine
BOS	Balance of system
BP	An international company for solar cell
BPWM	Bipolar Pulse Width Modulation
CHP	Combined Heat and Power generation
DC	Direct Current
DLL	Dynamically Linked Library
EL	Electrolyser component
ESMA	A company for manufactory supercapacitors
ESR	Equivalent Series Resistance
FC	Fuel cell
HHV	Higher Heating Value
HPWM	Hybrid Pulse Width Modulation
IEC	European Community in Ispra or International Electro-technical Commission
ISET	Institute of Solar Energy supply Technology
I-U	Current-Voltage
JRC	Joint Research Centre
LED	Light Emitting Diode
LHV	Lower Heating Value
MCFC	Molten Carbonate Fuel Cell
MEA	Membrane Electrode Assembly
MH	Metal Hydride
MPP	Maximum Power Point
MPPT	Maximum Power Point Tracker
MW	Megawatt
NOCT	Normal Operating Cell Temperature
PAFC	Phosphoric Acid Fuel Cell

PCU	Power Conditioning Unit
PEM	Proton Exchange Membrane or Electrolyte Membrane
PEMFC	Proton Exchange Membrane Fuel Cell
PNGV	"Partnership for New Generation of Vehicles" company
PR	Performance Ratio of the system
P-U	Power-Voltage
PV	Photovoltaic generator
PVFC	Photovoltaic-Fuel Cell
PWM	Pulse Width Modulation
Q1, Q2, and Q3	Quadratic Models
R&D	Research and Development
RMS	Root Mean Square value
SM	Synchronous Machine
SMA	A company for control systems
SOC	State OF Charge for hydrogen storage in the tank
SOFC	Solid Oxide Fuel Cell
SPFC	Solid Polymer Fuel Cell
STC	Standard Test Conditions
UPS	Uninterruptible Power Supply
UPWM	Unipolar Pulse Width Modulation
US	United States
Wp	Peak watt

Symbols

A_c	Cross section area of the electrode in electrochemical components,[m²]
A_{PV}	Surface area of PV generator, [m²]
a_i	Activity of species *i*, [-]
C_0, C_1, and C_3	Parameters of PCU Quadratic model Q3, [W,-, and 1/W]
$C1$	Capacitance of supercapacitor at the positive plate, [F]
$C2$	Capacitance of supercapacitor at the negative plate, [F]
C_{H_2}	Concentration of the hydrogen reduced, [-]
C_{H^+} and C_{H_2O}	Concentration of hydrogen protons and pure water, [-]
C_{O_2}	Concentration of the oxygen oxidized, [-]
C_{OH^-}	Concentration of the hydroxide ions OH^- at the anode with EL, [-]
d_e	Distance between electrodes (Electrode Gap), [cm]
EC	Equilibrium constant of chemical solutions, [-]
E_{Ld}	Daily average load consumption, [kWh/d]
E_{ELN}	Net energy supplied to H_2 storage tank by EL, [kWh]
E_{FCN}	Net energy consumed from H_2 storage tank by FC, [kWh]
E_{in}	Total input energy to the system, [kWh]
E_L	Energy consumed by the user load, [kWh]
$E_{PV,in}$	Total solar energy on PV generator, [kWh]
$E_{PV,out}$	Total output energy from PV generator, [kWh]
$E_{PV,STC}$	PV generator nominal energy, [kWh]
$E_{PV,use}$	PV generator part of the useful energy, [kWh]
E_s	Global solar radiation, [W/m²]
E_{sd}	Daily mean solar radiation energy, [kWh/m²/d]
E_{use}	Useful energy from the system, [kWh]
FF	Fill Factor, [-]
ΔF_e	Standard free energy activation for anode or cathode, [J/mol]
f_{air}	Surface factor of the electrode for air operation, [-]

F_{in}	Fuel input to the fuel cell (in power units), [W]
$F_{in,PV}$	PV generator fraction of the total input energy, [-]
F_{out}	Fuel output from electrolyser, [W]
ΔG_0	Change in Gibbs energy at STC, [J/mol]
ΔG	Change in Gibbs energy, [J/mol]
ΔH_0	Reaction enthalpy change at STC, [J/mol]
ΔH	Reaction enthalpy change, [J/mol]
$H_{2,cons}$	Hydrogen consumption by FC, [Nm³]
$H_{2,prod}$	Hydrogen production by EL, [Nm³]
I	Terminal current for electrochemical components, [A]
i_{coef}	Temperature coefficient of the short-circuit current, [A/°C]
I_d	Diode current, [A]
I_{dis}	Self-discharge current in the supercapacitor, [A]
I_n	Internal current loss in electrochemical components, [A]
I_{mpp}	Current at maximum power point, [A]
I_{ph}	Generated photocurrent, [A]
I_{rated}	Rated current for any component in the system, [A]
I_s	Output terminal current of the PV generator, [A]
I_{sh}	Current in shunt resistance, [A]
I_{sc}	Short circuit current, [A]
$I_{sc,STC}$	Short circuit current at STC, [A]
j	Anodic or cathodic current density, [A/cm²]
j_0	Anodic or cathodic exchange current density, [A/cm²]
$j_{0,a}^{ref}$ and $j_{0,c}^{ref}$	Anodic and cathodic standard exchange current density, [A/cm²]
j_L	Limiting current density for electrochemical components, [A/cm²]
j_n	Internal current density in PEM fuel cell, [A/cm²]
K_0, K_1, and K_2	Parameters of the PCU Quadratic model Q1 (self-consumption, voltage drops, and ohmic losses respectively), [W, -, and 1/W]
L_c	Capture losses in the system, [kWh/d/kWp]
L_s	System losses, [kWh/d/kWp]
m and n_o	Parameters of the PCU Quadratic model Q2 (Losses dependent and independent load respectively), [-]
Mf_{H_2O}	Molar fraction of water, [-]
$\dot{m}_{H_2}$	Hydrogen flow rate, [mol/s]
$\dot{m}_{H_{2,actual}}$	Actual hydrogen flow rate, [mol/s]
$\dot{m}_{H_2O}$	Water flow rate, [mol/s]
$\dot{m}_{H_{2,th}}$	Theoretical hydrogen flow rate, [mol/s]
Mm_{H_2O}, Mm_{KOH}	Molar mass of the H_2O and KOH, [g/mol]
$\dot{m}_{O_2}$	Oxygen flow rate, [mol/s]
M_i	Measured value of sample I
N_s	Number of cells in series, [-]
N_p	Number of cells in parallel, [-]
P_1, P_2, P_3, and P_4	Constant parameters for the one-diode PV model, [Am²/W, m²/W, 1/K, and A/K³]
P_1, P_2, P_{01}, and P_{02}	Constant parameters for the two-diode PV model, [A.m²/W, A.m²/W.K, A/K³ and A/K$^{5/2}$]
p	Pressure inside the storage tank, [Pa]
$p_{H_2}^O$ and $p_{O_2}^O$	Operating pressure of hydrogen and oxygen, [Pa]
p_0	Reference pressure or pressure at standard test conditions, [Pa]
P_{el}	Electrical input power to the electrolyser, [W]
P_{fc}	Electrical output power of the fuel cell, [W]

$P_{fc,r}$	Rated output power of the fuel cell, [W]
p_{H_2}	Partial pressure of species H_2, [Pa]
$p_{H_2O,\ r}$	Saturated vapour pressure of pure water, [Pa]
p_i	Partial pressure of species *i*, [Pa]
P_{in} and P_{out}	Input and output power of the power conditions units, [W]
p_{O_2}	Partial pressure of species O_2, [Pa]
P_{LDI} and P_{LDM}	Minimum and maximum load power, [W]
P_{Load} or P_L	User load power demand, [W]
P_{loss}	Power losses of the power conditioning units, [W]
P_{max}	Maximum power of the power conditioning units, [W]
P_{periph}	Peripheral power of the fuel cell system, [W]
P_{PV}	PV generator output power, [W]
$P_{PV,STC}$	PV generator output power at standard test conditions, [W_p]
P_{rated}	Rated power for any component in the system, [W]
P_S	Output power from PV generator, [W]
P_{SCap}	Supercapacitor charge or discharge power, [W]
$P_{standby}$	Standby consumption power of the power conditioning units, [W]
P_{STC}	Output power from the PV generator at STC, [W]
R_{el}	Internal resistance of the electrolyser, [Ω]
R_{fc}	Internal resistance of the fuel cell, [Ω]
R_i	Total cell resistance for electrochemical components, [Ω.cm²]
R_{in}	Internal resistance of the supercapacitor, [Ω]
R_s	Series resistance of the PV model, [Ω]
R_{sh}	Shunt resistance of the PV model, [Ω]
ΔS_0	Reaction entropy change at STC, [J/K/mol]
ΔS	Reaction entropy change, [J/K/mol]
S_i	Simulated value of sample *i*
T	Electrochemical cell temperature, [K]
T_a	Ambient temperature, [°C]
T_j	Junction cell temperature of the PV model, [K]
T_{SCap}	Temperature of the supercapacitor, [°C]
U_0	Ideal cell voltage of electrochemical components at standard test conditions, [V]
U_{act}	Activation over-voltage, [V]
U_{actual}	Actual cell voltage of electrochemical components, [V]
U_{anode}	Voltage at the anode, [V]
$U_{cathode}$	Voltage at the cathode, [V]
u_{coef}	Temperature coefficient of the open-circuit voltage, [V/°C]
U_{conc}	Concentration or diffusion over-voltage, [V]
U_{mpp}	Voltage at maximum power point, [V]
U_{oc}	Open circuit voltage, [V]
$U_{oc,STC}$	Open circuit voltage at STC, [V]
U_{ohm}	Ohmic over-voltage, [V]
U_{rated}	Rated voltage for any component in the system, [V]
U_s	Output terminal voltage of the PV generator, [V]
U_{SCap}	Terminal voltage of the supercapacitor, [V]
U_{th}	Theoretical cell voltage of electrochemical components, [V]
V	Volume of the storage tank, [m³]
Y_a	Array yield in the system, [kWh/d/kWp]
Y_f	Final yield in the system, [kWh/d/kWp]
Y_r	Reference yield in the system, [kWh/d/kWp]
z	Ionic valence of cations or anions, [-]

η_{10}	Efficiency at 10% of the rated power, [%]
η_{100}	Efficiency at 100% of the rated power, [%]
η_{BOS}	Overall balance of the system efficiency, [%]
η_{el}	Electrolyser efficiency, [%]
η_F	Faraday's efficiency of electrochemical components, [%]
η_{fc}	Efficiency of the fuel cell, [%]
$\eta_{fc,stack}$	Stack efficiency of the fuel cell, [%]
$\eta_{fc,system}$	Total efficiency of the fuel cell system, [%]
η_{out}	Output efficiency of the power conditions units, [%]
$\eta_{PCU,FC}$	Efficiency of the PCU used with the fuel cell, [%]
η_{PV}	PV generator efficiency, [%]
$\eta_{PV,STC}$	PV generator efficiency at STC, [%]
η_{rated}	Rated efficiency of the power conditioning units, [%]
$\eta_{sub\text{-}sys}$	H_2 subsystem efficiency, [%]
η_{sys}	Total system efficiency taking into account the PV conversion efficiency, wires, diodes, chemical conversion, electricity regeneration, regulator, PCU, etc, [%]
ζ_i	Faraday's efficiency parameters (i=1 to 5), [%, m^2/A, $m^2/A.°C$, m^4/A, $m^4/A^2.°C$]
γ_{H_2} and γ_{O_2}	Fugacity coefficients of hydrogen and oxygen, [-]
γ_{H_2O}	Fugacity coefficient of water, [-]
γ_{OH^-}	Fugacity coefficient of OH^- ions, [-]
α_a and α_c	Anodic and cathodic transfer coefficient, [-]
σ	Electrical conductivity of the electrolyte membrane in FC, [1/ Ω.cm]
σ_k	Electrical conductivity of the electrolyte KOH in EL, [1/ Ω.cm]
λ	Water content, [-]
ϕ	Water vapour activity, [-]

1. INTRODUCTIONN

1.1 Motivation

The conventional fossil fuel energy sources such as petroleum, natural gas, and coal which meet most of the world's energy demand today are being depleted rapidly. Also, their combustion products are causing global problems such as the greenhouse effect and pollution which are posing great danger for our environment and eventually for the entire life on our planet [Veziroglu-04]. The renewable energy sources (solar, wind, tidal, geothermal etc.) are attracting more attention as an alternative energy. Among the renewable energy sources, the photovoltaic (PV) energy has been widely utilized in low power applications. It is also the most promising candidate for research and development for large scale users as the fabrication of low cost PV devices becomes a reality.

Photovoltaic generators which directly convert solar radiation into electricity have a lot of significant advantages such as being inexhaustible and pollution free, silent, with no rotating parts, and with size-independent electric conversion efficiency. Due to harmless environmental effect of PV generators, they are replacing electricity generated by other polluting ways and even more popular for electricity generator where none was available before. With increasing penetration of solar photovoltaic devices, various anti-pollution apparatus can be operated by solar PV power; for example, water purification by electrochemical processing or stopping desert expansion by PV water pumping with tree implantation.

From an operational point of view, a PV power generation experiences large variations in its output power due to intermittent weather conditions. Those phenomena may cause operational problems at the power station, such as excessive frequency deviations. In many regions of the world, the fluctuating nature of solar radiation means that purely PV power generators for off-grid applications must be large and thus expensive. One method to overcome this problem is to integrate the photovoltaic plant with other power sources such as diesel, fuel cell (FC), or battery back-up [Krauter-00], [Hollmuller-00], and [Almonacid-98]. The diesel back-up generator for PV power is able to ensure a continuous 24-hour. However, it has a number of significant disadvantages such as noise and exhaust gases pollution. In addition, reasonably reliable diesel back-up generators are available only for the power range above about 5kW, which is too much high for a large number of applications [Benz-03]. In the middle and small power range this technology cannot be used in an effective way.

The fuel cell beak-up power supply is a very attractive option to be used with an intermittent power generation source like PV power because the fuel cell power system is characterized with many attractive features such as efficiency, fast load-response, modular production and fuel flexibility. Its feasibility in co-ordination with a PV system has been successfully realised for

both grid-connected and stand-alone power applications. Due to the fast responding capability of the fuel cell power system, a photovoltaic-fuel cell (PVFC) hybrid system may be able to solve the photovoltaic's inherent problem of intermittent power generation. Unlike a storage battery, which also represents an attractive back-up option, such as fast response, modular construction and flexibility, the fuel cell power can produce electricity for unlimited time to support the PV power generator. Therefore, a continuous supply of high quality power generated from the PVFC hybrid system is possible day and night.

Environmental impacts of the fuel cell power generation are relatively small in contrast to other fossil fuel power sources. Since chemical reactions inside the fuel cell stack are accomplished by catalysts, it requires a low sulphur-content fuel [Hoogers-03]. Low-emission characteristics of the fuel cell power system may allow some utilities to offset the costs of installing additional emission control equipment. Moreover, their high efficiency results in low fossil fuel CO_2 emissions, which will help in reducing the rate of global warming [Hirschenhofer-99]. Therefore, the fuel cell power system has a great potential for being co-ordinated with the PV generator to smooth out the photovoltaic power's fluctuations.

1.2 Objectives of the Study

It has been well-proven that a photovoltaic power source should be integrated with other power sources, whether used in either a stand-alone or grid-connected mode. Stand-alone power systems are very popular, especially in remote sites. The system under study in this dissertation is a stand-alone hydrogen PVFC hybrid power system, which is constituted of a photovoltaic generator, an alkaline water electrolyser, a proton exchange membrane (PEM) fuel cell, a short-term supercapacitor storage, and gas storage tanks. This system is intended to be a future competitor of hybrid PV/Diesel systems, especially from an environmental point of view (low noise and zero emission) and operational costs point of view [Mayer-01]. Hydrogen production in this system is produced by electrolysing water molecules electrically through the electrolyser and is used to produce electricity via the PEM fuel cells. This method is a very effective way for producing and using pure hydrogen. Therefore, the hydrogen in this system drastically reduces global pollution emissions of CO_2.

The development of appropriate simulation tools will help in dealing with modelling, simulation, design and energy management of the system under study. A simulation software program known as Simplorer has been used to simulate the system performance. The system design and performance analysis could thus be achieved through computer modelling and simulation prior to practical realization. This dissertation aims towards:

- Proper data collecting and/or data synthesising that describes the system operation and the load profile,
- Visualizing and analysing the system dynamic behaviour using power flow trace over long-term duration, for example, one year,

- Creating an accurate simulation system model to predict the real performance of the hydrogen PVFC hybrid system, and then
- Undertaking detailed analysis of the effect of changes in the system configurations, power conditioning units, and sites to choose an optimal system design.

The objective of the study is to reach a design that optimises the operation of a hydrogen PVFC hybrid system. All components of this system have been selected for an optimal operation of the complete system. The data of the component models was taken from real projects or manufacturer's data sheet. The methodology selected is to simulate a number of different system topologies based on the type of coupling between the components system, e.g., DC or AC coupling. A library of the system models is produced under the designation "ISET Alternative Power Library for Simplorer". Models of this library are developed and under continuous enhancement by new models in the Institute of Solar Energy supply Technology ISET (university Kassel, Germany) to improve the hybrid power systems operation. The component models of the system are verified with component's experimental data to assure the accuracy of these models before being implemented into the system simulation study. Also, this study evaluates the hydrogen gas storage for the long term as well as for the short term operation.

1.3 Outline of the Dissertation

Chapter 1 gives an introduction to the concept of photovoltaic hybrid system and the objectives of study. **Chapter 2** gives a description of different hybrid power systems configurations, and includes notes about the hybrid power system topologies, modularisation, and standardisation. **Chapter 3** covers the background information about all components used in the system study, such as photovoltaic generator, hydrogen energy subsystems (PEM fuel cell, electrolyser, and hydrogen storage tank), supercapacitor module, and power conditioning units. **Chapter 4** deals with the mathematical models of the all components used for the hydrogen PVFC hybrid system. The described models here are used to study the long-term energy performance of the system. **Chapter 5** describes the identification and validation of the hydrogen PVFC hybrid system component models that are modelled in chapter 4. The evaluation of these models is based on measured data given by the components manufacturer's data sheet or from actual system operation. **Chapter 6** simulates the overall system that uses solar radiation as the primary energy input and hydrogen as energy storage over one year. A comparison between different topologies such as DC or AC coupled systems at different locations on the basis of energy point of view is studied. **Chapter 7** summarizes and concludes the thesis, and proposes recommendations for future work. References are given in **Chapter 8**, and Appendices in **Chapter 9**.

2. STATE OF THE ART HYBRID SYSTEMS

In hybrid power systems, a number of power generators and storage components are combined to meet the energy demand of remote or rural area, or even a whole community. In addition to PV generators, diesel generators, wind generators, small hydro plants, and others sources of electrical energy can be added as needed to meet the energy demand in a way that fits the local geography and other specifics. Before developing a hybrid electric system for a specific site, it is essential to know the particular energy demand and the resources available at that site. Therefore, energy planners must study the solar energy, wind, and other potential resources at the site, in addition to the energy demand. This will allow them to design the kind of hybrid power system that meets the demands of the facility at best. In this chapter, a brief technical description of some different hybrid power system configurations is considered. It also includes notes about hybrid power system topologies, modularisation, and standardisation.

2.1 Introduction

The utility grid extension to remote and inaccessible areas is not a cost effective option and sometimes technically not feasible, and the need for stand-alone power systems is essential. The first solution to provide electricity to these areas is achieved by using diesel generators which have low investment costs but high running costs, particularly for the smaller units. Their power generation costs increase when meeting short period peak loads, especially encountered in small communities with low consumer diversity and similar social habits. Therefore, systems are often over-dimensioned by installing multiple diesel units in order to compensate the peak periods, causing low efficiency and higher maintenance costs. The first hybridisation step is taken by adding a PV generator or a wind turbine generator to such conventional power generation systems, which increases the operational problems. As the power has to be supplied continuously, these generators must run continuously to meet any instantaneous deficit caused by load increase or renewable resource fluctuations. In such a hybrid system, the renewable energy generators serve as fuel saving units. Nonetheless, renewably generated power serves to decrease further the average loading ratio of the diesel plant, and consequently the increased maintenance costs may outweigh fuel savings. The addition of some kind of energy storage partially solves the problem of the diesel by shutting down the conventional power generator when the generated renewable energy plus the stored energy is higher than the user load demand [Schmid-97]. Moreover, integration of a storage medium enhances the renewable energy usability.

Different stand-alone hybrid systems based mainly on a PV generator combined with a battery as a storage medium and an auxiliary diesel generator have been installed and operated in different climates and applications for several years [Protogeropoulos-97], [Sayigh-97], [Kansteiner-98] and [Strauss-00].

2.2 Description of different Hybrid Power System Configurations

2.2.1 Photovoltaic-Battery-Diesel Hybrid System

The PV hybrid system may be an economical alternative to a large stand-alone PV system, because the PV generator doesn't have to be sized large enough for worst case weather conditions. A diesel generator (genset) combined with a battery charger can supply power to the user load when the PV generator fails. If the PV generator is sized for average user load, then during periods of higher user loads, the diesel generator supplies the difference. When batteries are low, the diesel generator supplies the loads as well as the battery charger to recharge the batteries. If the PV generator is sized smaller than needed for normal load, the diesel generator can supply peak loads, such as pumping water, and simultaneously the battery charger to charge battery system. Diesel generator and battery bank sizes must be chosen carefully for reliable system operation [Strauss-00].

The disadvantages of this system are:

(1) Batteries must be well loaded to release electricity with a good yield.
(2) Batteries produce dangerous gases such as H_2 and O_2, so they can be dangerous when installed in confined places.
(3) Diesel generators have a bad yield percentage of power needed (approximately 40%).
(4) Batteries have a relatively short lifetime compared to other system components.

The advantages are:

(1) Diesel generators could be operated and maintained by a major part of an unqualified population.
(2) Maintenance, consumables and spare parts are generally available.
(3) Batteries have reached an important maturity degree.
(4) Advanced battery technologies quickly becoming commercially available.

2.2.2 Photovoltaic-Battery-Fuel cell Hybrid System

The diesel generator in this system is replaced by a fuel cell system. The fuel cell system is used as a back-up generator, when the batteries reach the minimum allowable charging level and the load exceeds the power produced by the PV generator. The advantages of this system are in general the same as for a Photovoltaic-Battery-Diesel hybrid system with regard to the PV generator size and batteries availability. Some principle differences exist between a diesel generator and a fuel cell which affect the design, sizing and the operating strategy of such a hybrid system. For example, a diesel generator will provide the rated power to the load in a few seconds after start up, but a fuel cell system needs more time to provide the rated power and the output should only be increased slowly after start up. The increasing operating temperature which occurs during operation does improve the efficiency of a fuel cell significantly [Ulleberg-

98]. According to the load profile, the feasible fuel cell capacity can be determined, whereas a diesel generator should be operating at the rated power as much as possible.

A significant advantage of the fuel cell as a back-up generator over the diesel or petrol generator is the high conversion efficiency of the fuel cell. Whereas a 1kW diesel generator achieves total efficiencies between 8-15% [Benz-03], a similar fuel cell system can achieve up to 50% efficiency when operated with H_2 and O_2. Diesel generators need high maintenance costs and they are noisy and emit exhaust gases continuously. In contrast, the fuel cells have very good technical properties which make them interesting for stand-alone power systems, such as low noise level and clean exhaust gases, especially when pure hydrogen is used as a fuel. Due to their very low maintenance cost, the fuel cells are expected to generate electricity at lower cost than conventional diesel generators in spite of their higher initial investment cost.

Lower investment cost and higher life time of fuel cell systems are expected in the future, when mass production and technical improvements are realized.

2.2.3 Photovoltaic-Electrolyser-Fuel cell System

For many applications, a loss of feeding loads is not acceptable. In order to achieve no loss of feeding load probabilities with a PV generator, the system must be designed according to the worst case climate and load conditions. Therefore, another source of energy is necessary to realise energy storage. In this system, the excess energy is stored in the form of compressed hydrogen via conversion through the electrolyser. The fuel cell is used to produce power if the load power exceeds that produced from the PV generator. It can also function as an emergency generator, if the PV generator system fails.

With a total efficiency of the storage system in the range of 50%, a suitable storage volume can be achieved and the PV generator capacity can be reduced significantly [Busquet-00]. This compensates partially the extra cost of the hydrogen system. Based on the site climate, the load profile, the characteristic of the components, and the storage volume can be optimised.

For many years, a number of hybrid systems have been realised using hydrogen for seasonal energy storage. Different system topologies have been used. Most common is the DC connection of PV generator, electrolyser, and fuel cell with, or even without, a DC/DC converter. All these system topologies will be studied in details in this work.

Technically, this system can possible store not only the hydrogen but also the oxygen. Due to safety problems and extra costs, the oxygen is not used and the fuel cell may be operated with the oxygen from air [Ulleberg-98].

2.3 Topologies of Hybrid Power Systems

From the application's point of view, hybrid power systems which combine conventional and renewable power conversion systems can be classified as DC or AC coupled topologies [Preiser-97]. A DC coupled hybrid power system is a system whose different power sources are connected to a main DC bus-bar and through this bus they are connected to the AC grid or AC user load. An AC coupled hybrid power system is a system whose different power sources are connected to the AC grid or AC user load without an intermediate DC bus-bar connecting them.

2.3.1 DC Coupled System Topology

In this topology, all generator and storage units are tied to the DC bus-bar, Fig. 2.1. The output of all AC power sources, if available, is converted into DC, then added to the output of all DC power sources to a main DC bus-bar, which is connected to the AC user load through a main DC/AC inverter. This inverter converts the generated DC power from different generators and storages to AC of the desired voltage and frequency to satisfy the AC user load demand. This inverter should be adequate to cover the peak load demands, while the back-up generator capacity (diesel or fuel cell generator) should be able to meet the peak load and charge the short-term storage units simultaneously. Referring to Fig. 2.1, it can be seen that each power source is connected to the DC bus-bar through its own DC/DC converter. The DC/DC converters which connect the battery or hydrogen fuel cell system to the DC bus-bar differs from the others by being bi-directional, instead of unidirectional, in order to allow charge and discharge of battery as well as hydrogen storage by electrolyser and fuel cell. These converters are used in order to produce a constant DC voltage on their outputs regardless of the voltage variations on their inputs.

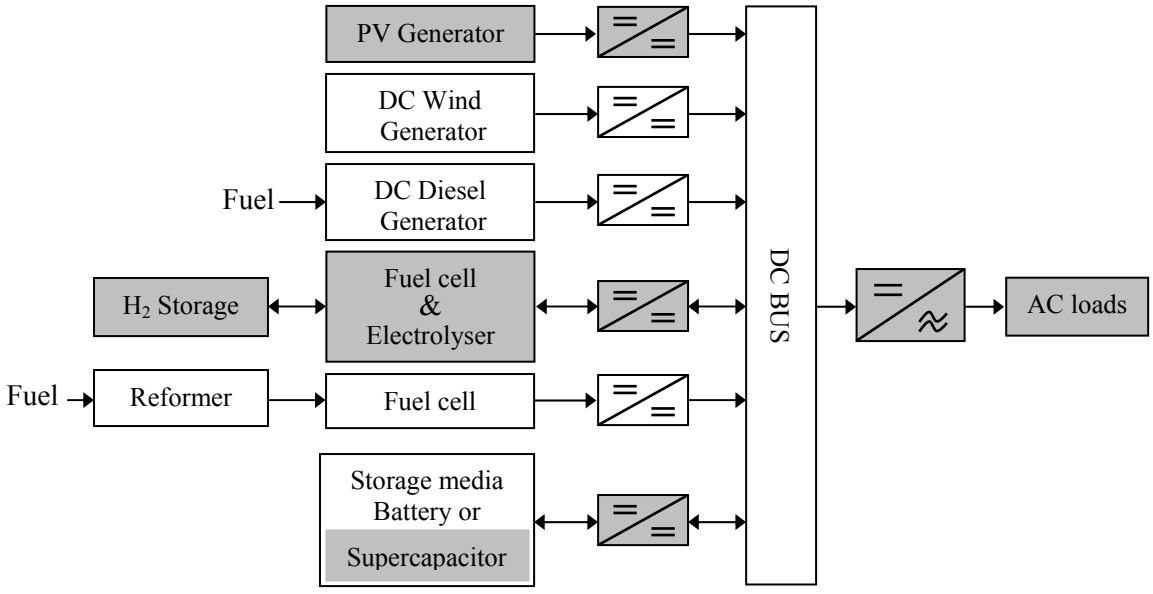

Fig. 2.1: Block diagram of the DC coupled hybrid power systems.

The advantage of this topology is that the load demand is satisfied without interruption even when the generators charge the short-term storage units. The design principles of this topology are rather easy to implement. Its serious disadvantages are low overall conversion efficiency, and limited control by the diesel generator in case of being incorporated in the system. Furthermore, expanding the system by increasing a component capacity's or adding further generators is very complicated due to the limited nominal capacity of the DC/AC inverter [Ibrahim-02].

2.3.2 AC Coupled System Topology

All system components in this topology are connected to the AC user load via the AC bus-bar, Fig 2.2. The AC coupled system topology has a superior performance compared to the DC coupled configuration since each inverter can be synchronized to its generator so that it can supply the load independently and simultaneously with other inverters [Kleinkauf-94]. This offers some flexibility for the energy sources to meet the user load demand. In case of low load demand, all the inverters of the generators and storages are in standby mode operation without one inverter, for example the PV generator inverter, to cover the load demand. However, during high load demands or peak times, some generators and storage units or all are operated in parallel to cover the user load demand. Because of this parallel operation capability, the capacities of the power conditioning units (PCUs) and the generators are reduced. This topology has several advantages compared to the DC coupled topology such as higher overall efficiency, smaller sizes of the PCUs while keeping a high level of energy availability, and optimal operation of the diesel generator due to reducing its operating time and consequently its maintenance cost. The operation and control of this topology are sophisticated due to the synchronization process required between the components. The development of an advanced PCU simplifies the control and the load dispatch problem. Therefore, advanced control algorithms which build and stabilize the isolated grid and allow parallel operation of different renewable and conventional generators as well as the integration of storage media have been developed, for example by [Engler-01]. Moreover, due to continuous developing of power conditioning units, such complicated control tasks become reliable in their applications. In this way, the expansion or modification of the hybrid system configurations can easily be carried out in order to cover the demand growth or change in demand behaviour.
In this work, the coloured (gray) components in Figs. 2.1 and 2.2 will be studied in details in the next chapters.

2.4 Modular Hybrid Power System Technology

Recent developments allow coupling all components of a PV hybrid system on the AC side in a standardized way. Main features of this way are system expandability, general adaptability, utility-grid compatibility, cost reduction, and simple system design and installation. The overall system control needs not to be changed with any change in the size of the system components [Schmid-97].

The design and construction technique of the complex hybrid power systems decisively influence their flexibility, functioning, quality and economic performance. The modular technique can cope varied requirements of the electrification. It can be

- generally adapted to satisfy diverse load-specific requirements,
- modularly expanded as a single or three phase PV hybrid system to cover increasing energy and power needs, and
- easily connected to a conventional grid, if available.

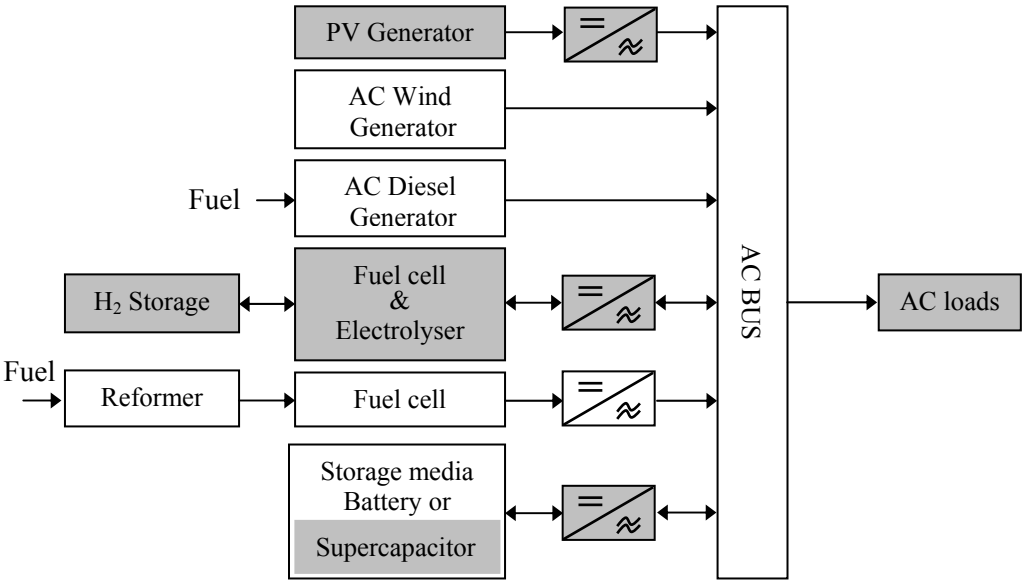

Fig. 2.2: Block diagram of the AC coupled hybrid power systems.

Based on the standardization of system design, the construction of hybrid power systems, especially power conditioning units, has the potential to strongly reduce the cost [Kleinkauf-03]. Using a small set of inverter types with a global-market-oriented degree of modularisation, such as PV string inverters or PV module integrated ones; the whole PV application spectrum for supplying power can be covered. "The advantages of modularisation of power supply units appear mainly in the kilowatt-range and can be extended up to the MW power scale" [Kleinkauf-03].

Figure 2.3 shows a general modular system technology for reliable hybrid power systems as defined by [Kleinkauf-94], [Kleinkauf-95], [Engler-97], and [Caselitz-03]. This structure contains two connection buses which are called the energy and communication buses. The energy bus couples the system's components among each other and with the user load. All components are considered to be connected on the AC side as recommended in the modular system concept. The communication bus connects all system components and the user load with the supervisory controller. The task of this bus, in practice, is to transfer signals, which describe

the status of the subsystem components for monitoring and control purposes of the hybrid system. Upon this information and based on the predefined settings, the supervisory energy dispatch decisions which are signalled back via the same communication line to the corresponding component's controller or actuator.

For the modular AC coupled power generation and storage units, the well established standard 230V/50Hz or 110V/60Hz is most suitable with the energy bus. Defined units are integrated with a standard interface, hence one unit being compatible with another [Kleinkauf-95]. This approach has worked on modularisation and standardization at the component level which is a more satisfactory solution than standardization at the system level. Consequently, serial production is achievable, which in itself leads to cost reduction and improves the supply reliability. The modular low power hybrid systems in single and three phase technology which are based on PV generator and battery storage components are being developed and tested at ISET together with partners from industry and research.

2.5 Conclusion

Hybridisation through combining different energy sources in one supply system offers the best possibility to use locally available renewable energies. The nature of hybridisation is mainly based on the special features and economic potential of various energy conversion processes and on the power range. Hybrid system technology mainly covers stand-alone systems as well as isolated grids of small and medium power ranges. The modular hybrid power system coupling all generators, storage media and user loads on the AC side come out with numerous advantages, such as simplicity in system design, high reliability, and expandability. Moreover, the AC side structure provides standardisation, quality assurance and serial production which also results in a considerable potential of cost reduction. Due to the features of modular expandability and general adaptability a family of hybrid systems in megawatt-range is initiated in order to cover a multitude of different stand-alone applications.

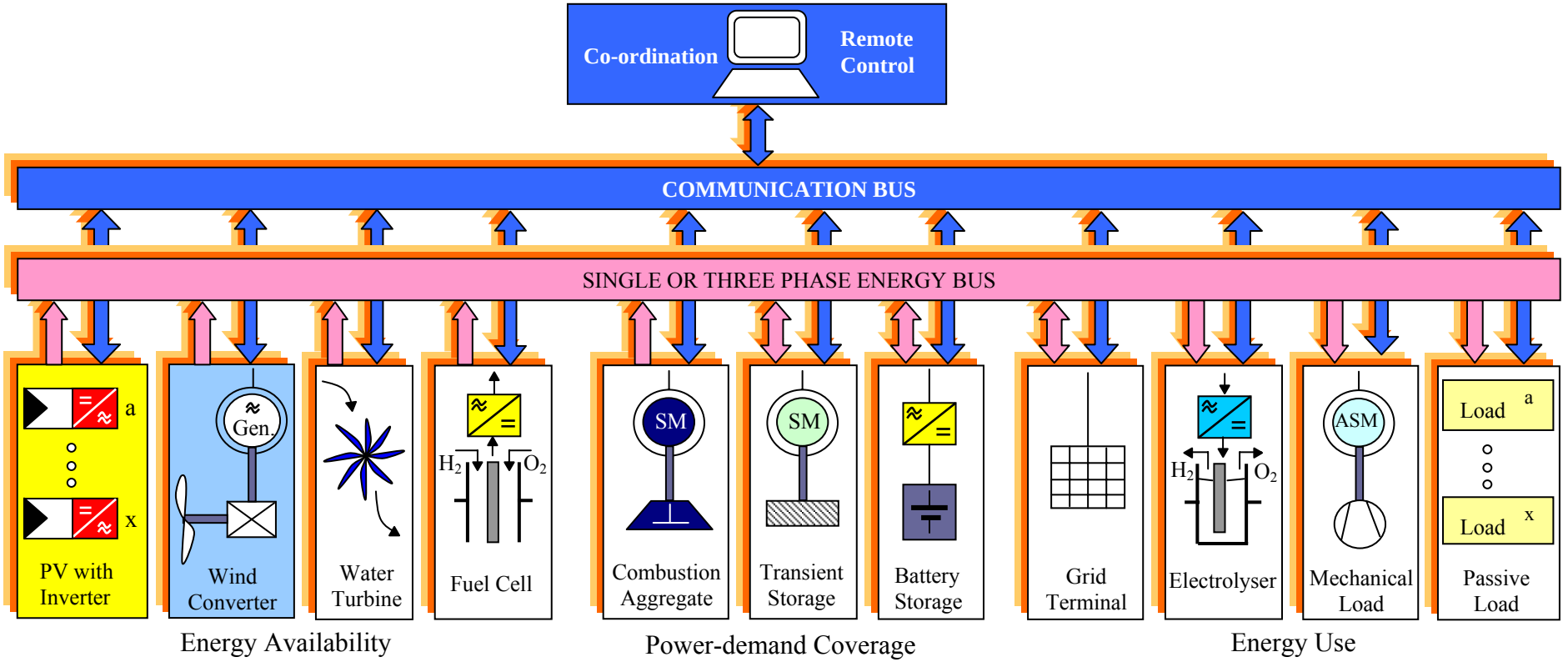

Fig. 2.3: General modular hybrid system with AC coupled components and standardized modules.

3. DESCRIPTION OF HYDROGEN PVFC HYBRID SYSTEM COMPONENTS

The utilization of intermittent natural energy resources such as solar, wind, and hydro energy requires some form of energy storage. The concept of utilizing hydrogen as a substance for storage of energy is shown in Fig. 3.1. In this work, a hybrid system based on hydrogen technology is considered which needs a hydrogen producing unit (Electrolyser), a hydrogen storing unit (Tanks), and a hydrogen utilizing unit (PEM Fuel Cell). However, the system based on intermittent energy sources and is likely to experience large minutely, hourly, and daily fluctuations in energy input. Thus, it should be emphasized that the main purpose of the hydrogen storage system is to store energy over short and long periods of time, i.e., hour to hour and season to season. Other small short-term energy storage such as a secondary battery or supercapacitor must also be included for the safe operation of the fuel cell component and also to supply power during transient load conditions. In addition, a control system is required to monitor and guide the operation of the components of the system. This chapter consists of four sections: (1) photovoltaic generator; (2) hydrogen energy system and components; (3) supercapacitor; and (4) power conditioning units (PCUs). In these sections, a brief description of the mentioned components will be given to make the hydrogen PVFC hybrid system easy to understand in this dissertation.

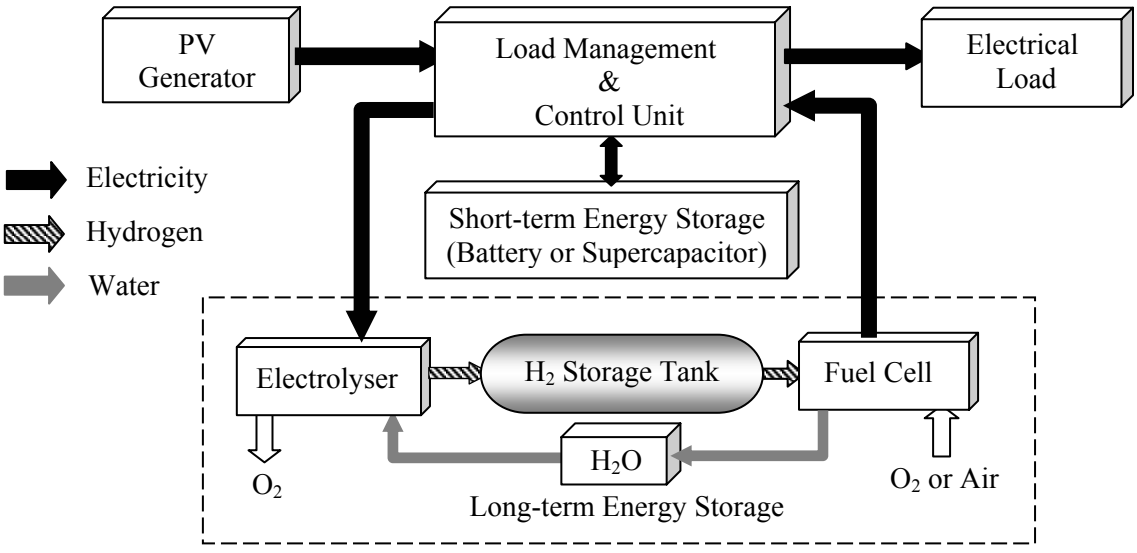

Fig. 3.1: Concept of hydrogen PVFC hybrid system.

3.1 Photovoltaic Generator

In the early 1980's, the photovoltaic industries attracted the interest of large energy companies and government agencies. With their capital investment, a tremendous acceleration in PV modules' development took place. Today whole product lines are available with PV modules designed to withstand environmental wear for decades. As automation, better designs and

improved manufacturing techniques have been applied to PV technology; its price has dropped significantly [Hoffmann-01].

3.1.1 General Description of a Photovoltaic Cell

Photovoltaic cells convert solar radiation directly into DC electrical energy. The basic material for almost all the photovoltaic cells existing in the market, which is high purified silicon (Si), is obtained from sand or quartz. Basically three types of technology are used in the production of photovoltaic cells: monocrystalline; polycrystalline; and amorphous silicon [Fry-98]. The crystalline-Si technology is commonly used as a reference, or baseline, for the solar power generation technology. In general, the status of a photovoltaic cell technology depends on the cell efficiency, and manufacturing cost. The focus of R&D is on improving its efficiency and cost, where the optimal solution is based on a trade-off between the two. The efficiency of a photovoltaic cell is determined by the material's ability to absorb photon energy over a wide range, and on the band gap of the material. Approximate values of the band gap, maximum currents, and maximum theoretical efficiencies at room temperature of some used materials are given in Table 3.1 [Ulleberg-98].

Table 3.1: Band gap, maximum current density, and theoretical efficiency of some different semiconductor technologies

Material	Band gap [eV]	Max. current density [mA/cm²]	Max. theoretical efficiency [%]
Silicon, Si	1.12	43.4	28
Gallium arsenide, GaAs	1.4	31.8	30
Cadmium telluride, CdTe	1.5	28.5	29
Amorphous silicon, a-Si	1.65	21.7	27

Crystalline and polycrystalline silicon are the materials most commonly used in photovoltaic cells. The advantage of silicon cells is primarily the abundance of silicon on earth. The photovoltaic cell consists of several layers of semiconductor materials with different electronic properties. In a typical polycrystalline cell, the bulk of the material is silicon, doped with a small quantity of boron to give it a positive or *p*-type character. A thin layer on the front of the cell is doped with phosphorous to give it a negative or *n*-type character. The interface between these two layers produces an electric field and forms the so called a "cell junction" [Kininger-03].

When the cell is exposed to sunlight, a certain percentage of the incoming photons are absorbed in the region of the junction, freeing electrons in the silicon crystal. If the photons have enough energy, the electrons will be able to overcome the electric field at the junction and are free to move through the silicon and into an external circuit. The direction of the electrical current is opposite to its direction if the device operates as a diode.

A photovolatic generator consists of a number of modules, formed by the interconnection of photovoltaic cells, connected together in series and parallel to provide the required voltage and current. Therefore, the performance of the PV generator depends on the modules that comprise the generator and the cells that comprise the modules. The operating point of the generator is defined by the intersection of its I-U characteristics with the load line of the load connected to it.

3.1.2 I-U Characteristics of a Photovoltaic Module

The performance characteristics of a photovoltaic module depend on its basic materials, manufacturing technology and operating conditions. Figure 3.2 shows typical current-voltage I-U and power-voltage P-U curves of a *BP 585 High-Efficiency Monocrystalline Photovoltaic Module* according to the variation of solar radiation level and cell temperature.

Three points in these curves are of particular interest:

1. *Short circuit point*, where the voltage over the module is zero and the current is at its maximum (*short circuit current* I_{sc}).
2. *Maximum power point or MPP*, where the product of current and voltage has its maximum (defined by $I_{mpp} \times U_{mpp}$).
3. *Open circuit point*, where the current is zero and the voltage has its maximum (*open circuit voltage* U_{oc}).

The measurements taken for obtaining an I-U curve depend on controlling the load current. At open circuit, when no load current is generated, a first characteristic value can be measured; the *open circuit voltage* U_{oc}. Decreasing the load fed by the photovoltaic module leads to a decreasing voltage U with an increasing current I. In other words, by increasing the load current from zero to its maximum value, the operating point moves from the open circuit voltage at zero current to the short circuit current I_{sc} at zero voltage. The series of all measured pairs (U, I) yields the characteristic I-U curve of the module.

From the characteristic curves of the module, it is clear that the open circuit voltage of the photovoltaic module, the point of intersection of the curve with the horizontal axis, varies little with solar radiation changes. It is inversely proportional to temperature, i.e., a rise in temperature produces a decrease in voltage. Short circuit current, the point of intersection of the curve with the vertical axis, is directly proportional to solar radiation and is relatively steady with temperature variations. Actually, the photovoltaic module acts like a constant current source for most parts of its I-U curve.

As demonstrated in Fig. 3.2, an increase in solar radiation causes the output current to increase and the horizontal part of the curve moves upward. An increase in cell temperature causes the voltage to move leftward, while decreasing temperature produces the opposite effect. Thus, the

I-U curves display how a photovoltaic module responds to all possible loads under different solar radiation and cell temperature conditions.

An operating point of a photovoltaic module will move by varying solar radiation, cell temperature, and load values. For a given solar radiation and operating temperature, the output power depends on the value of the load. As the load increases, the operating point moves along the curve towards the right. So, only one load value produces a PV maximum power. The maximum power points line, which is positioned at the knees of the I-U curves, has a nearly constant output voltage at varying solar radiation conditions. When the temperature varies, the maximum power points are generated in such a manner that the output current stays approximately constant.

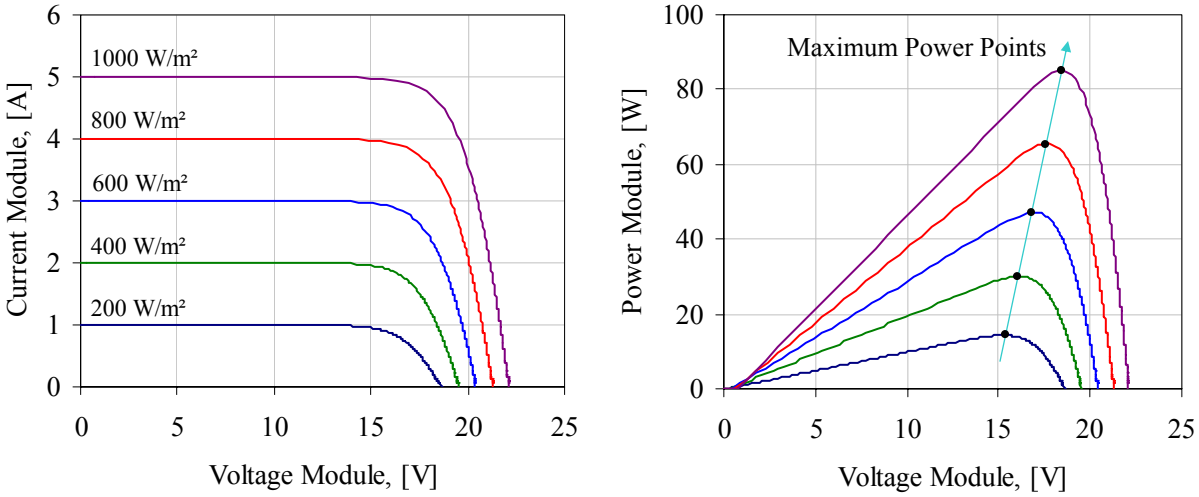

(a) Influence of solar radiation (cell temperature T_J= 25°C)

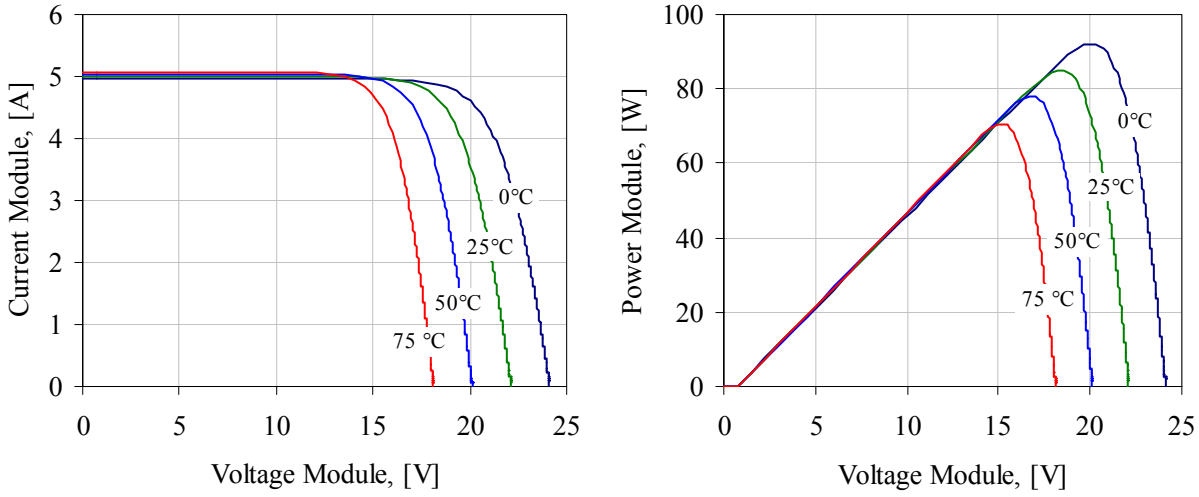

(b) Influence of cell temperature (solar radiation E_0=1kW/m²)

Fig. 3.2: I-U characteristics of BP 585 High-Efficiency Monocrystalline PV Module.

The *fill factor (FF)* of a photovoltaic generator is defined as the ratio of output power at MPP to the power computed by multiplying U_{oc} by I_{sc}. It determines the shape of the photovoltaic generator characteristics. The factors which affect the fill factor are the series and shunt resistances of the photovoltaic generator. A good fill factor is between 0.6-0.8 [Dumbs-99]. As the photovoltaic generator degrades with age, its series resistance tends to increase resulting in a lower fill factor.

3.1.3 Sources of Losses in a Photovoltaic Generator

The losses occurring in the field operation of a PV generator have to be considered in order to calculate precisely its real electric power output. The following losses have to be taken into account.

- ***Reflection Losses*:** when the incidence angle of the solar radiation differs from the perpendicular direction on the surface of a PV generator, reflection losses occur which will cause an overestimation of the PV yield under field conditions. These losses are reduced by coating the surface with antireflection layer [Kininger-03].

- ***Spectral Losses*:** the solar radiation is characterized by a wide spectral distribution because the Air Mass (AM) value changes during the day. The solar radiation contains photons with extremely different energies. Photons with smaller energy than the band gap energy are not absorbed and thus are unused. In case of photons with larger energy than the band gap energy, only an amount of energy equals to the band gap energy is useful, regardless of the value of a photon's energy. The excess energy is simply dissipated as heat into the crystal lattice.

- ***Mismatch Losses:*** the I-U characteristic of PV modules from the same type and the same manufacturer can vary from one module to another. According to the information of the suppliers, the MPP of a module under STC can deviate up to 10% from the data sheet characteristics. By series and parallel connection of the modules in a PV generator, the different I-U characteristics will produce power losses which are called mismatch losses. As example, for quantifying the mismatch losses, measurements were performed in which the PV generator was made up of 36 identical modules and then compared with calculations in which the manufacturer's parameters of the individual 36 modules were used, and the results showed mismatch losses of about 3% [Duzat-00].

- ***Shadowing Losses*:** the characteristics of the PV generators are affected by the presence of the partial shadowing especially the value of maximum output power, the fill factor, and the efficiency of PV generator. Therefore, it is very important to choose the suitable site for the PV generator to prevent partial shadowing during the operation of the PV system [Ahmad-97].

- ***External losses*:** in a real system, the PV generator output power is not exactly equal to the input power to the connected power conditioning unit. In order to calculate this input power, the

losses caused by the voltage drop due to cable resistances and the blocking diodes have to be considered. The losses caused by resistance of the connecting cables (ohmic losses) form the PV generator have to be calculated based on cables length and diameter. This resistance is considered as a series resistance of the PV model, see chapter 4. In each string that forms the PV generator, blocking diodes are connected in series with these strings. If a short circuit occurs in one or more of these strings, the blocking diodes will prevent the currents to flow from the perfect strings to the faulty strings. During operation there is a voltage drop through each diode of approximately 0.7V. This value has to be subtracted from the output voltage of the PV generator.

3.1.4 Maximum Power Point Tracker (MPPT)

The position of the maximum power points on the PV generator characteristic depends strongly on the solar radiation and the cells temperature, as shown in Fig. 3.2. It is used to adjust the actual operating voltage and current of the PV generator so that the actual power approaches the optimum value as closely as possible. Operation of the PV generator at its MPP involves matching the impedance of the load to that of the generator. For this purpose, an electronic device, normally a power conditioning unit, capable of performing the function of a MPPT has to be connected between PV generator and the load. Therefore, a tracking of the MPP is only meaningful, if components for processing are available and the tracking of the working point does not bring additional energy losses and at small additional costs. Many different techniques have been developed to provide maximum power tracking of PV generators [Kuo-01] and [Jantsch-97]. These techniques can be classified as either direct or indirect methods. The direct methods are based on a searching algorithm to determine the maximum of the power curve without interruption of the normal operation of the PV generator. For a certain working point, the corresponding voltage is changed around by a certain increment. Consequently, if the output power becomes larger than the last value calculated, then the search direction is maintained for the next step. Otherwise, it will be shifted in the opposite direction. The indirect methods use an outside signal to estimate the MPP. Such outside signals may be given by measuring the solar radiation, the module temperature, the short circuit current, or the open circuit voltage of a reference PV cell. A set of physical parameters has to be given, and the MPP set point is derived from the monitored signal. In this dissertation, the direct method is used and a MPPT model is available in the PV generator model.

3.2 Hydrogen Energy System and Components

Hydrogen is one of the most promising alternative fuels for the future because it has the capability of storing energy of high quality. Therefore, the hydrogen has been visualized to become the cornerstone of future energy systems based on PV energy and other renewable energy sources. The concept of using hydrogen as an energy carrier in storage and transport of energy has been studied by many scientists from all around the world [Hottinen-01] and [Ogden-02].

Hydrogen can be produced from water via water electrolysis, because of the abundance of water on the earth. The basic overall chemical reaction for splitting water in hydrogen and oxygen is:

$$H_2O \Rightarrow H_2 + ½\, O_2 \qquad 3.1$$

For this reaction to occur, a certain amount of energy is needed, while the opposite reaction releases energy. The oxygen in water electrolysis is usually released to the atmosphere. If hydrogen is produced from natural energy resources, the hydrogen cycle is an excellent environmentally benign energy cycle, as shown in Fig. 3.3. Because PV energy for all practical purposes can be regarded as an infinite source of energy, the hydrogen cycle is one of the best options for a sustainable future.

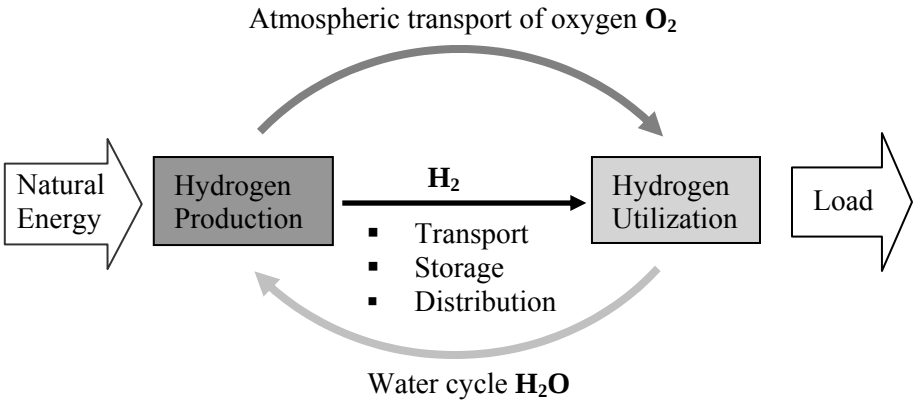

Fig. 3.3: The natural energy hydrogen cycle [Ulleberg-98].

3.2.1 Fuel Cell

The conversion of hydrogen into electricity can be achieved by different methods such as fuel cell and combustion reactions. The advantage of the fuel cell reaction is its higher overall conversion efficiencies. Therefore, the fuel cell will be the topic of interest in this dissertation.

3.2.1.1 Historical development of fuel cell technology

The fuel cell principle was discovered by the Englishman William Robert Grove in 1839 [Möller-00]. The technical development of fuel cells started shortly after World War II when Francis T. Bacon of Cambridge, England, successfully developed a high pressure fuel cell. Subsequently alkaline fuel cells (AFC) and proton exchange membrane fuel cells (PEMFC) were developed for space programs (Gemini, Apollo, Space-lab). In the early 1970s, the development of phosphoric acid fuel cells (PAFC), high temperature molten carbonate (MCFC), and solid oxide fuel cells (SOFC) started [Wurster-99]. PEMFC was not investigated with significant efforts before the late 1970s. These intensified activities, mainly by Ballard, Siemens, H Power, International Fuel Cells and several US universities and research centres,

resulted in significantly improved Membrane Electrode Assemblies (MEA). Therefore, weight and cost of the PEMFC could be reduced drastically and their performance increased dramatically. The first commercial power plant for the PEMFC began operation in 1992 with the 200kW PC25^{TM} [Möller-00]. With the formation of the Partnership for a New Generation of Vehicles (PNGV) by Chrysler, Ford, General Motors and the US Government in 1993, a new focus was set on transportation applications of fuel cells. Their aims are lower amounts of resources for longer distances with fewer emissions.

3.2.1.2 Fuel cell types and their fields of application

Fuel cells are classified as power generators because they can operate continuously, or for as long as fuel and oxidant are supplied. The application of fuel cells largely depends on the operation conditions such as the values of the typical operation temperature and efficiency. Fuel cell types are listed in Table 3.2 according to the order of operating temperature. The most probable fields of application for the different fuel cell types are given in Table 3.3.

Table 3.2: Overview of the fuel cell technologies [Hirschenhofer-99]

Fuel Cell Type	Electrolyte	Temperature, [°C]	Electrical Efficiency, [%]
PEMFC	Polymer	~ 80	60-65
AFC	Potassium hydroxide, KOH	~ 100	60-70
PAFC	Concentrated phosphoric acid, H_3PO_4	~ 200	40-45
MCFC	Molten carbonate melts, Li_2CO_3	~ 650	53-57
SOFC	Yttrium-stabilized zirkondioxide, ZrO_2	~ 1000	55-65

Table 3.3: Overview of the fuel cell application [Wurster-99]

FC Type	Fields of Application	Availability
PEMFC	- Stationary applications for domestic power and heat production - Stationary applications for dedicated power and heat production - Mobile applications for buses, service vehicles - Mobile applications for railroad systems	2000/2001 2002/2003 2001-2003 2003
AFC	- Space and Special military applications	today
PAFC	- Stationary applications for dedicated power and heat production - Mobile applications	1998 > 2000
MCFC	- Stationary applications for combined power and vapor production - Stationary applications for utility use	2001 > 2005
SOFC	- Stationary applications for domestic heat and power production - Stationary applications for commerical heat and power production - Stationary applications for utility use	2000 2001-2003 > 2005

SOFC and MCFC operate at high temperatures, and are therefore most suitable for large power plants. PAFC is today commercially available and can be used over a large power range, from a few kW to several MW. However, it operates at medium high temperatures and is typically

most suitable for co-generation (Combined Heat and Power generation, CHP). The two low temperature fuel cells AFC and PEMFC are attractive options for stand-alone power systems due to their low operation temperatures.

3.2.1.3 Advantages and disadvantages of fuel cells

The fuel cell is important for terrestrial applications of the hydrogen technology, because it combines a relatively high efficiency with a very low environmental emission. In addition, it operates at a constant temperature, and the heat from the electrochemical reaction is available for co-generation applications. Fuel cell power plants can be configured to use a wide variety of fuels and produce a wide range of electrical outputs. Also, these plants by operating on hydrogen and oxygen offer high energy density. Therefore, large energy outputs can be produced from a system with a relatively small weight and volume. Thus, a fuel cell is a preferred power generator in remote applications where system weight and volume are important parameters. Other ***advantages*** of fuel cells and fuel cell plants [Gomatom-03] and [Hoogers-03] are:

- Direct conversion of chemical to electrical energy.
- Excellent characteristics, even with partial loading.
- High availability of lower temperature units.
- Fuel flexibility.
- Zero or very low noise except for occasional vibrations.

Disadvantages:

- Relatively high costs compared to conventional power sources.
- Life time limitations (no confirmed knowledge about real life time).
- Decreasing electrical efficiency as function of the operating life time.
- Special treatment of fuel (H_2) is necessary.
- Noble materials are needed for membranes and electrodes, e.g., platinum is one of the most effective catalysts.

3.2.1.4 Cost of the fuel cell

The cost is a barrier for all types of fuel cells across all applications. The cost of fuel cells is determined by the market segment, by costs of the competing technologies and by the energy economic developments (energy taxation) [Taylor-03]. Due to the higher efficiency of fuel cell systems, the fuel and the maintenance costs are lower compared to other systems such as gas turbines. The following factors can influence the operational costs of fuel cell systems: (1) the cost of natural gas; (2) the operation mode (heat conducted, electricity conducted, or combinations); (3) the lifetime of the system (costs for stack replacement).

To reduced the investment costs of fuel cell systems, various measures have to be taken: (1) improving fuel cell stack design to increase the power density; (2) using lower cost materials;

and (3) minimizing temperature constraints (e.g. lowering SOFC operating temperature to use lower cost materials).

The cost of fuel cells varies widely depending on size, power electronics requirements, and reformer requirements. Two autonomous remote renewable energy systems, a small 356W radio repeater station and a 148kW village power system are analysed in detail in [Cotrell-03]. The capital cost of a PEMFC is 5000$/kW for the radio repeater station because of its small size. This cost was reduced to 3000$/kW for the other system to account for its large size. The cost issues facing portable and standby power applications are less acute than the challenges facing transportation and stationary applications.

3.2.1.5 Hydrogen/Oxygen PEM fuel cell operation

In the case of a H_2/O_2 PEM fuel cell, H_2 and O_2 are the fuel and oxidant respectively. The product is pure water H_2O and electricity. The cell reactions are:

Anodic half reaction:	$H_2 \Rightarrow 2H^+ + 2e^-$	3.2.a
Cathodic half reaction:	$½O_2 + 2H^+ + 2e^- \Rightarrow H_2O$	3.2.b
The overall reaction:	$H_2 + ½O_2 \Rightarrow H_2O$	3.2.c

Hydrogen is oxidized on the anode and oxygen is reduced on the cathode. Protons are transported from the anode to the cathode through a PEM and electrons are carried to the cathode over an external circuit. On the cathode, oxygen reacts with protons and electrons forming water and producing heat. Both the anode and the cathode contain a catalyst to speed up the electrochemical processes. Basic description of a PEM fuel cell operation is shown in Fig. 3.4.

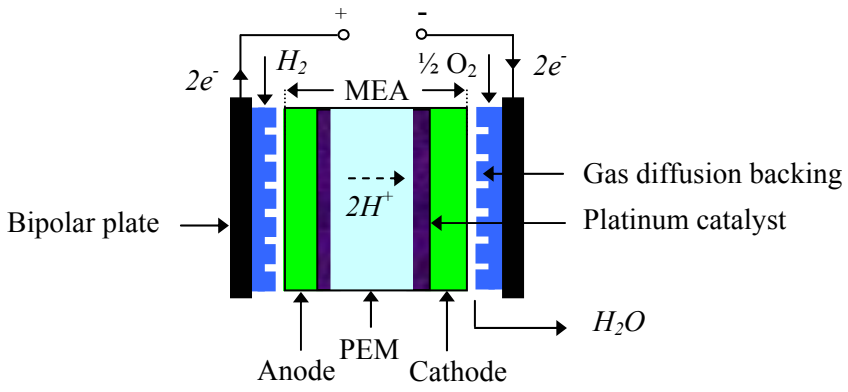

Fig. 3.4: Basic description of a PEM fuel cell operation [Ulleberg-98].

The theoretical cell voltage for a PEM fuel cell (U_{th}) is about 1.23V at standard conditions. The cell voltage decreases because of over-voltages, which can be divided into the activation, ohmic and concentration (diffusion) over-voltages. The activation over-voltage is due to the slow charge transfer of the oxygen reduction and it is the major source of losses. The ohmic over-voltage is due to the resistance of the membrane, other materials, and their junctions. The

concentration over-voltage arises when the mass transportation is limiting the reaction. All these losses will be discussed and calculated in detail in chapter 4.

A single fuel cell produces a limited voltage, usually less than 1V. In order to produce a useful voltage for practical applications, several cells are connected in series to form a fuel cell stack. The output voltage depends on the number of the cells in the stack. A view of a PEM fuel cell structure and a PEMFC stack are presented in Fig. 3.5.

The main part of a single cell is the Membrane Electrode Assembly (MEA) which consists of an anode, electrolyte membrane (PEM), and cathode. These components are pressed between two gas diffusion backings and two bipolar current collector plates. The **Anode** (fuel electrode) must provide a common interface for the fuel and electrolyte, catalyse the fuel oxidation reaction, and conduct electrons from the reaction site to the external circuit. The **Cathode** (oxygen electrode) must provide a common interface for the oxygen and the electrolyte, catalyse the oxygen reduction reaction, and conduct electrons from the external circuit to the oxygen electrode reaction site. The **Electrolyte Membrane** (PEM) must transport one of the ionic species involved in the fuel and oxygen electrode reactions, while preventing the conduction of electrons (electron conduction in the electrolyte causes a short circuit).

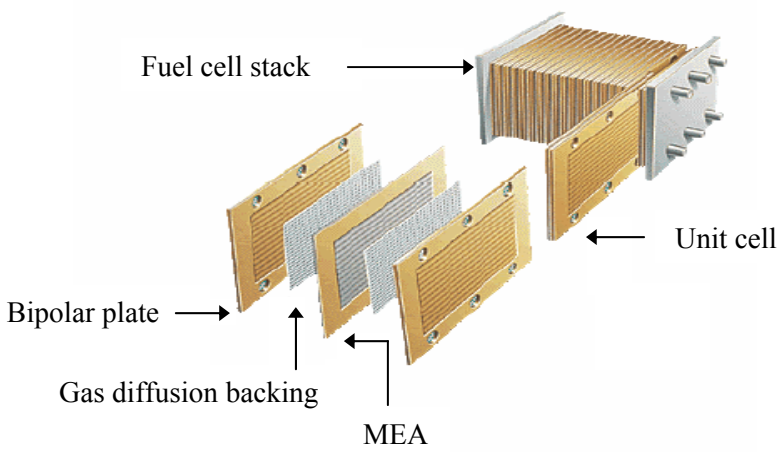

Fig. 3.5: A view of a PEM unit cell structure and a PEMFC stack [Mikkola-01].

In a PEM fuel cell, the gas diffusion backings provide electrical contact between the electrodes and the bipolar plates, and distribute reactants to the electrodes. Also, they allow the reaction product water to exit the electrode's surface and permit passage of water between the electrodes and the flow channels. These layers are made of a porous, electrically conductive material, usually carbon paper. In a fuel cell stack, bipolar plates or separator plates separate the reactant gases of adjacent cells, connect the cells electrically, and act as a support structure. Bipolar plate materials must have high conductivity and be impermeable to gases.

3.2.1.6 PEM fuel cell characteristics

The I-U and I-P characteristics of a PEM fuel cell are presented in Fig. 3.6. They can be divided into three regions, which are governed by different over-voltages. Activation over-voltage dominates at low current densities in region I. Region II is governed by the ohmic losses and in region III bending down of the polarization curves due to the concentration over-voltage. Some fuel cells are not operated at high enough currents to ever see the effects of losses in region III.

Hydrogen and oxygen pressures in a H_2/O_2 PEM fuel cell during operation are kept fairly constant. In an H_2/Air PEM fuel cell, a fan is usually used to force atmospheric air across the cathode side. The overall performance of the PEM fuel cell can be improved by increasing one or all of the following conditions: (1) temperature of the PEM fuel cell (20-80°C); (2) hydrogen and/or oxygen pressure (1-5 Bar); (3) flow rates of hydrogen and oxygen [Ulleberg-98].

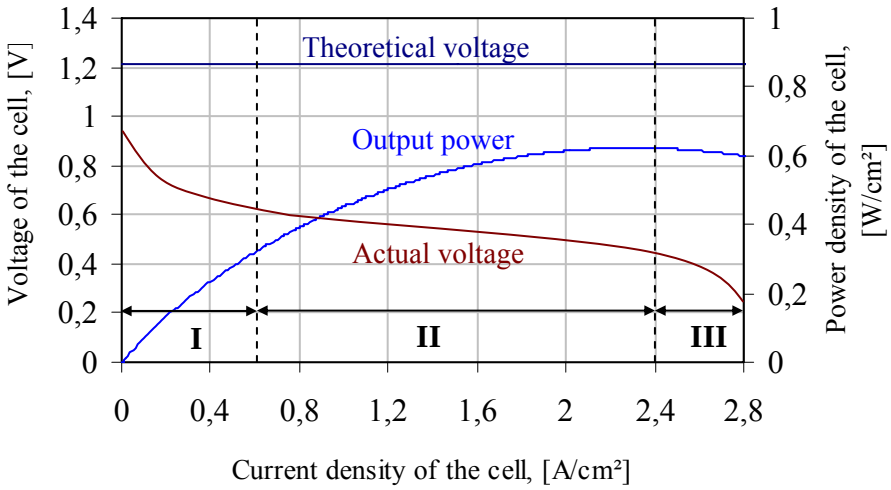

Fig. 3.6: Characteristic curves of a typical PEM fuel cell.

3.2.2 Electrolyser

An electrolyser converts electricity into chemical energy which produces hydrogen. Hydrogen can be stored for example into pressure tanks or metal hydrides. Hydrogen can be produced from water electrolysis in several ways such as alkaline, acidic, and solar photo production. Alkaline and acidic water electrolysers are commercially available today. Alkaline water electrolyser will be the main topic of interest in this dissertation and will be discussed in detail in this section.

One of the most promising types of acidic electrolysers is proton (polymer) exchange membrane (PEM) electrolyser, which resembles that of PEM fuel cell described in section 3.2.1. Actually, if properly designed, the same PEM unit can be operated as an electrolyser to produce hydrogen, as well as hydrogen driven fuel cell to produce electricity. The basic difference between the PEM electrolyser and PEM fuel cell is that the hydrogen and oxygen reactions on the electrodes

are opposite. Therefore, the electrolyser produces H_2 at the cathode and O_2 at the anode, while the fuel cell consumes H_2 at the anode and O_2 at the cathode. Also, the decomposition of water into H_2 and O_2 in the electrolyser is non-spontaneous and requires an electric power for the reaction to occur, while the opposite fuel cell reaction is spontaneous and produces an electric power. In both cases the reversible voltage is constant and equal to 1.23V. On the other hand, one can use the same equations to model PEM electrolysers as to model PEM fuel cells, only the model's parameters might have different signs. The investment cost for PEM electrolyser is over 1000$/kW [Kato-03]. The high cost of the components is the main drawback of this technology.

The solar photo production methods are futuristic forms of hydrogen production. According to PV energy driven water splitting systems, two important systems should be considered for future R&D. These systems are PV and electrolyser systems, and photo electrochemical systems. From a practical point of view, the systems of most interest are the combination of PVs and electrolysers. This is due to the relatively mature of the alkaline electrolyser technology, and the rapid and development of the silicon photovoltaic technology. The photo electrochemical systems have the advantage of combining the PV generator and electrolyser into one system without wires. A solar to hydrogen conversion efficiency with this design is approximately 15% [Miller-00].

3.2.2.1 Alkaline water electrolyser types

- ***Conventional Alkaline Water Electrolyser***

The electrolyte used in an alkaline water electrolyser has been aqueous potassium hydroxide (KOH) mostly with solutions of 20-30 wt.%. This concentration range gives the optimal conductivity and corrosion resistance of stainless steel [Wendt-90] and [Pyle-94]. The typical operating temperatures and pressures of this electrolyser are 70-100°C and 1-30bar respectively. Physically an electrolyser consists of several electrolytic cells, connected in parallel. Two distinct cell designs exist: mono-polar and bipolar. In mono-polar cells the electrodes are either negative or positive while bipolar cells have electrodes that are negative on one side and positive on the other side separated by an electrical insulator, as shown in Fig. 3.7a [Ulleberg-98]. The bipolar electrolyser stacks is more compact than the mono-polar ones. The bipolar electrolyser operates at higher pressures (up to 30 bar), and this is another advantage, because it reduces the compression work required to store the hydrogen produced by the electrolyser. Mono-polar systems operate at atmospheric pressure. The advantage of the compactness of the bipolar cell design leads to shorter current paths in the electrical wires and electrodes compared to the mono-polar cell design. This reduces the losses due to internal ohmic resistance of the electrolyte, and therefore increases the electrolyser efficiency. However, there are some disadvantages of bipolar cells, for example a single cell failure leads to malfunctioning of the whole stack. Mono-polar cells can be connected individually in the stack depending on the voltage-current demands, a single cell can be disconnected in the case of failure without

seriously disturbing performance. Furthermore, the compactness and high pressures of the bipolar electrolysers require relatively sophisticated and complex system design. The relatively simple and study mono-polar electrolysers systems are in comparison less costly to manufacture. Nevertheless, most alkaline water electrolysers manufactured today are bipolar.

- ***Advanced Alkaline Water Electrolyser***

The main aims of the advanced water electrolysers are: (1) to reduce the practical cell voltages to reduce the unit cost of electrical power and thereby the operational costs; and (2) to increase the current density and thereby reduce the investment costs [Wendt-90]. Actually these two aims are conflicting with each other because increasing the current densities yield increasing the cell voltage due to increasing the ohmic resistance as well as increasing the over-voltages at the anodes and cathodes. In practice, three basic improvements of alkaline water electrolyser are considered to reach the two aims stated above.

(1) Developing new cell configurations to reduce the surface-specific cell resistance despite increased current densities (e.g., zero-gap cells and low-resistance diaphragms).
(2) Processing at higher temperatures (up to 60°C) to increase electric conductivity of the electrolyte, i.e., to reduce the electric cell resistance.
(3) Developing new electrocatalysts that reduce anodic and cathodic over-voltages.

In the zero-gap cell design, as shown in Fig. 3.7b, the electrode materials are pressed on either side of the diaphragm so that the hydrogen and oxygen gases are forced to leave the electrodes at the rear. Most manufacturers are already adopting this design. The investment cost of this type is approximately 500$/kW [Kato-03].

3.2.2.2 Alkaline water electrolyser cost

Standard alkaline water electrolyser, which makes use of fossil fuel sources of electricity, is much cheaper than renewable electrolyser, which makes use of solar or wind power sources of electricity. However, the standard alkaline water electrolyser suffers the environmental penalties resulting from fossil fuel burning in power plants, and represents very little progress away from the current energy regime. The capital costs of standard alkaline water electrolysers range from 300$/kW to 600$/kW [Bafna-02]. For example, a 2MW alkaline water electrolyser with an efficiency of approximately 80% would cost roughly 600$/kW and the price of hydrogen produced is approximately 20$/GJ [Bafna-02]. Although the environmental benefits of the renewable electrolyser far surpass other methods, its use is not recommended in the short-term. Renewable methods of electricity production are themselves a developing technology. The cost of hydrogen production from a renewable electrolysis is simply high to be economical. However, as a long-term goal, this production method is quite promising. The cost of the electrolyser remains decreasing, as component materials continue to be changed and developed.

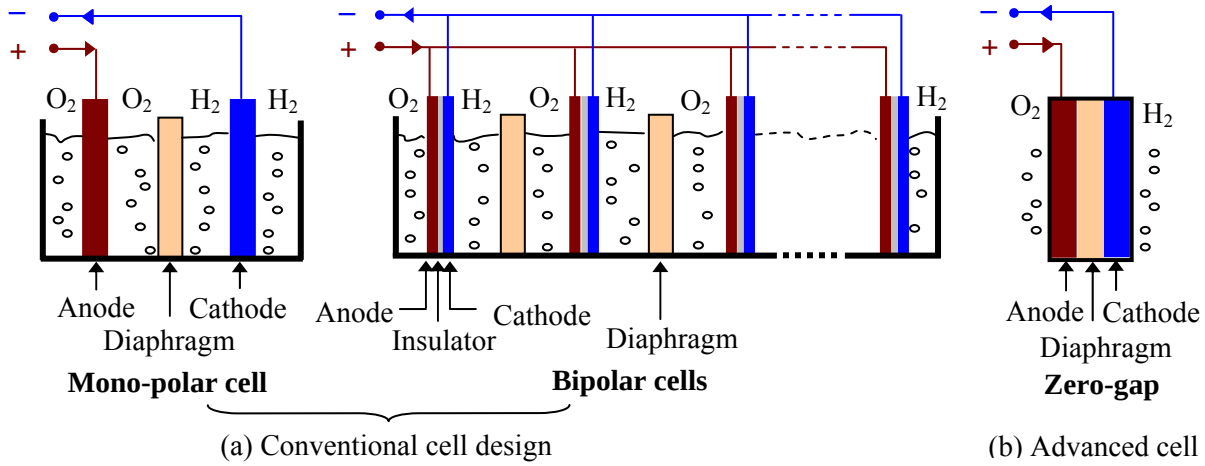

Fig. 3.7: Principle of alkaline water electrolyser cell designs.

3.2.2.3 Alkaline water electrolyser operation and I-U characteristics

The decomposition of water into hydrogen and oxygen can be achieved by passing a DC electric current between two electrodes separated by a KOH electrolyte with good ionic conductivity. Water is a very poor ionic conductor and for this reason a conductive electrolyte must be used, so that the reaction can proceed at a technically acceptable cell voltage. The half cell reactions and the overall reaction are:

Anodic half reaction:	$2OH^- \Rightarrow \frac{1}{2}O_2 + H_2O + 2e^-$	3.3.a
Cathodic half reaction:	$2H_2O + 2e^- \Rightarrow H_2 + 2OH^-$	3.3.b
The overall reaction:	$H_2O \Rightarrow H_2 + \frac{1}{2}O_2$	3.3.c

A plot of the theoretical and actual voltages (U_{th}, U_{actual}) for an alkaline water electrolyser cell versus the current density at high and low operating temperatures are shown in Fig. 3.8. The difference between the two I-U curves is mainly due to the temperature dependence of the over-voltages.

3.2.3 Hydrogen Storage

Before discussing some methods of hydrogen storage, the properties and characteristics of hydrogen must be mentioned. Hydrogen is the simplest and most abundant element in the Universe. It is clean and pollution free. Some characteristics of hydrogen are [VLEEM-02] and [Barbir-03]:

- It is colourless, odourless, and has no taste.
- It is the lightest of all elements (molecular weight = 2.016g/mol). Its density is about 14 times less than air (0.08376kg/m³ at standard temperature and pressure), it has a very high diffusion rate.
- It is liquid at temperatures below 20.3K at atmospheric pressure. The density as liquid is 70.8 kg/m³.
- It contains the highest energy per unit mass of all fuels (HHV = 141.9MJ/kg or 11.89MJ/m³, and LHV = 119.9MJ/kg or 10.043MJ/m³). One pound of hydrogen has three times the energy content of one pound of gasoline.
- It has a small molecular size, allowing it to leak more easily through porous materials than other common gases at equivalent pressures. At the same holes or joints, it is leak about 1.26 to 2.8 times faster than a natural gas.
- It is generally non-corrosive and non-reactive with typical container materials.
- It is non-toxic and non-poisonous. In contrast, the combustion products of diesel and other conventional fuels are more toxic from an inhalation standpoint.

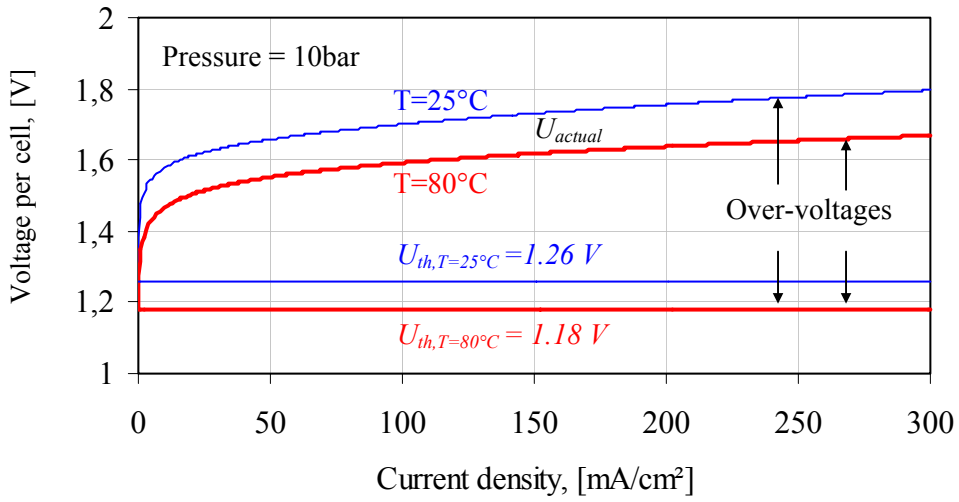

Fig. 3.8: I-U curves for an electrolyser cell at high and low temperatures.

When an energy system is totally based on renewable or intermittent power systems, the problem arises that the energy demand pattern cannot be fully fulfilled by on line power generation. An energy storage system must be put in between the power generation and the power utilization. Hydrogen has been proposed as the core medium for solving this problem. Hydrogen is not a primary energy source, but it is utilized as an energy carrier between power generation and the power utilization. Power is generated from hydrogen either by conversion in a fuel cell, or by combustion in an internal combustion or turbine engine. In this dissertation, a hydrogen fuel cell system will be studied in detail. Hydrogen is characterized by a low density under normal conditions, so that its storage is difficult compared with liquid fuels. It can be

stored in many basic configurations such as: (1) pressurized (compressed) hydrogen gas in tanks or in underground reservoirs; or (2) liquid hydrogen in tiny micro spheres; or (3) Metal hydride compounds, i.e., H_2 is stored in a metal or an alloy. The various storage types have different characteristics. The selection of a specific storage type depends on these characteristics, and mainly on energy density and cost of each type.

3.2.3.1 Compressed gaseous hydrogen storage

Compressed gaseous hydrogen can be stored in pressure tanks at ambient temperature and 200 up to 700bar pressure. The most common materials used for hydrogen tanks are steel and aluminum. From all storage technologies, the compressed gaseous hydrogen has the longest history and cheapest price. This storage type is suitable for electroysers, which can produce hydrogen at high pressures. The theoretical gravimetric energy density of hydrogen can be calculated the molar mass of hydrogen molecule (2.016g/mol) to be 39.4kWh/kg [Hottinen-01]. The actual gravimetric energy density of stored hydrogen is largely dependent on the material of the container since light materials usually do not tolerate pressure as well as heavier ones. With a traditional steel tank energy density of about 0.45kWh/kg could be achieved, which is equivalent to 1.14% of the weight of stored hydrogen. The material development of tanks has taken a tremendous step with the development of different composites. Therefore, with these composite tanks, the energy density is increased to 4.45kWh/kg, which is equivalent to 11.3% of the weight of stored hydrogen [WS-qtww-03]. Compressed gaseous hydrogen can be stored either in aboveground portable or stationary tanks or in different kinds of earth caves. The aboveground hydrogen storage tanks vary in size but are typical in standard pressure. One of the best properties of the aboveground tanks is that they do not leak. The losses of the storage capacity are thus virtually non-existent [VLEEM-02]. Some leaks may occur through connectors but with proper fittings and regulators these leaks could be minimized. The underground caves are an easy and relatively cheap method for large size storage of hydrogen. The pressure in earth caves varies between 80-160bar and thus the volumetric energy density is about 250-465kWh/m³ [Hottinen-01]. The losses caused by the leaks in earth caves are about 1-3% of the total volume per year.

3.2.3.2 Liquid hydrogen storage

Liquid hydrogen has been used as a fuel in space technology for several years [Hottinen-01]. It is light and has less potential risks in terms of storage pressure compared with the compressed gas. The hydrogen liquefies to a colourless liquid at –253°C (20.3K) and thus the storage tanks require sophisticated insulation techniques. Liquid hydrogen is stored in standing or lying tanks of 3-75m³ under a pressure of 12bar [Möller-00]. The energy needed to liquefy the hydrogen is about 20 to 30% of the energy content of hydrogen. This is one of the largest problems concerning the use of liquid hydrogen. However, this loss of energy is quite compensated with high energy density of liquid hydrogen. An amount of 1%/day of the stored hydrogen must be evaporated to keep the low temperature. The gravimetric storage density of the liquid hydrogen

in storage containers is about 25.9 wt.% (10.2 kWh/kg) and the volumetric energy density is about 2760kWh/m³ [Hottinen-01]. The improvements in insulation techniques and pressurization of the tank will have some effect on these figures. This type of storage has fast refuelling (125 liter tank of liquid hydrogen can be refuelled within only 3 minutes) [Barbir-03].

3.2.3.3 Metal hydrides storage

A special way of hydrogen storage is done by using metal hydride. Metal hydride is a metal or an alloy, which is able to bind the hydrogen chemically. This metal or alloy can store multiple hundreds of its capacity of hydrogen. When a hydride is formed with a metal or an alloy, heat is generated, i.e., the process is exothermic. Conversely, in order to release hydrogen from a metal hydride, heat must be supplied, i.e., the process is endothermic. These processes can be represented by the following chemical reations [Ulleberg-98]:

Charging or Absorption process:	$M + xH_2 \Rightarrow MH_{2X}$	3.4
Discharging or Desorption process:	$MH_{2X} \Rightarrow M + xH_2$	3.5

where M represents the hydriding substance, a metal or an alloy. The rate of these reactions increases with the surface area. Therefore, in general, the hydriding substances are used a powder to speed up the reactions. MH is the metal hydride, x is ratio of the number of hydrogen atoms to the number of hydriding substance atoms. During the formation of the metal hydride hydrogen molecules are split and hydrogen atoms are inserted in spaces inside the lattice of the metals or alloys. In such a way an effective storage is created comparable to the density of liquid hydrogen. However, when the mass of the metal or alloy is taken into account then the metal hydride gravimetric storage density is comparable to storage of pressurised hydrogen. The best achievable gravimetric and volumetric hydrogen storage densities are about 0.07kg/kg of metal, and 101kg/m³ of metal respectiviely, for a high temperature hydride such as MgH_2. Also, the gravimetric and volumetric energy storage densities of this metal hydride are 2.8kWh/kg and 4000kWh/m³, respectively [WS-qtww-03] and [Noponen-00]. During the storage process (charging) heat is released which must be removed in order to achieve the continuity of the reaction. During the hydrogen release process (discharging) heat must be supplied to the storage tank.

Two ways can be used for storing electric energy in hydriding substances. In one of the methods, DC energy is used to electrolyse the water, and the hydrogen produced is stored in a hydriding substance. When electric energy is needed, the hydrogen is released from the hydriding substance by heating and used in a fuel cell to produce DC energy. Heat from fuel cell can be used to release hydrogen from the metal hydride. In the second method, one electrode of the electrolyser is covered with a hydriding substance [Barbir-03]. During the electroysis of water, the hydrogen produced on the electrode surface is immediately absorbed by the hydriding substance covering the electrode. Then, when electric energy is needed, the

electrolyser operates in a reverse mode as a fuel cell using the hydrogen released from the metal hydride to produce electric energy.

Metal hydride process is expensive and sensitive against impurities and has finite lifetime. On the other hand, this kind of storage is relatively safe because the hydrogen is bound to a metal.

3.3 Supercapacitor

3.3.1 Background information

Supercapacitors were first practically used in 1979 for memory backup in computers and are now manufactured by many companies [Namisnyk-03]. The term "supercapacitor" reflects orders of magnitude of improvement in the energy density of DC capacitors through state of the art selection and processing of electrode materials [Burke-00]. It differs from common dielectric capacitor, because it stores energy in a polarized liquid layer at the interface between a conducting ionic electrolyte and a conducting electrode such like a battery (first generation). The electrodes are fabricated from a high surface area, porous material having pores of diameter in the nanometre range. The surface area of the electrode materials used in supercapacitor in much greater than that used in conventional capacitor electrodes, being in the order of 1500-2000m²/g. Thus, the energy stored by such capacitors may reach 50-60J/g. Electric charge is stored in the micro pores at or near the interface between the solid electrode material and the electrolyte, as shown in Fig. 3.9. The electric charge and energy stored are given by the same expressions for the simple dielectric capacitor [Namisnyk-03]. This kind of supercapacitors is the so-called symmetric design, where the positive and negative electrodes are made of similar materials (activated carbon material) each with the same capacitance, i.e., *C1=C2*.

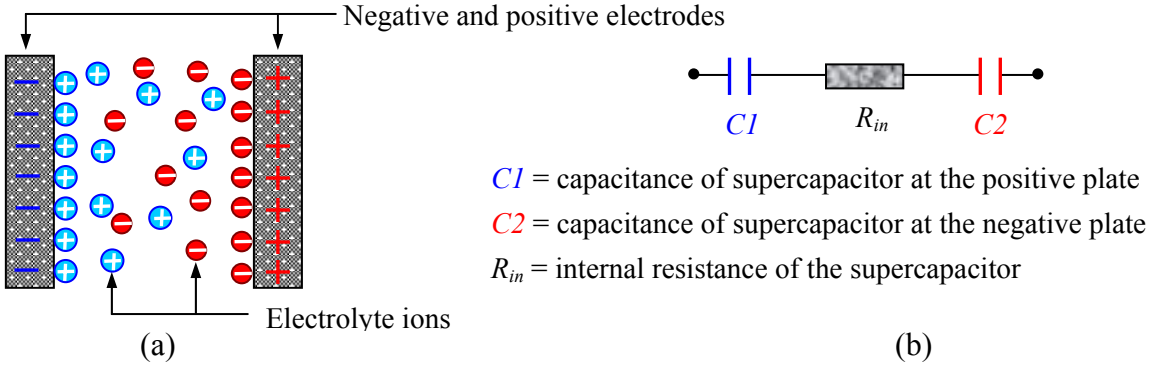

Fig. 3.9: Supercapacitor: (a) structure; (b) simplified equivalent circuit.

Second generation supercapacitors use also the symmetric design but with organic rather than aqueous electrolyte. Organic electrolyte allows higher operating voltage (cell voltage 2.5–3V) and energy density. The third generation of supercapacitors uses a negative electrode made of activated carbon material and a positive electrode that contains nickel hydroxide as a basic active material component. This technology is called asymmetric design. The capacitance at

the positive electrode is significantly greater than the capacitance at a negative electrode having the same dimensions, i.e., *C1>>C2*. It has almost a twofold increase in capacitance compared to a symmetric capacitor, and this increases the energy stored by an asymmetric design. As a result, the energy density in an asymmetric design is 4 to 5 times as much as that of a conventional carbon/carbon symmetric design using aqueous electrolyte [WS-esma-04]. Many of these products are targeting many applications such as hybrid electric vehicles, power quality improving systems, supplement to a battery or fuel cell, and stand alone PVFC systems.

The supercapacitor has the ability to store greater amounts of energy than conventional capacitors, and is able to deliver more power than batteries. The current position of the supercapacitor is easily visualised by means of a Ragone plot, as shown in Fig. 3.10, which graphically represents each device energy and power capabilities. Table 3.4 shows that the supercapacitor fits between conventional capacitor and battery in terms time constant, energy density, power density, and life cycle. A supercapacitor can also store or release energy very quickly, and can operate over a wide range of temperatures. Other advantages of supercapacitors are:

- State of charge is easily determined by measuring the terminal voltage.
- Self-discharge rate is very low.
- Recharging efficiencies approaching 99%.
- A minimal maintenance is required.

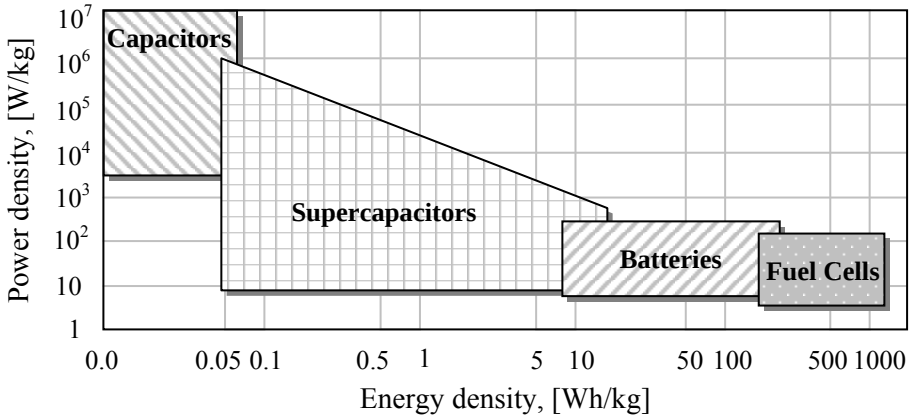

Fig. 3.10: Ragone plot of various energy storage devices [Braun-00] and [Schneuwly-02].

Table 3.4: Comparison of various energy storage devices [Key-03]

Parameter	Conventional Capacitors	Supercapacitors	Batteries
Time constant, [S]	< 0.1	0.2 – 10	> 100
Energy density, [kJ/kg]	0.1 – 0.5	0.5 – 30	> 100
Power density, [kW/kg]	> 10	~ 0.5 - 1	~ 0.1 – 0.5
Life cycle, [cycles]	> 1000 000	500 000 – 1000 000	< 1500

3.3.2 System design and voltage balancing

A number of supercapacitors are combined in series to form modules to achieve the required voltage level for most applications, much like a string of batteries. Today, standard modules with voltages of 14, 28 and 42V are available [Schneuwly-02]. This connection increases the total equivalent series resistance (ESR) of the modules. If the ESR needs to be reduced additional strings of series capacitors will have to be connected in parallel. The variation of capacitance and resistance in the individual supercapacitors will produce an unequal voltage distribution across the modules. This can be hazardous because if the voltage of an individual supercapacitor is greater than the electrolyte's breakdown voltage of a parallel supercapacitor, a destruction of the module would results. Therefore, a voltage balancing circuitry is required when making use of a supercapacitor module.

Manufacturers have developed two methods to deal with voltage balance. The first is a passive circuit solution which uses; series resistors or zener diodes connected in parallel with the capacitors [Namisnyk-03], [Jeong-02] and [Barrade-02]. The second method is an active circuit solution which uses one of different circuits such as a buck/boost converter; a fly-back converter; or a comparator circuit [Barrade-00], [Barrade-03], [Rufer-02] and [Prophet-03]. Each supercapacitor is coupled with one of these circuits. Therefore, this technique is very expensive but offers a maximum isolation of each capacitance, a maximum energy stored with a high efficiency, and a very good availability. In the following, a passive circuit solution is discussed.

A common way to equalize the voltages of supercapacitor cells is to connect across each of them a resistor. Figure 3.11 shows a supercapacitor module, in which each capacitor is connected by using a copper bus-bar to reduce the ohmic resistance of the connecting wire. Figure 3.12 shows an electric circuit diagram of a supercapacitor with cell balancing resistor and a fault detection branch. The supercapacitor fault detection branch has a LED and a driving resistor, so that the damaged cell can easily be detected without time consuming. The main disadvantage of this solution is the power dissipated in each resistor. There is always a current flowing in the resistor, deteriorating the self-discharge behaviour of the system.

(a) (b)

Fig. 3.11: (a) Supercapacitor module; (b) An enlarged photograph of (a) [Schneuwly-02].

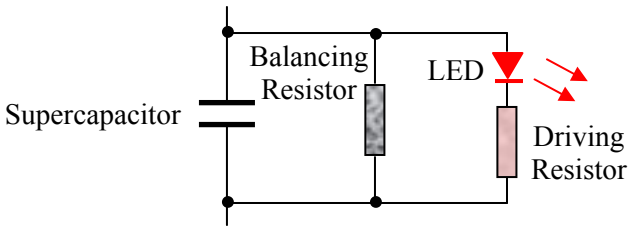

Fig. 3.12: Supercapacitor cell balancing and fault detection circuit.

A circuitry similar to the resistor balancing circuit uses a zener diode instead of the balancing resistor across each capacitor. The zener diode has to limit the voltage of the supercapacitor cells at the maximum allowable value. There is no power dissipation as long as all the voltages are less than the limiting voltage. But the power dissipation could be high if many cells reach their voltage limit [Schneuwly-02].

Energy losses for voltage balancing with resistors and zener diodes are simulated and compared in details in [Barrade-00]. In both cases, four 1000F and one 800F supercapacitors were connected in series and charged from 0V to 12.5V (maximum cell voltage 2.5V). The energy stored at the end of the charging process amounted to 15kJ. In case of the voltage balancing resistors (each 0.1Ω), 120kJ was required to fully charge the supercapacitors, resulting in an efficiency of 12.5%. It is clear that large amount of power is dissipated in each resistor. In addition, the charging process was slow and took 400sec to equalize the voltages of all the capacitors. When zener diodes were used only 16.3kJ was required, resulting in an efficiency of 92%, and it took only 40sec to equalize the voltages of all the capacitors. Therefore, the charging efficiency and equalizing time are improved by using zener diodes for voltage balancing instead of resistors.

3.3.3 Supercapacitor characteristic

The supercapacitor can be charged and discharged extremely quickly (in micro to milliseconds). The actual charge and discharge current limits depend on the size of the supercapacitor and the internal losses. Typically small capacitors can deliver current over 10A and large one can deliver current over 1000A [HILTech-01]. The internal resistance of the supercapacitor prevents it from discharging instantaneously. Indeed most supercapacitors have a time constant between 1 to 2 seconds and it takes approximately 5 time constants to completely discharge in a resistor circuit.

The supercapacitor's voltage comprises two components; a capacitive component, and a resistive component. The capacitive component represents the voltage due to the charge or discharge energy within the capacitor. The resistive component represents the voltage change due to the internal resistance of the supercapacitor. Figure 3.13 shows these two components for a constant current discharge. The charge profile will be similar, but in a reverse way such that the terminal voltage of the supercapacitor increases with charging time.

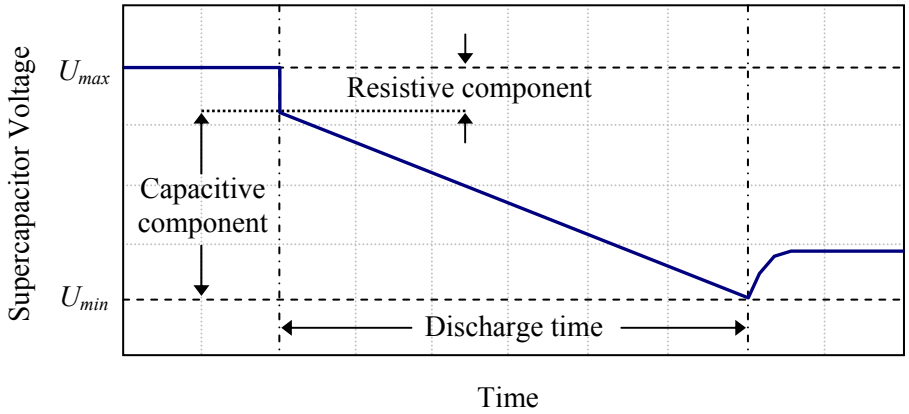

Fig. 3.13: Supercapacitor discharge profile [HILTech-01] and [Kim-03].

3.3.4 Supercapacitor with PVFC hybrid system

PVFC hybrid systems derive their energy from intermittent source. Using supercapacitors have a number of advantages over the commonly used batteries. The repeated charge and discharge cycles every day for a battery in a PV hybrid system have a detrimental effect on it, resulting in shorting its life to 3 years till at most 7 years for high quality batteries. Contrarily, supercapacitors are able to withstand a large number of charge and discharge cycles without suffering significant losses in performance, and thus only need to be replaced every 20 years, which is the lifetime of the PV generator itself [Namisnyk-03].

Energy efficiency is always of primary concern in renewable power generation, and supercapacitors provide higher charging efficiency than battery. A lead acid battery, for example, can lose up to 30% of the energy during charging. Supercapacitor, on the other hand, may only lose 10% [Namisnyk-03]. The ability to operate efficiently over a wider range of temperatures is also an advantage of supercapacitors. Some remote stations may be located in a cold climate and if batteries are used for energy storage their temperatures have to be maintained close to room temperature by auxiliary systems, representing additional cost and energy consumption.

In this dissertation, a PVFC hybrid system is combined with a supercapacitor to provide a more robust power response to changes in system loading. The supercapacitor will be used to improve the load following characteristics of a PEM fuel cell. During motor's start or any other sudden variation in load, the supercapacitor will provide the balance of active and reactive power needed during the momentary load variation period. During sudden loss of load, the supercapacitor will absorb excess energy from the generator source. Adding supercapacitor energy storage to the system will improve power quality and efficiency. Also, it is used to reduce the capital expenses by allowing the system to be sized more closely to the steady state power requirements, rather than over-sizing the generator to meet transient loading

requirements. Therefore, the hybrid fuel cell and supercapacitor combination can serve dynamic loads and also provide power conditioning for grid connected or stand alone system.

3.4 Power Conditioning Units (PCUs)

Photovoltaic or fuel cell power systems, which generate power as a direct current (DC), require power conversion units to convert the power from DC to alternating current (AC). This power could be connected to the transmission and distribution network of a utility grid. There are other applications, where it is necessary to be able to control power flow in both directions between the AC and DC sides. For all these cases power conditioning units are used. Power conditioning units (PCUs) are defined generally as electronic units that transform DC power to AC power (inverters), AC power to DC power (rectifiers), both (bi-directional power electronic converters), or convert DC power at one voltage level to DC power at another voltage level.

3.4.1 Using PCUs in hydrogen PVFC hybrid power systems

In PVFC hybrid power systems, the input power of the system varies continuously with time. The output characteristics of a PV generator have peak power points that depend on solar radiation and cell temperature. Therefore, it may be advantageous to use an MPPT to optimally utilize the input power source. PVFC hybrid power systems can use the power conditioning units for this purpose and also to prevent the expensive electrochemical units such as fuel cell or electrolyser from damage, to step-up voltage for electrochemical units, to invert, to regulate, and to wave-shape the output voltage from all components.

An inverter is also needed to connect the system to the AC consumer loads. When all components of the system are directly connected, the two electrochemical components (fuel cell and electrolyser) have a relatively low output voltage. Therefore, the feasible system must enclose PCUs to adapt the energy flow like DC/DC converters and DC/AC inverters, and also to prevent the expensive electrochemical devices from damage. It seems reasonable that problems concerning efficiency are mainly caused by technical components of this system. For example PV hydrogen plant in Jülich, has up to 30% of the energy lost in the PCUs [Solmecke-94], which can be attributed to operating the converters most of the time at very low power levels. Therefore, an accurate design of the components is very important. Most improvements in the circuit design of the PCU to increase the efficiency are in the use of modern power semiconductors with low conduction and driving losses, and in the use of recently developed designs of the integrated control circuits.

The cost reduction of storing energy in hybrid systems can be achieved by increasing the efficiency and decreasing the cost of the PCU. The power conditioning sensitivity in hybrid systems, which is studied in detail in [Vosen-99], has the greatest effect relative to other components in the system (Electrolyser, Fuel cell, Battery, and PV cell array). When an

increase in the PCU efficiency by 1% is achieved, the cost of electric power generated is reduced by 0.94%.

- ***Using PCU with PV generators***

In order to achieve the optimal system design from its energetic and economic points of view, it is necessary to select the proper PCU. The optimal size of the PCU as a function of the peak power of the PV generator (value of the PV output power at MPPT under STC) is determined by the minimum ratio between the rated power of the PCU to the peak power of the PV generator for optimum operation. This allows maximum energy production and consequently best global efficiency of the system to be achieved. According to different sites in Europe, the recommended sizing ranges that lead to a maximum power conditioning efficiency are: 0.65 to 0.8 (north); 0.75 to 0.9 (central); 0.85 to 1 (south). These values are discussed in detail in [Jantsch-92], [Caamano-95] and [Solmecke-97]. It is worth observing that the tilt angle has no significant influence on the optimal size of the PCU, at least for Mediterranean climate data [Louche-94].

- ***Using PCU with electrolyser or fuel cell components***

The electrolyser is supplied by a proper PCU from the bus-bar. The PCU steps the bus-voltage down to the low electrolyser voltage and serves as a positioning element for the energy management. The fuel cell is connected with a step up PCU to increase the fuel cell voltage up to the high bus voltage. A direct connection of the electrolyser to the PV generator is possible but it is not the best in general. Usually, there is no need to use both the fuel cell and the electrolyser at the same time. If both components are connected to a DC bus-bar and operate at the same output, it is possible to replace the two unidirectional units by one bi-directional DC/DC converter. This will save space and money. Also, for AC bus-bar it is possible to replace the two unidirectional units, step-down AC/DC rectifier with electrolyser and step-up DC/AC inverter with fuel cell, by one DC/AC bi-directional inverter. Therefore, the overall PVFC hybrid power system's efficiency depends on the PCU efficiency, size and cost. To improve the efficiency of these systems, low loss bi-directional units must be used. A simple bi-directional DC/DC converter is preferred for high efficiency, small size and low cost which perfectly matches the specific requirements of the electrochemical units, as developed and described in [Solmecke-97].

3.4.2 Different PCU Technologies used in Renewable Power Systems

P. Redi [Redi-01] developed a new grid connected DC/AC inverter (2kW/3kW rated power) of high efficiency for powers in the range between 2.5% and 100% of the rated power. This inverter is capable of working at high efficiencies even at low solar radiation values. Therefore, it opens the way to higher efficiency PV plants and thus to a reduction in costs of the energy produced. Increasing the overall conversion efficiency in one year of about 3% to 5% is a possible target particularly in Europe where the number of hours of low solar radiation is

considerable. This inverter is based on using two separate power units operating in parallel and automatically matched with the actual power generated by the PV generator. Recently developed electronic digital components are used in order to reduce the losses and reduce the production costs.

H. Solmecke [Solmecke-97] developed a new type of bi-directional DC/DC converter with high efficiency and small size at low cost which perfectly matches the PV supplied hydrogen storage systems. However, because of its modular construction and flexible control electronic, it can also be used in battery systems with low battery voltages as well. For use in hydrogen storage systems, special security mechanisms are provided to prevent the very expensive electrochemical devices from damage. This converter works only with an inductor instead of a transformer so that losses caused by transformers, usually used, are avoided. Practically, the converter used in the solar hydrogen plant in the KFA Jülich (Germany) was compared with a commercial step-up converter of the same power and voltage range. The efficiency improvement was between 10% and 15% more than the commercial one. Its size was only 50% of the size of the commercial converter and the number of its power electronics components was approximately 20% of number used in the commercial one.

K.H. Edelmoser [Edelmoser-97] designed a high efficiency DC/AC inverter suitable for stand-alone and grid connected systems. This inverter uses only off-line switches to generate the AC voltage. It has only one active switch in the main path. This can be obtained by applying a diode with controlled turn-off capability, thus two active switches in the main path are avoided. It leads to improved efficiency and is therefore well suited for solar and renewable energy as well as for aerospace applications. The comparison of this topology with the DC/AC inverter that uses two switches in the main path emphasizes the superiority of the new inverter. Also, the reduction of the number of active elements leads to higher reliability and lower costs.

J. Myrzik [Myrzik-97] presented two new transformers-less inverter topologies, which are suitable for modular solar cell applications. These topologies work in a power range of 200 to 600W and are derived from two bi-directional Zeta and Cuk converters. Each of the converters may be seen as an individual two port, which is connected in parallel-series connection. The Zeta inverter has a significant high efficiency of about 93%. The total harmonic distortion (THD) in the Zeta inverter is less than 4% for load variation range of 40 to 100%. It was compared with a common inverter of the same power range, which was available in the market, and the achievable weight and costs reductions were 50% and 30%, respectively. Also, the Cuk inverter has approximately the same behaviour as the Zeta inverter.

R. Lai [Lai-95] proposed a new PWM method for the reduction of switching losses in a full bridge inverter. This method is called the hybrid PWM method, or HPWM. Only two of the four switches in the full bridge inverter operate at high frequency, thus reducing the switching losses in the other two switches, which operate at low frequency. 50kW HPWM, UPWM, and

BPWM inverters have been simulated and their switching losses are compared. From the comparison, the HPWM got the lowest total losses among the three switching schemes.

3.5 Conclusion

This chapter reviews all components of the hydrogen PVFC hybrid system. From the characteristics of the main components of this system such as the PV generator, the fuel cell, and the electrolyser, a number of comments are worth to be mentioned:

1. To increase the available energy efficiency of the PVFC hybrid system, the PV energy must be generated with highest efficiency before converting and storing it in the form of hydrogen.

2. The compressed hydrogen storage process is the best alternative relative to other storage processes where energy densities are not critical. The usefulness of compressed hydrogen might rise if its container is made from some composite materials, which enable increasing pressured hydrogen gravimetric energy density and thus decreasing the storage costs. Liquefied hydrogen suits for large size applications where the additional cost of the liquefaction facility does not matter. Metal hydrides might be the best for small size applications because of its high energy storage ability [Noponen-00].

3. A short term storage energy device, represented in this dissertation by a supercapacitor, is important to provide the balance of active and reactive power needed during the momentary load variation period. It also improves the power quality and efficiency of the systems. Also, it is used to reduce the capital expenses by allowing the systems to be sized more closely to the steady state power requirements, rather than over-sizing the generator to meet transient loading requirements. Therefore, the photovoltaic hydrogen fuel cell hybrid system with supercapacitor can serve dynamic loads and also provide power conditioning for grid connected or stand alone system.

4. PCU are important for a PVFC hybrid system because: (a) they are used with a PV generator to track the MPP, which give the highest possible power output; (b) they are used with the expensive electrochemical units (fuel cell and electrolyser) to prevent theirs from damage and step-up the voltages of these units, especially for large scale systems; (c) they are used also with all components of the system to invert, to regulate and to wave-shape the output characteristics.

4. MODELLING OF THE INDIVIDUAL SYSTEM COMPONENTS

Modelling is the basis for computer simulation of a real system. It is usually based on a theoretical analysis of the various physical processes occurring in the system and of all factors influencing these processes. Mathematical models describing the system characteristics are formulated and translated into computer codes to be used in the simulation process. Apart from physical models, empirical data obtained from measurement of system components characteristic can also be used in simulation models.

The hydrogen PVFC hybrid system is composed of various components which interact with each other in different ways, but within the limits imposed by certain strategies used to control the system as a whole. The schematic layouts of different topologies for the hydrogen PVFC hybrid system are shown in Fig. 6.1 and Fig. 6.2, see chapter 6.

The modelling of the components of such a system involves the knowledge of various disciplines (meteorology, physics, power electronics, etc), and requires a good understanding of the interactions between them. In this chapter, simulation models for the hydrogen PVFC hybrid system are presented. Based on the theoretical analysis, which will be given in the next sections, and on some measurements made on the system components, physical models of the operational characteristics of these components are developed and later implemented in a computer simulation program to establish a model of the complete system. The following sections give a detailed description of the different component models which are used for simulation of the system. The models will be validated by comparing the simulation results with the measured characteristics data in chapter 5. All models described here focus on the study of long-term energy performance of the hydrogen PVFC hybrid system over one year duration time, i.e., they assume a steady state mode of operation. These models are PV cells, PEM fuel cell and alkaline water electrolyser, power conditioning units, supercapacitors, and gas storage tanks.

4.1 Photovoltaic Cell Model

A detailed approach to PV cell module or array modelling based on a mathematical description of the equivalent electrical circuit of a PV cell is given in [Ulleberg-98] and [Dumbs-99]. Three models are used to describe the equivalent electrical circuit of a PV cell module or array: the one-diode, the two-diode, and the empirical model. The most commonly used configuration is the one-diode model that represents the electrical behaviour of the *pn*-junction. The two-diode model allows for a more detailed description of the recombination process of charge carriers both on the surface and in the bulk material. The empirical model is a good fit for the measured I-U curve and has a less number of parameters than in the other two models. The parameters of this model (P_{max}, I_{sc}, U_{oc}, etc) are usually given in the manufacturer's data sheet, which allows modelling with an acceptable accuracy.

4.1.1 One-Diode Model

The photovoltaic cell is represented as an equivalent circuit containing a current generator (modelling the conversion of solar radiation to electric energy), a diode (accounting for the physical properties of the semiconductor cells) and two resistances, shunt and series resistances, see Appendix A. The four variables generating this model are the two input variables, solar radiation E_s [W/m²] and ambient temperature T_a [°C], as well as the two output terminal variables, PV cell current I_s [A] and voltage U_s [V], as shown in Fig. 4.1.

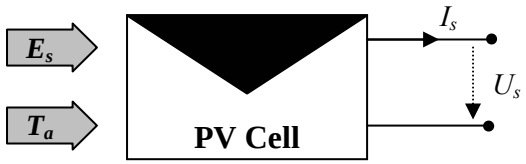

Fig. 4.1: Block diagram of the PV cell with input/output variables.

From Appendix A, the relations between input and output variables are:

$$I_s = P_1 E_s [1 + P_2 (E_s - E_0) + P_3 (T_j - T_0)] - P_4 T_j^3 \exp(-\frac{E_g}{kT_j}) \left[\exp(\frac{e_0}{a_f N_s k} \frac{U_s + R_s I_s}{T_j}) - 1 \right] - \frac{U_s + R_s I_s}{R_{sh}} \quad 4.1$$

$$T_j = (T_a + 273.15) + \frac{E_s}{800 W/m^2} (NOCT - 20) \quad 4.2$$

Where

P_1, P_2, P_3, and P_4	constant parameters, [Am²/W, m²/W, 1/K, and A/K³]
T_j	junction temperature, [K]
e_0	electron charge, [C]
a_f	ideality factor of the PV cell array, ≈1
N_s	number of cells in series
k	Boltzmann's constant, [J/K]
R_s, R_{sh}	series and shunt resistances respectively, [Ω]
E_g	gap energy voltage, [eV]
E_0	reference solar radiation, [W/m²]
T_0	reference junction temperature, [K]
$NOCT$	normal operating cell temperature ≈ 45-49°C

The set of parameters (P_1, P_2, P_3, P_4, R_s and R_{sh}) can be obtained from the modules manufacturer's data sheet. Table 4.1 gives these parameters for the *photo watt BPX 47-451A 45Wp Si* PV module [Dumbs-99].

Table 4.1: Parameters of the one-diode model of the *photo watt BPX 47-451A* PV module

Parameters	P_1	P_2	P_3	P_4	R_s	R_{sh}
Value	2.96	-8.6E-4	0.0037	1272.3	1.29	154.1

4.1.2 Two-Diode Model

The two-diode model, described in detail in Appendix A, is derived from the same equivalent circuit of the one-diode model, with the main difference that the recombination current I_d is replaced by two currents I_{d1} and I_{d2}. Recombination of minority carriers, both on the surface and in the bulk material, is the major determinant of the open-circuit voltage, occurring readily at trapping levels of the depletion zone. When modelling the recombination phenomena, the first diode is associated with neutral (base and emitter) regions, whereas the second diode simulates the space-charge recombination effect by incorporating a separate current component I_{d2} with its own exponential voltage dependence [Dumbs-99]. The advantage of this model is its accuracy, while the disadvantage is that it requires more parameters than the one-diode model. Thus, the model is only suitable when detailed PV cell and module experiments can be performed in advance [Ulleberg-98]. The relationship between the voltage U_s [V] of a PV cell and the current I_s [A] is given by the two-diode model as:

$$I_s = (P_1 + P_2 T_j) E_s - P_{01} T_j^3 \exp\left(-\frac{E_g}{kT_j}\right)\left(\exp\left(\frac{e_0}{\alpha \cdot a_f N_s k}\frac{U_s + R_s I_s}{T_j}\right) - 1\right)$$
$$- P_{02} T_j^{\frac{5}{2}} \exp\left(-\frac{E_g}{2kT_j}\right)\left(\exp\left(\frac{e_0}{\beta \cdot a_f N_s k}\frac{U_s + R_s I_s}{T_j}\right) - 1\right) - \frac{U_s + R_s I_s}{R_{sh}} \qquad 4.3$$

Where

P_1, P_2, P_{01}, and P_{02} constant parameters, [A.m²/W, A.m²/W.K, A/K³ and A/K$^{5/2}$]

α and β fit diode parameters, equal 1 and 2 respectively

The other parameters in Equation 4.3 are the same as for the one-diode model. The set of parameters (P_1, P_2, P_{01}, P_{02}, R_s and R_{sh}) can be obtained from the modules manufacturer's data sheet. Table 4.2 gives these parameters for the PV module SM50 [Duzat-00].

Table 4.2: Parameters of the two-diode model of the photovoltaic module SM50

Parameters	P_1	P_2	P_{01}	P_{02}	R_s	R_{sh}
Value	0.306	0.179E-4	1.708E-4	1.880	1.381E-4	0.13

4.1.3 Empirical Model

Many parameters are used within the one-diode and two-diode models. Some of them have known values and others are physical constants (see Appendix D). The "Normal Operating Cell Temperature" *NOCT* as well as the number of elementary series cells N_s is given in the PV cell module manufacturer's data sheet. Normally, *NOCT*=45°C, and N_s=36. The factor a_f is called the ideality factor of the diode in the PV cell model. If no other information is available, a_f=1 may be used as a default setting [Fry-98]. The remaining 6 parameters (see Tables 4.1 and 4.2) must be determined before using either one of these two models. These parameters are difficult to measure with high accuracy. Therefore, the empirical model is developed to give a sufficiently good fit for the measured I-U curve of a PV cell module and array. This model uses only three easily measurable parameters which are the open-circuit voltage U_{oc}, the short-circuit current I_{sc}, and the maximum power P_{max}. With an additional three parameters ($\partial U_{oc}/\partial T_j$; $\partial U_{oc}/\partial E_s$; $\partial I_{sc}/\partial T_j$), it is possible to describe any I-U curve taking into account the junction cell temperature T_j and the solar radiation E_s.

This method has been tested on various PV modules. The difference between the real curve and the proposed fit was found to be less than 3% for a fixed cell temperature and solar radiation and about 6% for various combinations of temperatures and solar radiations [Singer-84]. All equations and the equivalent circuit are given in Appendix A.

The values of I_{sc}, U_{oc}, and P_{max} can be calculated according to the actual conditions apart from the manufacturer's parameters under standard test conditions. In addition to this, the above parameters can be used to calculate R_s, see Appendix A. The relationship between the voltage U_s [V] of a PV cell and the current I_s [A] is given by this model as:

$$U_s = U_{oc}\left[1+\frac{1}{20.7}\ln\frac{I_{sc}-I_s}{I_{sc}}\right]-R_s I_s \qquad 4.4$$

4.2 Electrochemical Component Models

Theoretically, the processes occurring in the fuel cell and electrolyser are quite similar. Therefore, before going into modelling details of these individual components, it is useful to give a brief overview of the fundamentals of electrochemical reactors which are important for modelling these components.

A chemical reaction will take place as long as the reacting system is at non-equilibrium conditions. The general description of the equilibrium condition of a chemical reaction is:

$$\chi A + \gamma B \Leftrightarrow \zeta C + \varepsilon D \quad 4.5$$

Where; A, B, C, and D represent chemical species and χ, γ, ζ, and ε are their stoichiometry coefficients in the balanced equation. The Equilibrium Constant (EC) is given by [Kordesch-96]:

$$EC = \frac{a_C^{\zeta} \times a_D^{\varepsilon}}{a_A^{\chi} \times a_B^{\gamma}} \quad 4.6$$

Where; a_i is the activity of species i, which can be calculated from the concentration or pressure. For example, the activity of a species in terms of pressure is $a_i = p_i / p_0$, where p_i is the partial pressure of species i and p_0 is a reference pressure (usually 100kPa). The activities of gases are usually taken as their partial pressures and the activities of solutes such as ions are usually taken as their molar concentrations [WS-water-04].

The chemical energy from a spontaneous oxidation-reduction reaction is converted into electrical energy to produce an electromotive force (emf) in form of the theoretical (equilibrium) cell voltage U_{th} [V]. The relationship between the theoretical cell voltage U_{th} of an electrochemical component and the concentration is given by the Nernst equation [Hirschenhofer-99]:

$$U_{th} = U_0 - \frac{RT}{nF} \ln[EC] \quad 4.7$$

Where, U_0 [V] is the equilibrium cell voltage at the standard conditions (reference pressure p_0 = 100kPa, reference cell temperature T_0 = 298.15K), R is the universal gas constant (8.31451 J/K/mol), T [K] is the cell temperature, n is the charge number (i.e., the number of moles of electrons), and F is the Faraday's constant (96485.309C/mol).

4.2.1 PEM Fuel Cell Model

The fuel cell model here depends on the physical and theoretical analysis, so-called analytical model. The first step to model this unit is defined by its ideal performance. Once the ideal performance is determined, the losses can be calculated and then deducted from the ideal performance to give the actual operation. Also, to simplify the analysis of the model, water management analysis has to be excluded.

4.2.1.1 Reversible performance of PEM fuel cell model

The ideal performance of a fuel cell depends on the electrochemical reactions that occur with different fuels and oxygen [Barbir-97]. The theoretical PEM fuel cell voltage is analysed in details in Appendix B and is given by:

$$U_{th} = U_0 - (T - 298.15) \times \frac{\Delta S}{nF} + \frac{RT}{nF} \times \ln\left[\frac{p_{H_2} \times p_{O_2}^{1/2}}{p_0^{3/2}}\right] \quad 4.8$$

Where ΔS [J/K/mol] is the reaction entropy change and p_{H_2}, p_{O_2} [Pa] are the partial pressures of species H_2 and O_2 respectively. This equation is based on the following assumptions:

- Gases behave ideally with pressure variation.
- The temperature of the fuel cell is constant at all points in the fuel cell stack.
- $\Delta G \cong \Delta H_0 - T\Delta S_0$ (Equation B.4), i.e. the fuel cell variations are isothermal, and in addition the change in the molar enthalpy and the change in molar entropy at varying temperature are equal to their value at the standard temperature.
- p_{H_2O} = 100kPa for water.

4.2.1.2 Actual PEM fuel cell model

Useful amount of electrical energy could be obtained from a fuel cell only when a reasonable current is drawn from it. The actual cell voltage U_{actual} is lower than the theoretically voltage U_{th} due to various irreversible loss mechanisms. These losses, which are often called polarization or over-voltage losses, originate primarily from three sources: activation over-voltage U_{act}; concentration or diffusion over-voltage U_{conc}; resistive or ohmic over-voltage U_{ohm}. These losses are calculated and discussed in detail in Appendix B, thus, the actual cell voltage is:

$$U_{actual} = U_{th} - U_{anode} - U_{cathode} - U_{ohm} \quad 4.9$$

Figure 4.2 shows the simplified circuit diagram of the actual PEM fuel cell.

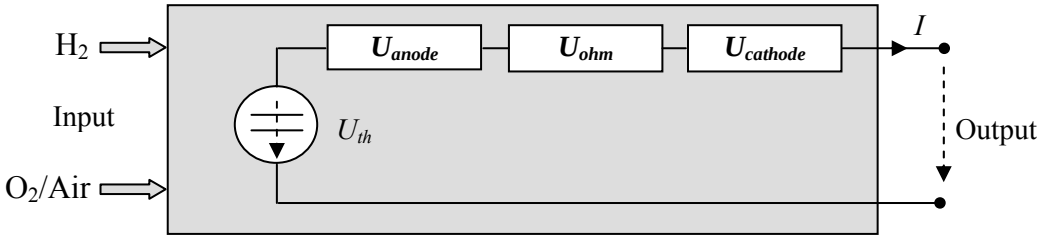

Fig. 4.2: Simplified circuit diagram of the actual PEM fuel cell.

The goal of fuel cell developers is to minimize the over-voltage, so that U_{actual} approaches U_{th}. This goal is approached by making modifications in the fuel cell design (improvement in electrode structures, better electro-catalysis, more conductive electrolyte, thinner cell components, etc.). For a given cell design, it is possible to improve the cell performance by modifying the operating conditions (e.g., higher gas pressure, higher temperature, lower gas

impurities content) [Hirschenhofer-99]. At open circuit, when no load is connected to the fuel cell and consequently no power is being generated, the voltage of the PEM fuel cells is usually different from the theoretical open circuit voltage, or electromotive force calculated on the basis of thermodynamics reactions due to the activation loss.

4.2.1.3 Efficiency of PEM fuel cell

The efficiency of a fuel cell is the ratio between the electrical power output and the fuel input (in power units), both of which must be in same units [W], i.e.

$$\eta_{fc} = \frac{P_{fc}}{F_{in}} \tag{4.10}$$

Where P_{fc} is the electrical power output of the fuel cell and F_{in} is its input fuel (in power units). The ideal efficiency of a fuel cell could also be given by:

$$\eta_{fc} = \frac{\Delta G}{\Delta H} \tag{4.11}$$

Where ΔG [J/mol] is the change in Gibbs energy which represents the electrical energy output of the fuel cell and ΔH [J/mol] is the reaction enthalpy change which represents the thermal input energy.

The most widely used efficiency value of fuel cells is based on the change in the standard free energy of the cell reaction. In H_2/O_2 PEM fuel cell, the chemical reaction produces water in the liquid form. At standard conditions of 25°C (298K) and 100kPa, the thermal input energy ΔH_0 in the H_2/O_2 reaction is –286kJ/mole, and the free energy available for useful work is -237.3kJ/mole. Thus, the maximum theoretical H_2/O_2 fuel cell efficiency is 0.83.

The efficiency of an actual fuel cell stack $\eta_{fc,Stack}$ can be expressed as the ratio of the operating cell voltage (U_{actual}) to the reversible cell voltage (U_{th}). The actual cell voltage is less than the reversible cell voltage because of the losses associated with cell over-voltages, as discussed in Appendix B. Therefore, the efficiency of the actual fuel cell stack can be written as:

$$\eta_{fc,Stack} = 0.83 \times \frac{U_{actual}}{U_{th}} \tag{4.12}$$

As mentioned in Appendix B, the reversible cell voltage of a pure H_2/O_2 reaction at reference conditions is 1.2297V. Thus, the efficiency of an actual fuel cell stack at reference conditions, based on the higher heating value of hydrogen, is given by:

$$\eta_{fc,Stack} = \frac{0.83 \times U_{actual}}{U_{th}} = \frac{0.83 \times U_{actual}}{1.2297} = 0.675 \times U_{actual} \tag{4.13}$$

A fuel cell can be operated at different current densities. The corresponding cell voltage then determines the fuel cell efficiency. Decreasing the current density increases the cell voltage,

thereby increasing the fuel cell efficiency. As the current density is decreased, the active cell area must be increased to obtain the required amount of power. Thus, designing the fuel cell for higher efficiency increases the capital cost, but decreases the operating cost, and a trade-off must be made.

The total efficiency of the fuel cell system $\eta_{fc,System}$ including the losses of the peripheral power components P_{periph} [W] such as air blower, control system, reformer, heat exchanger, compressor, etc is given by [Bocklisch-03]:

$$\eta_{fc,System} = \frac{P_{fc}}{F_{in} + P_{periph}} = \frac{\eta_{fc,stack}}{1 + \frac{P_{periph}}{1.482 \times N_s \times I}} \tag{4.14}$$

Where N_s is the number of cells in the stack and I [A] is the output current of the fuel cell. The value 1.482 is the theoretical thermal voltage of the cell at standard conditions in volts (see Appendix B).

4.2.1.4 Hydrogen fuel cell consumption

According to Faraday's law, the consumption of hydrogen supplied to a fuel cell is directly proportional to the rate of transfer of electrons at the electrodes, which is equivalent to the output current to the external circuit. Hence, the total hydrogen flow rate consumption to a fuel cell, which consists of several cells connected in series, can be expressed by [Busquet-03]:

$$\dot{m}_{H_2} = \frac{N_s \times I}{n \times F} \times \frac{1}{\eta_F} \tag{4.15}$$

Where $\dot{m}_{H_2}$ [mol/s] is the hydrogen flow rate, n=2 is the number of electrons per mole, and η_F is the Faraday's efficiency.

In an actual PEM fuel cell, hydrogen is usually supplied at flow rates slightly higher than the theoretical maximum value (stoichiometry). This amount of hydrogen reduces the current efficiency, or Faraday's efficiency of the fuel cell. The Faraday's efficiency η_F is defined as the ratio between the theoretical maximum value of hydrogen consumed in the fuel cell and the actual value. Therefore, Faraday's efficiency can be calculated from:

$$\eta_F = \frac{\dot{m}_{H_{2,th}}}{\dot{m}_{H_{2,actual}}} \tag{4.16}$$

Where $\dot{m}_{H_{2,th}}$, $\dot{m}_{H_{2,actual}}$ [mol/s] are the theoretical and actual hydrogen flow rate respectively.

An increase in temperature leads to a lower resistance, more current losses, and lower Faraday's efficiency [Ulleberg-98]. Thus, an empirical expression of the Faraday's efficiency η_F that accurately depicts these phenomena is the non-linear relationship:

$$\eta_F = \zeta_1 \exp\left(\frac{\zeta_2 + \zeta_3 T}{I/A_c} + \frac{\zeta_4 + \zeta_5 T}{(I/A_c)^2}\right) \quad 4.17$$

Where ζ_i Faraday's parameters (i=1…….5)

T temperature of the fuel cell, [°C]

I fuel cell current, [A]

A_c area of electrode, [m²]

The water production rate $\dot{m}_{H_2O}$ and oxygen consumption rate $\dot{m}_{O_2}$ are simply found from the stoichiometry of Equation 3.2.c, which on a molar basis is:

$$\dot{m}_{H_2O} = \dot{m}_{H_2} = 2\dot{m}_{O_2} \quad 4.18$$

4.2.2 Alkaline Water Electrolyser Model

An actual alkaline water electrolyser consists of several electrolyser cells connected in series. The electrolyser model considered here is based on the characteristics of individual cells. The calculations of the required operation voltage and the mass flow rates of hydrogen and oxygen are all done on a per cell basis, while the corresponding values for the whole electrolyser unit are simply found by multiplying by the number of series cells. This method is also used with PEM fuel cell model in section 4.2.1.

The equation that describes the behaviour of the electrolyser is:

$$U_{actual} = U_{th} + U_{anode} + U_{cathode} + U_{ohm} \quad 4.19$$

This equation is the same form as for fuel cell, while the over-voltages represent here the surplus of electrical voltages necessary to activate the electrode reactions and to overcome the concentration gradients. All the over-voltages depend on current density and are calculated by the same manner for the fuel cell. The detailed analysis of Equation 4.19 is given in Appendix C. Figure 4.3 shows the simplified circuit diagram of an alkaline water electrolyser cell according to Equation 4.19. The efficiency of an electrolyser can be calculated in the same manner as of the fuel cell.

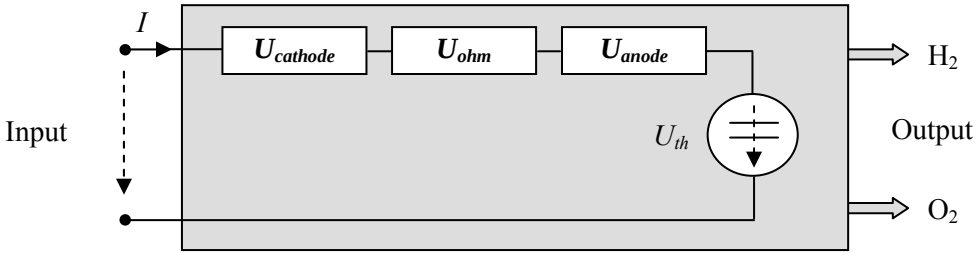

Fig. 4.3: Simplified circuit diagram of the actual alkaline water electrolyser cell.

The actual flow rates of hydrogen and oxygen production or water consumption in an electrolyser cell can be calculated by [Ulleberg-98] and [Busquet-03]:

$$\dot{m}_{H_2} = 2\dot{m}_{O_2} = \dot{m}_{H_2O} = \eta_F \frac{N_s \times I}{n \times F} \qquad 4.20$$

Where

$\dot{m}_{H_2}$	hydrogen production rate, [mol/s]
$\dot{m}_{O_2}$	oxygen production rate, [mol/s]
$\dot{m}_{H_2O}$	water consumption rate, [mol/s]
η_F	Faraday's efficiency, [-]
N_s	number of series cells, [-]
I	Input current to electrolyser, [A]
n	number of electrons per mole, $n = 2$
F	Faraday's constant, [C/mol]

4.3 Power Conditioning Unit Models

The PCU models in this work are described as energy conversion models, which are characterized by a certain efficiency curve. The function of a PCU model within the renewable energy system depends on the application requirements. Therefore, different modelling variables may be considered:

(a) For stand-alone power systems without energy storage, the output power P_{out} of the PCU is equal to the load demand and the PCU determines the power to be provided by the PV system. Consequently, the efficiency η of the PCU will be expressed in terms of P_{out}, e.g. $\eta = f(P_{out})$.

(b) For stand-alone power systems with energy storage or for grid-connected systems, the situation is more difficult. During normal operation the input power P_{in} will determine the power supplied through the PCU and the energy conversion function becomes $\eta = f(P_{in})$.

Therefore, in order to make the PCU model applicable to virtually any operation modes, a function of the form $P_{out} = f(P_{in})$ is established. Three different models which are used to describe the PCU as an energy conversion are linear, quadratic, and piecewise linear models.

4.3.1 Linear PCU Model

In this model, the output power P_{out} is described by three parameters: the input power P_{in}, the standby power consumption $P_{standby}$ corresponding to the operation at no loads (open circuit), and the efficiency of the model η_{rated} at rated power.

$$P_{out} = \eta_{rated} \times (P_{in} - P_{standby}) \qquad P_{in} \geq P_{standby} \qquad 4.21$$

Where $P_{standby} = 0.01 \times P_{rated}$

For $P_{in} < P_{standby}$, the model efficiency is assumed to be zero. When P_{in} approaches the rated power P_{rated}, the standby power consumption is negligible in comparison with the model input power and consequently the model operates at its rated efficiency η_{rated}. A slightly modified model is given by:

$$P_{out} = \eta_{out} \times (P_{in} - P_{standby}) \qquad P_{in} \geq P_{standby} \qquad 4.22$$

Where $\eta_{out} = \dfrac{\eta_{rated} \times P_{rated}}{P_{rated} - P_{s\tan dby}}$, and $P_{standby} = 0.01 \times P_{rated}$

This model is easy to implement, as it requires only two to three parameters, $P_{standby}$, η_{rated} and P_{rated}. These parameters are given in the manufacturer's data sheet. However, the model is inaccurate for a small range of the input power and gives an underestimation of the inverter's efficiency of about 5% to 10% for high values of P_{in} [Dumbs-99].

4.3.2 Quadratic PCU Model

- *Model 1 (Q1)*

This model is the most currently used, despite its limited accuracy at low input power levels. It requires only three parameters that can be extracted from experimental data by the least-squares method. The model results are quite satisfactory in the range of high input power. The parameters of the power curve are calculated from pairs (η, P_{in}) of the efficiency and the input power of the model. Only when the model is switched off, is the power consumption zero (P_{in} =0).

$$P_{out} = \begin{cases} P_{in} - P_{loss} & P_{s\tan dby} \leq P_{in} \leq P_{in,\max} \\ 0 & otherwise \end{cases} \qquad 4.23$$

Where $P_{loss} = K_0 + K_1 P_{out} + K_2 P^2_{out}$

K_0 load independent losses (self power consumption, equals $P_{standby}$), [W]
K_1 load linear proportional losses (voltage drops in semiconductors), [-]
K_2 load ohmic losses (magnetic and all other losses are included in this parameter), [1/W]

Magnetic and all other losses in transformers, capacitors, etc. are represented by these parameters too [Jantsch-92]. This model was for 35 commercial inverters [Caamano-95]. Table 4.3 shows the average and best values of the parameters of this model. Figure 4.4 shows the effect of changing these parameters on the efficiency curve. The effect of the reduction of voltage drops and ohmic losses are approximately the same over the low and medium range of the curve. As output power is closer to the rated value, the ohmic losses have more influence on the efficiency, due to voltage drops. Therefore, the reduction of these losses mainly increases the rated power efficiency of the model. The reduction of self-power consumption parameter improves the low and medium power efficiency, which is the most important for solar applications. For solar application, the solar radiation is zero for approximately 50% of the time. This factor is also very important for the reduction of the PCU standby power consumption.

From the above discussion it is clear that all parameters are important to improve the efficiency over all ranges of the power model as shown in Fig. 4.4.

Table 4.3: Average and best values of the parameters of the PCU first model

Parameters	K_0	K_1	K_2
Average Value	0.02 P_{rated}	0.025	0.08/P_{rated}
Best Value	0.0035 P_{rated}	0.005	0.01/P_{rated}

Two other quadratic models are also used to represent the PCU models and give the same accuracy of the above model. One model gives the conversion efficiency of the model while the other represents the power curve by a relation between the input and output power.

- *Model 2 (Q_2)*

The efficiency of the PCU can be calculated as [Macagnan-92]:

$$\eta = \frac{P}{P + n_0 + mP^2} \qquad 4.24$$

Where $P = P_{out} / P_{rated}$,

$n_0 = \frac{1}{99}\left(\frac{10}{\eta_{10}} - \frac{1}{\eta_{100}} - 9\right)$ load independent losses,

$m = \left(1/\eta_{100}\right) - n_0 - 1$ load dependent losses,

η_{10} efficiency of the PCU at 10% of the rated power (P_{rated}), and

η_{100} efficiency of the PCU at 100% of the rated power

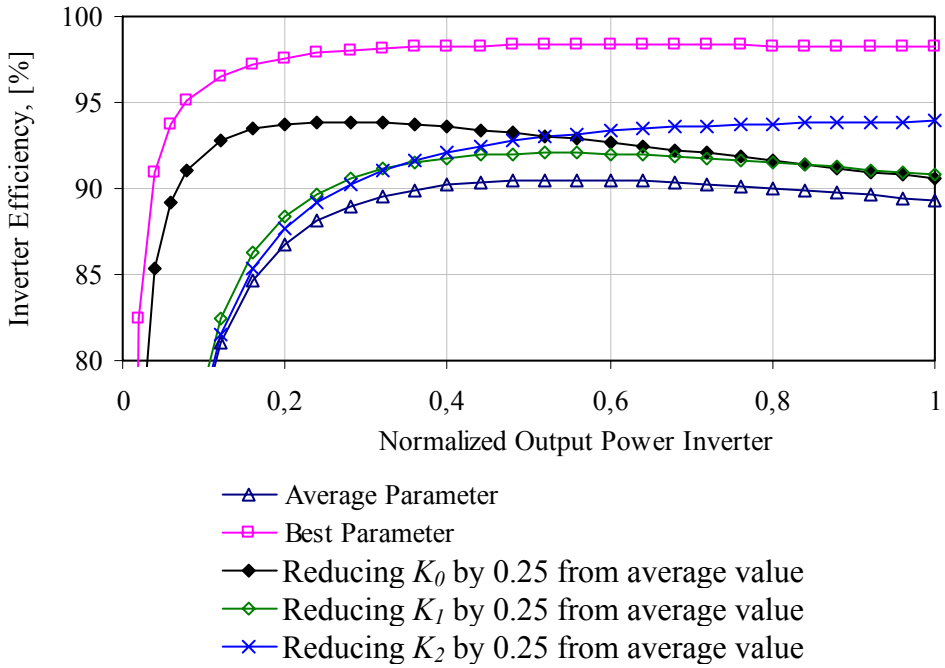

Fig. 4.4: Effects of parameters reduction on the inverter efficiency.

- *Model 3 (Q_3)*

The output power in this model can be represented as:

$$P_{out} = \begin{cases} C_0 + C_1 P_{in} + C_2 P_{in}^2 & P_{s\tan dby} \le P_{in} \le P_{in,\max} \\ 0 & otherwise \end{cases} \quad 4.25$$

The parameters of this model (C_0, C_1, and C_2) are extracted from experimental data using the last-squares method. In this model, the value of C_0 is always a negative and gives an indication of the average power consumption of the model at no load (P_{out}=0). The numerical value of this power consumption is typically in the range of 1% of the PCU rated power.

4.3.3 Piecewise linear PCU model

The piecewise linear PCU model is based on a linear interpolation between measured efficiency values for corresponding PCU input power values. The measured values are saved in "2D Lookup Table". This model can predict the efficiency of the PCU with equal accuracy over the full range of electrical input power. Rather than fitting a polynomial to a measured, non-linear relationship between the input power and the output efficiency of the PCU, this model divide the input power into values at equal intervals and measure the PCU efficiency corresponding each of these values. For a given PCU input power, the efficiency is calculated by linear interpolation between the measured efficiency values (η_{low} and η_{up}) at the lower and upper ends of the selected interval from measured input power ($P_{in,low}$ and $P_{in,up}$). The efficiency calculated η at any intermediate level P_{in} is then given by:

$$\eta = \eta_{low} + \frac{(P_{in} - P_{in,low}) \times (\eta_{up} - \eta_{low})}{(P_{in,up} - P_{in,low})} \qquad 4.26$$

An interval size of 5% of the rated power of the PCU has been reported to represent a satisfactory compromise between an adequate resolution of the model and a reasonable demand for measured efficiency values.

4.4 Supercapacitor Model

According to the ISET Alternative Power Library (ISET-APL) for Simplorer program, two characteristics are used to describe the supercapacitor model; its self-discharge current I_{dis} and internal equivalent series resistance (*ESR*). The self-discharge current depends on the temperature T_{SCap} [°C] and the voltage U_{SCap} [V] of the capacitor, while the *ESR* depends only on the temperature. Therefore, the model used in this work requires the following characteristics:

- Characteristic of the self-discharge current, $I_{dis} = f(U_{SCap}\ ,\ T_{SCap})$, [$A$].
- Characteristic of the internal resistance, $ESR = f(T_{SCap})$, [ohm].

Figure 4.5 shows the equivalent circuit of a supercapacitor, which consists of an equivalent series resistance ESR and a capacitance C. The equivalent series resistance accounts for the losses in the supercapacitor.

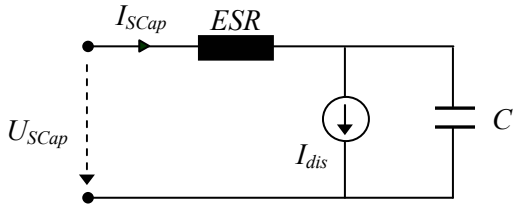

Fig. 4.5: Equivalent circuit for the supercapacitor module.

As shown in Fig. 4.5, U_{SCap} and I_{SCap} are the terminal voltage and the current flowing into the supercapacitor respectively. The voltage-current relationship of the supercapacitor is then expressed by:

$$U_{SCap} = ESR \times I_{SCap} + \frac{1}{C}\int_0^t (I_{SCap} - I_{dis})dt + U_{Scap}(0) \qquad 4.27$$

Where $U_{SCap}(0)$ is the initial voltage across the capacitance C.

To achieve higher voltage and current ratings, series and parallel connections of the supercapacitors are used to form a supercapacitor module. The voltage across the

supercapacitor module might swing above and below the common DC bus voltage considerably due to the excessive incoming and outgoing currents during the operation. This necessitates an intermediate bi-directional DC/DC power converter, which is capable of operating in both up and down modes.

4.5 Gas Storage Tank Model

The traditional way of storing hydrogen is as compressed gas in tanks. Since hydrogen behaves very much like an ideal gas in the ambient temperature. Therefore, the mathematical model for the hydrogen pressure p in a storage tank can be calculated from:

$$p = \frac{nRT}{V} \tag{4.28}$$

Where
- p hydrogen pressure inside the tank, [Pa]
- n number of moles, [mol]
- R universal gas constant (8.31451), [J/K/mol]
- T temperature of the gas, [K] and
- V volume of the tank, [m³]

4.6 Conclusion

The individual component models of the hydrogen PVFC hybrid system have been described in this chapter. These models are mainly based on electrical and electrochemical theories. The models of PV generator, PEM fuel cell, alkaline water electrolyser, and power conditioning units are described of detail, but that for the supercapacitor and the gas storage tank are presented as simple models.

Three PV generator models have been presented, whereas the empirical model is simpler than other one or two diode models. While for the one or two diode models six parameters must be determined, and these parameters are difficult to measure precisely to obtain an acceptable accuracy of the models, the empirical model uses five parameters which can be found in the manufacturer's data sheet of the PV module.

The models of electrochemical components (PEM fuel cell and alkaline water electrolyser) presented here are analytical models that depend on physical and theoretical analysis. Therefore, these models include a high number of parameters that have to be identified. Consequently, to simplify the analysis of these models, water management analysis has to be excluded.

Different power conditioning unit models have been presented. Whereas the quadratic model relating the input and output power is expected to give reasonable accurate results, it has the advantage of being easy to implement since only three parameters are generating the model.

5. IDENTIFICATION AND VALIDATION OF THE SYSTEM COMPONENTS MODELS

The identification and validation of the system components' models are necessary before using these models for an optimum design of the system. All the components models were programmed by using C++ language and interfaced with the simulation software program Simplorer. Once the source code for each component is created, it is built into a Dynamically Linked Library (DLL) that allows the components' models to be used at any time. All models of the system under study are produced within the ISET project under the name of "ISET Alternative Power Library (APL) for Simplorer". This library is available by "Ansoft Corporation" since 2003 [Caselitz-03]. This chapter describes the identification and validation of the major hydrogen PVFC hybrid system components' models that were developed in chapter 4 and are required for the system simulation in the next chapter. The evaluation of these models is based on the components measured data taken from the manufacturer's data sheet or from actual system operation.

5.1 PV Generator

This section evaluates the different PV generator models, which are studied in chapter 4, to select the best model to be used in this work. All PV generator models include a maximum power point tracker algorithm, while losses in the MPPT due to inefficiencies are considered in the PCU models, section 5.5. However, in an actual system, the MPPT is a device external to the PV generator. The models are tested against measured data over one day operation in Kassel/Germany every 15sec. interval by using 85W PV module.

5.1.1 The Comparison between PV Models Using Operational Data

At first, the parameters of the characteristic equations of the models are calculated by using the manufacturer's data sheet and the method of the "Effective Solar Cell Characteristic", which is described in detail in [Wagner-00] and [Bendel-03]. The "Effective Solar Cell Characteristic" method is used to calculate the parameters of the one and two-diodes models without a shunt resistance from the measured values of I_{sc}, U_{oc}, I_{mpp}, and U_{mpp}. The shunt resistance has to be determined from the available manufacturer's information. The primary effect of the shunt resistance on the I-U characteristic is to change the short-circuit slope. Thus, it is logical to use the measured value of this slope to estimate the value of R_{sh}. The short-circuit slope is not usually included in the manufacturer's specifications. However, it is possible to approximate this value if the I-U curve is available. In order to determine the mathematical relationship between the short-circuit slope and the shunt resistance, it is necessary to differentiate between the I-U expression for one or two diode models and determine the value of I_{sc} corresponding to U=0 at standard test conditions. By using the values for the other parameters which had been

previously determined using the "Effective Solar Cell Characteristic" method and estimating the value of the short-circuit slope from the I-U curve, the shunt resistance is determined. This method was discussed in detail in [Fry-98]. All the parameters of 85-Watt high efficiency Monocrystalline PV Module are given in Table 5.1.

Table 5.1: Optimised simulation parameters for the 85-Watt High-Efficiency Monocrystalline PV Module (see Appendix E.1)

One-diode model	P_1 [Am²/kW]	P_2 [m²/W]	P_3 [1/K]	P_4 [A/K³]	R_s [Ω]	R_{sh} [kΩ]
	5	-8.52×10^{-6}	51.65×10^{-6}	66.67	0.4	1.14
Two-diode model	P_1 [Am²/kW]	P_2 [Am²/WK]	P_{01} [A/K³]	P_{02} [A/K$^{5/2}$]	R_s [Ω]	R_{sh} [Ω]
	4.14	2.896×10^{-6}	66.67	-0.06×10^{-3}	0.4	1.14
Empirical model	P_{STC} [W]	$U_{oc,STC}$ [V]	$I_{sc,STC}$ [A]	u_{coef} [V/°C]	i_{coef} [A/°C]	-
	85	22.1	5	-77×10^{-3}	1.39×10^{-3}	-

The next step is to compare the performance of the models with operational data using short-term simulations. The results in Fig. 5.1 show that there is an excellent agreement between simulated and measured data. In the simulated models the inputs, solar radiation E_s and cell junction temperature T_j, were set equal to actual measured data. Figure 5.1 also shows that the errors in the simulated relative to the measured output power are very small. Table 5.2 shows the total simulated energy produced, RMS and percentage mean error for 15-hour time period in this day. The RMS and percentage mean error are calculated from the equations given in Appendix D. It can be concluded that the differences between the models are not significant. Therefore, each model can be used to depict the I-U curve of a PV generator module. The one-diode and two-diode models need a lot of time to calculate their parameters, but all parameters of the empirical model are found directly in manufacturer's data sheet.

5.1.2 The Thermal Behaviour of the PV Generator

The I-U characteristics of a PV module are influenced by the temperature of the module cells. The temperature of the module is modelled based on the cell junction temperature T_j which can be calculated from Equations A.3 or A.20 in Appendix A. Equation A.3 depends on the normal operating cell temperature (NOCT), which is given in the manufacturer's data sheet of the PV module. The NOCT is used to describe the thermal properties of the module under no-load conditions (i.e., at zero efficiency): its value corresponds to the cell junction temperature T_j which is found at a solar radiation of E_s = 800W/m², an ambient temperature of T_a = 20°C and an average wind speed of 1m/s. Figures 5.2(a) and 5.2(b) show the variation of the equivalent NOCT obtained by solving Equation A.3 for a given T_j, T_a and E_s. NOCT is plotted as a function of the solar radiation and the time of the day respectively. A constant value for NOCT can be found at times between 8am and 6pm where the solar radiation is ≥300W/m². The main disadvantages of this equation can be summarized as follows:

- Temporary shading does only marginally affect the temperatures T_j and T_a, whereas the explicit dependence of this equation on the solar radiation E_s leads to short-term overestimations of T_j.
- Since no wind speed data are taken into account, a general overestimation of T_j is obtained during days of strong wind.

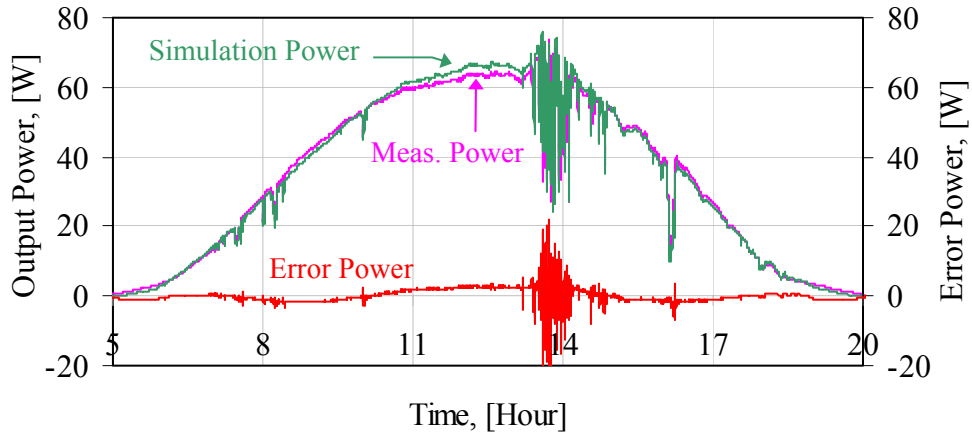

(a) One-diode model simulation and measured data.

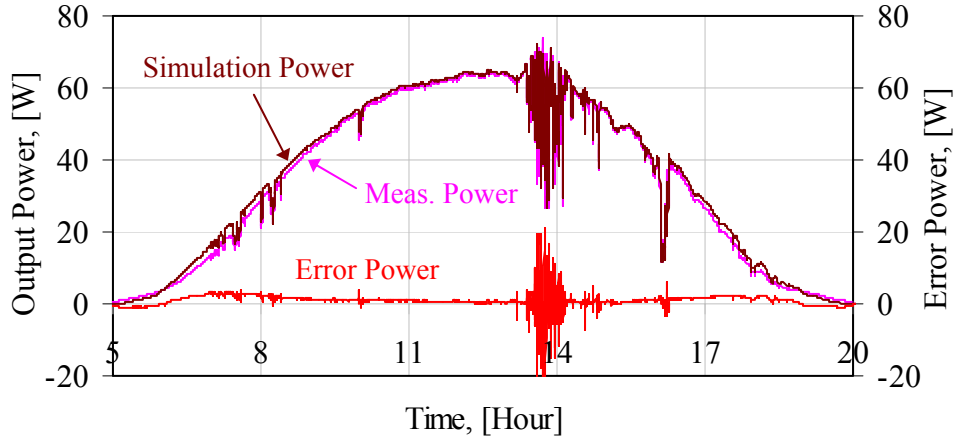

(b) Two-diode model simulation and measured data.

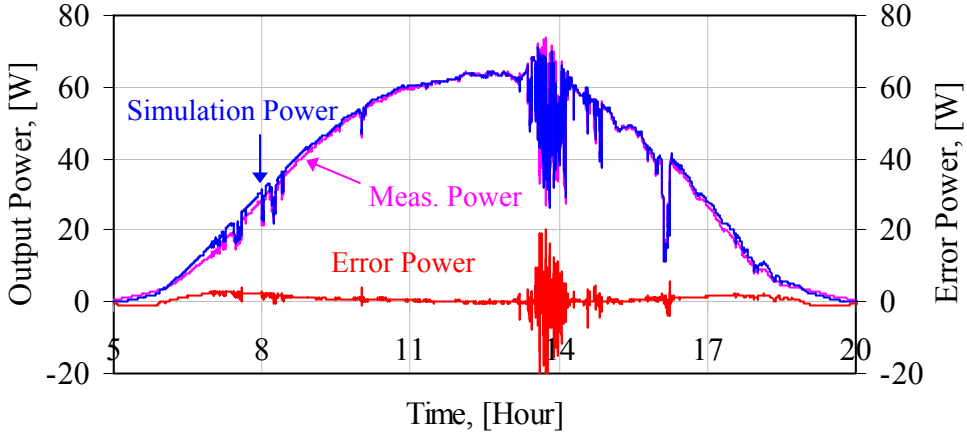

(c) Empirical model simulation and measured data.

Fig. 5.1: Simulated and measured power for 85W PV module, 01.08.2003 (Simulation inputs: Measured T_j, E_s and Δt = 15sec).

Table 5.2: Total simulated energy produced, RMS and percentage mean error (Total measured energy =0.51kWh/d)

Different Models	Simulated Energy, [kWh/d]	RMS Error, [W]	Mean Error, [%]
One-diode model	0.51	44.3	9.02
Two-diode model	0.53	42.5	11.12
Empirical model	0.52	40.0	10.47

The second relationship A.20 is used also to calculate the cell junction temperature using a simplified linear relation between the cell junction temperature and the solar radiation. The parameters of this equation can be determined by applying a regression analysis to the measured data at the site of the PV generator. For the PV generator installed in Kassel/Germany, the measured data (T_j, T_a, and E_s) were taken every 15sec for one day. The parameters calculated are A= -2.89°C and B=0.034°Cm²/W. Figure 5.3 shows the measured difference (T_j-T_a) and the calculated difference according to Equations A.3 and A.20 as function of the solar radiation E_s. It is clear from this figure, that Equation A.20 gives a better agreement with the measurement data than Equation A.3.

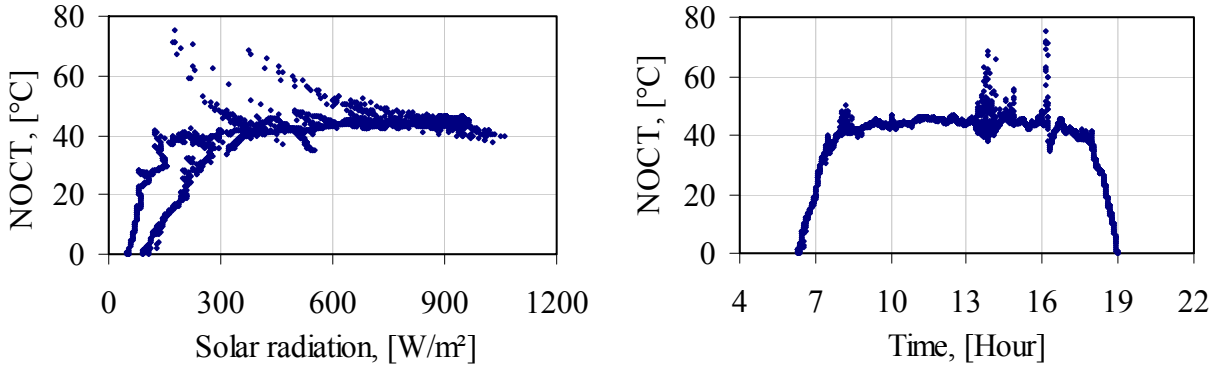

(a) NOCT versus solar radiation (b) NOCT versus time

Fig. 5.2: Evaluation of an equivalent NOCT based on measured data on 01.08.2003, in Kassel/Germany with BP 585 module.

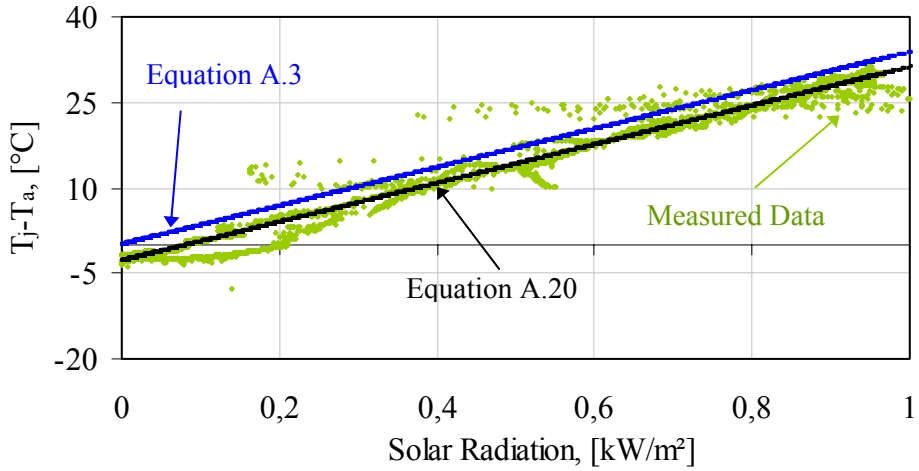

Fig. 5.3: Comparison between two Equations (A.3 and A.20) and the measurement difference (T_j-T_a) for the PB 585 module.

Figure 5.4 shows the output error power in PV generator when using the calculated cell junction temperature from ambient temperature using those equations instead of the cell junction temperature measured. Equation A.3 is simulated with a fixed value of NOCT=47°C, and the parameters of Equation A.20 are A= -2.89°C and B=0.034°Cm²/W. The overall PV generator energy when using the measured T_j during this day is 507.00Wh/d, as opposed to 507.07Wh/d or 502.20Wh/d when using T_a and Equation A.3 or Equation A.20, respectively. The corresponding error is approximately 0.96% for model Equation A.3 and 0.014% for model Equation A.20. Therefore, Equation A.20 represents the thermal behaviour of PV generator with a high accuracy.

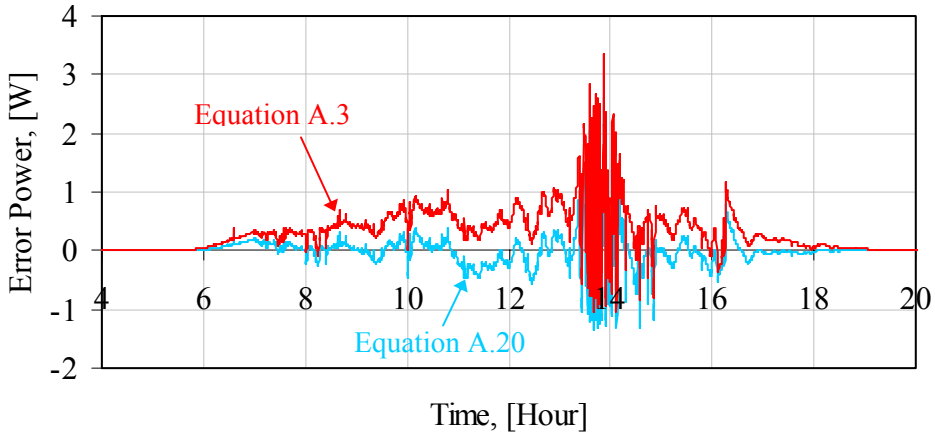

Fig. 5.4: Output error power from PB 585 module for one day.

5.2 PEM Fuel Cell

A 2.5kW two stacks PEM fuel cell was previously assembled at laboratory of the Institute of Solar Energy Technology (ISET) in Kassel. The testing and verification use one of these two identical stacks. Therefore, the maximum fuel cell output power is only 1.25kW. The fuel cell system here is not equipped with a fuel reformer and designed to operate directly from hydrogen tanks and air. In Appendix E.2, the technical data of the PEM fuel cell system are given and a photograph of the PEMFC complete system with all its components (PEMFC system, monitor system, electrical load, and network coupling inverter) used in the operation is shown [ZSW-02].

5.2.1 I-U Characteristics

The relationship that describes the current-voltage I-U characteristics of a PEMFC is given by Equation 4.8 in chapter 4. In the PEMFC at ISET, each of the two stacks has an electrode area of 126cm² and 50 cells connected in series, giving a maximum voltage of about 48V. The voltage at an operating temperature 52°C and a stack rated power of P_{rated}=1kW is about U_{rated} =30V. The operating pressures of air and hydrogen are fixed at p_{air}=100kPa and p_{H_2}=140kPa, respectively. The hydrogen consumption of each stack at rated power is approximately

0.8Nm³/h. A comparison between measured and simulated data is given in Fig. 5.5. The current and voltage values in Fig. 5.5 (176 points) are derived from one day operational data in ISET laboratory. The results show that there is an excellent agreement between the measured and simulated values; the RMS voltage error is about 14mV/cell and the percentage absolute error in the simulated relative to measured total energy yield is less than 2%. A plot of the stack's energy efficiency (Equation 4.13) and system energy efficiency (Equation 4.14) for a peripheral power of 70W against normalised rated power is provided in Fig. 5.6. The values of the stack and system efficiencies at the rated power are 40.7 and 39.5% respectively.

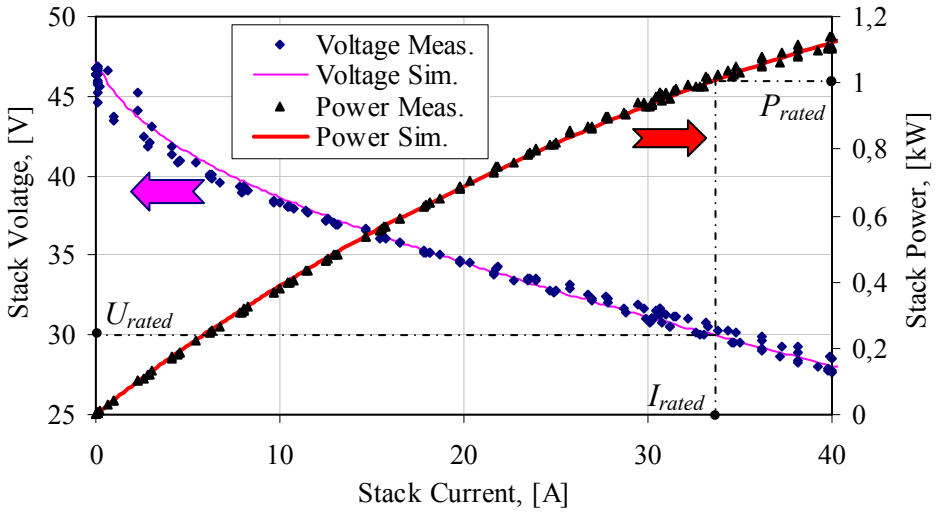

Fig. 5.5: Simulated and measured values for I-U-P characteristics of a PEMFC stack.

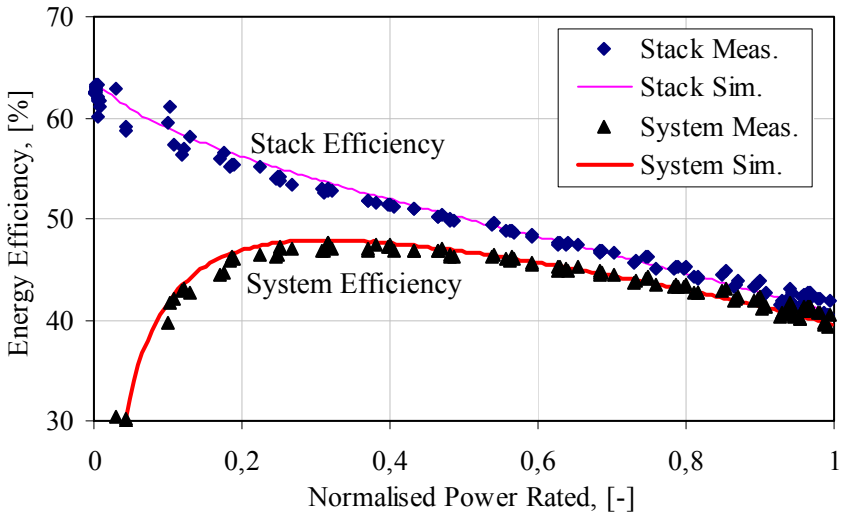

Fig. 5.6: Stack and system energy efficiencies of the PEMFC with 70W peripheral power.

Two aspects are worth to note about the characteristic curves. The first aspect is that the open circuit voltage per cell (0.97V) is not equal to the reversible voltage (1.23V). Therefore, the internal current (9.8mA/cm²) has to be considered to enhance the model accurate for open circuit and low currents. If modelling of the internal current would complicate the model then the internal current would have to be omitted from the model, and the model would be valid for currents above about 0.5A. The second aspect is that the concentration loss is not considered

into the model for these operating conditions and currents. The maximum current specified for the load is about 34A. With an electrode area of 126cm², the current density is 270mA/cm². Therefore, the model of the fuel cell in this work needs not to contain a concentration loss term. The model is thus accurate and as simple as possible, which is required.

The PEM fuel cell model presented here is based on the following assumptions:

- The PEM fuel cell operates under steady state conditions.
- The PEMFC stack is cooled by water therefore the operating temperature is assumed to be kept at a fixed level (~52°C in this work).
- All gases are assumed to be ideal and fully saturated with water vapour, so that the fugacity coefficients of hydrogen and oxygen (γ_{H_2} ,γ_{O_2}) are constant and equal to unity.
- The concentration of hydrogen protons (C_{H^+}) at the anode is assumed constant, and equals unity, throughout the reaction layer, and the concentration of pure water (C_{H_2O}) at the cathode equals also to unity.

5.2.2 Hydrogen Consumption

Measurements of the actual hydrogen consumption at various current densities for the ISET PEM fuel cell were only available for operating temperatures between 45 and 55°C. The parameters of Faraday's efficiency for the fuel cell are derived from these experimental data. Figure 5.7 shows the experimental results and the corresponding curve fit at an average temperature between 45°C and 55°C. The numerical values of the parameters of Equation 4.19 are given in Table 5.3, which gives also other operational parameters and electrode properties for the PEM fuel cell model.

A comparison between simulated and measured values of Faraday's efficiency is given in Fig. 5.7. It is clear that the coincidence between the simulated and measured values is good. Calculations of the RMS error in hydrogen consumption for 152 samples showed that RMS error=0.12Nm³/h. The total consumption of hydrogen for the whole samples was about 81.5Nm³/h. The percentage absolute error in the simulated relative to the measured hydrogen consumption in the PEM fuel cell does not exceed 1.8%. From Fig. 5.7 it is shown that the Faraday's efficiency based on the measured values for hydrogen flow and electrical current density is above 0.85 for the given operation conditions (T= 45-55°C and current density above 50mA/cm²). This efficiency achieved 0.935 at rated power operation.

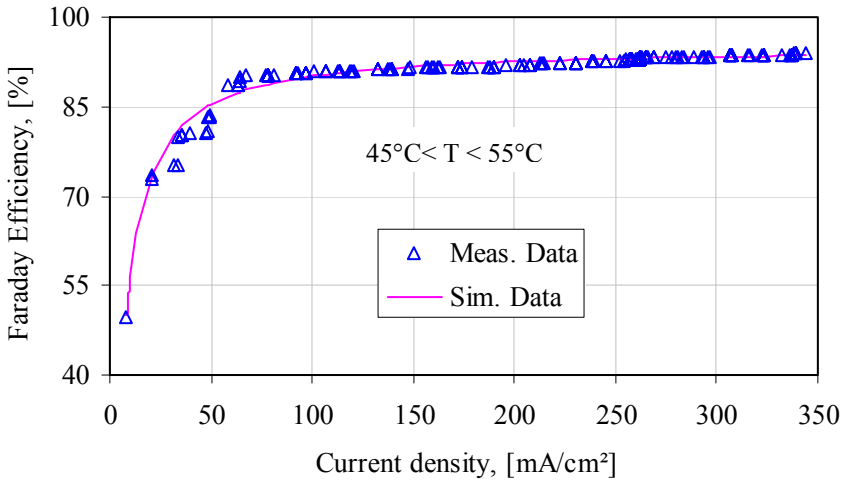

Fig. 5.7: Simulation versus measured Faraday's efficiency for PEM fuel cell in ISET.

Table 5.3: Operational parameters and electrode properties of the PEM fuel cell model

Parameters	Symbol	Value	Unit
1. Number of cells	N_s	50	-
2. Fuel cell temperature	T	52	°C
3. Cross section area of the electrolyte body	A_c	126	cm²
4. Distance between electrodes (Electrode Gap)	d_e	0.32×10^{-3}	cm
5. Internal current density	j_n	9.8×10^{-3}	A/cm²
6. Anodic transfer coefficient	α_a	0.5	-
7. Cathodic transfer coefficient	α_c	0.25	-
8. Anodic standard exchange current density	$j_{0,a}^{ref}$	0.5×10^{-3}	A/cm²
9. Cathodic standard exchange current density	$j_{0,c}^{ref}$	0.4×10^{-6}	A/cm²
10. Surface factor of the electrode for air operation	f_{air}	84	-
11. Standard free energy activation for anode or cathode	ΔF_e	50×10^{3}	J/mol
12. Peripheral power losses	P_{periph}	70	W
13. Faraday's efficiency parameters	ζ_1	95	%
	ζ_2	-9.58	m²/A
	ζ_3	-0.056	m²/A.°C
	ζ_4	302.71	m^4/A
	ζ_5	-70.80	m^4/A².°C

5.3 Alkaline Water Electrolyser

The alkaline water electrolyser analysed in this section consists of 30 series cells each of cross section area 150cm² and it can operate under a pressure of 3000kPa. At this pressure no parasitic load is needed to compress the hydrogen gas after its production in the electrolyser. The nominal operating point is 60A and 60V at temperature 80°C. It had a maximum power of 3.6kW and yielded about 0.8Nm³/h hydrogen gas at a pressure 3000kPa and a purity of 99.8% [Busquet-03]. The cells are circular, bipolar and have zero gap geometry. The electrolyte is a 30wt. % KOH solution. This electrolyser is installed at Agrate in Italy [WS-pvfcsys-04], see Appendix E.3. During one-day experimentation, on 30.03.2004, data was sampled every one minute to form the basis for the comparisons between simulated and measured data.

The current-voltage characteristics, or I-U curve, for an electrolyser is described by Equation 4.19. All voltages in this equation are function of temperature and pressure. A comparison between simulated and measured values for current and voltage over the day are presented in Fig. 5.8. The solid line represents a simulation fit at a temperature of 20°C, which is the average operating temperature of the electrolyser. An exponential rise due to the cathodic and anodic over-voltages is noticed below 30A, followed by a linear rise due to the ohmic over-voltage, yielding decreasing electrolyser efficiency with increasing current. The difference between measured and the simulated electrolyser output voltage using the parameters of Table 5.4 is shown in the right-hand graph of Fig. 5.8. Figure 5.8 demonstrates that the simulation ability of the proposed I-U model in Equation 4.19 is excellent; the maximum voltage difference is about ±1.5V and the percentage mean error is 0.94%.

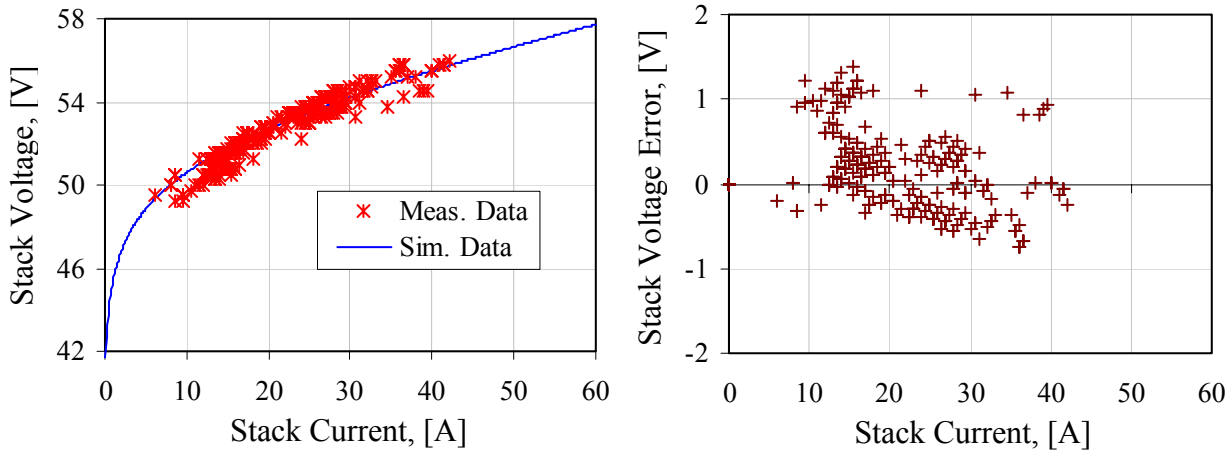

Fig. 5.8: Simulated versus measured values for I-U curve of a 3.6kW alkaline electrolyser on 30.03.2004 (Agrate, Italy), data measured at different temperatures between 10-40°C (crosses) and simulated at an average operating temperature of 20°C (solid line).

Measurements of the actual hydrogen produced at various current densities for the existing electrolyser are not available. However, detailed experiments of the Faraday's efficiency were performed on a similar two electrolysers installed at the PHOEBUS (Jülich/Germany) and HYSOLAR (Stuttgart/Germany) [Ulleberg-98]. Therefore, the parameters of the Faraday's efficiency for the existing electrolyser, see Table 5.4, could be derived from the experimental data of those electrolysers.

To test the accuracy of the electrolyser model with respect to the overall electrical power and energy demand of the electrolyser, a comparison between simulated and measured data for one day is performed. In this comparison, the input temperature of the electrolyser is assumed to be constant and equal to the mean value during the day. For this day, 30.03.2004, the simulated and measured energy are 5.29kWh and 5.28kWh, respectively. The percentage error in the total simulated relative to measured energy demand is thus less than 0.2%. Therefore, the approximate assumption of the input temperature is relatively little significance especially from an energy point of view. Figure 5.9 shows the simulated and measured voltage and power of the

electrolyser. Figure 5.10 shows the measured electrolyser stack temperature and hydrogen production versus time during one day operation. Note that, the hydrogen production is directly proportional to the power input to the electrolyser, see Fig. 5.9. The electrolyser temperature increases continuously at the start of the day during the operation of electrolyser then stabilizes, and decreases after a complete switching-off of the electrolyser.

Table 5.4: Operational parameters for an alkaline 3.6kW electrolyser

Parameters	Symbol	Value	Unit
1. Number of cells	N_s	30	-
2. Cross section area of the electrolyte body	A_c	150	cm²
3. Distance between electrodes (Electrode Gap)	d_e	Zero-Gap	cm
4. Surface factor of electrodes	f_{air}	44.5	-
5. Cathodic standard exchange current density	$j_{0,c}^{ref}$	0.12×10^{-3}	A/cm²
6. anodic standard exchange current density	$j_{0,a}^{ref}$	0.12×10^{-6}	A/cm²
7. Cathodic transfer factor	α_c	0.5	-
8. Anodic transfer factor	α_a	0.3	-
9. Standard free energy of activation for the anode	$\Delta F_{e,a}$	30000	J/mol
10. Standard free energy of activation for the cathode	$\Delta F_{e,c}$	68000	J/mol
11. Faraday's efficiency parameters	ζ_1	0.8756	%
	ζ_2	-9.5788	m²/A
	ζ_3	-0.0555	m²/A.°C
	ζ_4	1502.71	m^4/A
	ζ_5	-70.8	m^4/A².°C

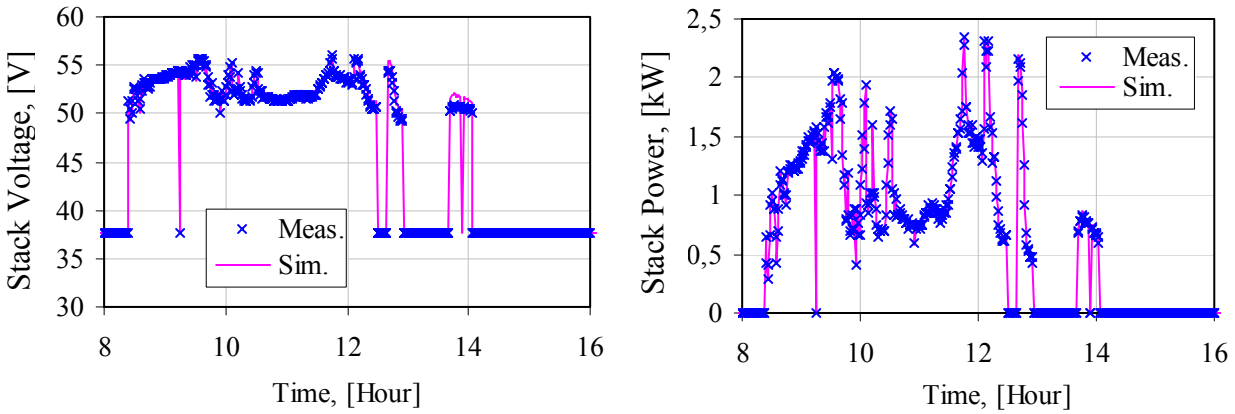

Fig. 5.9: Simulated and measured voltage and power for the electrolyser versus time during one day, on 30.03.2004.

Figure 5.11 shows the Faraday's and electrolyser efficiencies during one day. The variations in these efficiencies can be accounted for the conditions under which the system operates. When the input power to electrolyser is low, it runs at low current densities and the parasitic currents are high. As a result, the Faraday's efficiency takes the lowest values at low current densities. Conversely, higher current densities increase the voltage necessary for electrolysis, and have a negative effect on the electrolyser efficiency. For example, at 11:46, when Faraday's efficiency is at its maximum 0.99, the electrolyser efficiency is 0.68, the current density is 274mA/cm²,

and the electrolyser is operating at 1.84V/cell. At 8:45, Faraday's efficiency declines to 0.97 while electrolyser efficiency reaches its maximum 0.76. At this time the current density is only 53mA/cm² and the electrolyser voltage has dropped to 1.69V/cell.

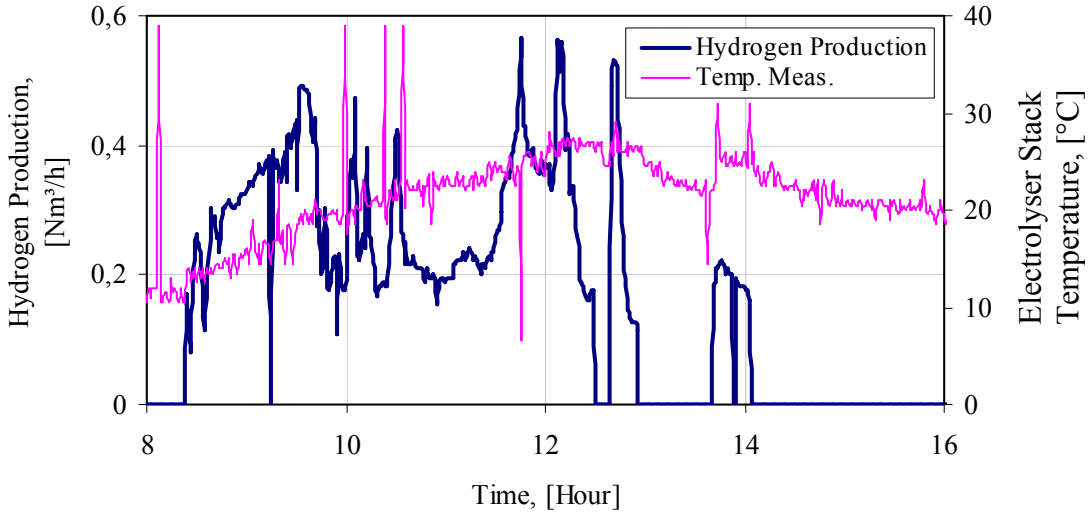

Fig. 5.10: Hydrogen production and electrolyser temperature versus time during one day, on 30.03.2004.

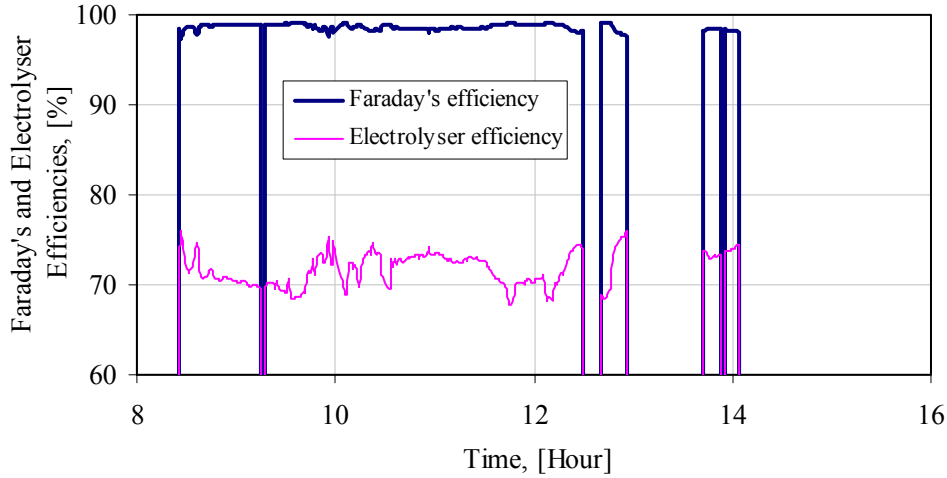

Fig. 5.11: Faraday's and electrolyser efficiencies versus time during one day, on 30.03.2004.

5.4 Supercapacitor

The hydrogen PVFC hybrid system necessarily uses a short-term energy storage source because it may need from time to time few seconds of stored energy to fulfil transient operating requirements, such as responding to momentary voltage changes. The choice between different supercapacitor technologies depends on the performance application. If a fast dynamic response is needed, symmetrical supercapacitors may be the best solution. However, if the application requires more energy, such as motor-starting current for several seconds in excess of the fuel cell's rating, asymmetrical supercapacitors are the preferred choice [Key-03].

The important performance characteristics of the supercapacitor considered for evaluation in this work are capacitance variation with load and temperature, equivalent series resistance (ESR),

and self-discharge rate. Two ESMA 20EC104S supercapacitor modules were selected for evaluation to be used in the system under study. Their technical characteristics and data are mentioned in Appendix E.4.

- ***Capacitance variation with load and temperature***

The capacitance variation with load is an important factor when selecting the proper size of the capacitor to ensure stable operation over its runtime. In many applications, the load is assumed a constant power load to improve the power quality, although the power can vary according to the load variation. For example, a UPS uses an inverter to convert the energy within the batteries to a constant output voltage. Similarly, if a supercapacitor is used to replace a battery, the inverter will regulate the discharge voltage of the capacitor to give a constant power to the load. However, the load may be variable because the user may or may not have loads. For this reason, the capacitance of the supercapacitor has been measured at various loads. The discharge profile of the supercapacitor module, under various discharge currents, is represented in Fig. 5.12. The test was conducted at 25°C. The module has been discharged under constant current, of values in range of 100A to 500A. The graph shows that the supercapacitor module under test demonstrates extremely stable capacitance over a wide range of discharge currents. Therefore, the supercapacitor module has adequate energy and capacitance stability.

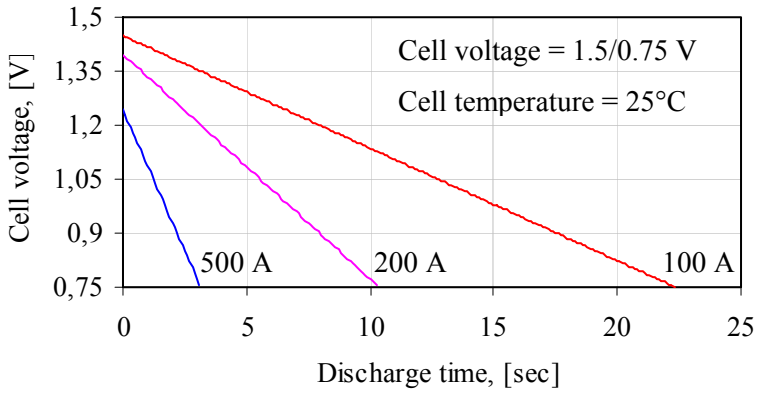

Fig. 5.12: Discharge characteristic of the EC104 supercapacitor cell.

The variation of capacitance with temperature determines the useful capacitance of the supercapacitor as temperature is changed. This is important when considering capacitors for use in uncontrolled environments. Many regions inside a manufacturing facility can reach temperatures above 40°C, and some applications in cold weathers may require operation below the freezing point. Understanding how temperature affects the capacitance of the supercapacitor is important for proper sizing and applications. Figure 5.13 shows a relationship between the percentage rated energy and the temperature for an ESMA supercapacitor. The percentage energy change is approximately 1%/°C. However, it is possible to compensate for the loss of energy at low temperatures by increasing the charging voltage. This is common, since many battery chargers offer temperature compensation.

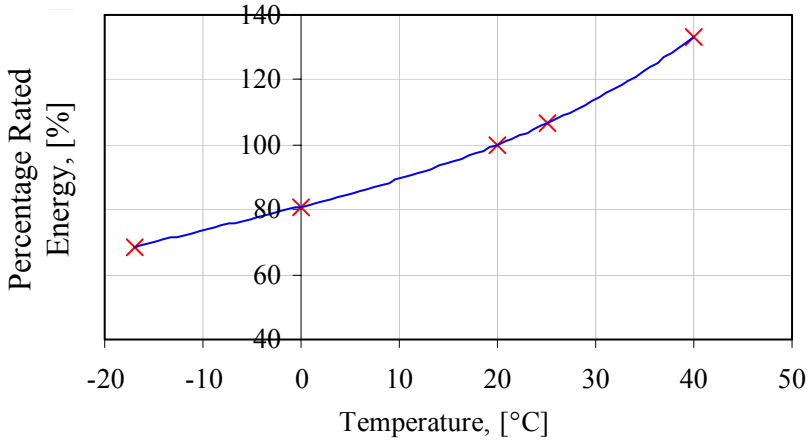

Fig. 5.13: Percentage rated energy versus temperature for ESMA EC203 supercapacitor [Key-03].

- ***Equivalent series resistance (ESR)***

Knowing the ESR is important because it determines how fast the supercapacitor charges and discharges. Also, the short-circuit current of the capacitor is limited by the ESR. A lower value of ESR is preferred because during charge and discharge, the ESR produces losses and heat. The ESR is calculated by dividing the change in voltage by the change in current (ESR=$\Delta U/\Delta I$). To simplify the measurement, an oscilloscope is used to measure the changes in capacitor voltage and current. Figure 5.14 shows that the ESR is weakly dependant on temperature [Klementov-01] and [Varakin-99].

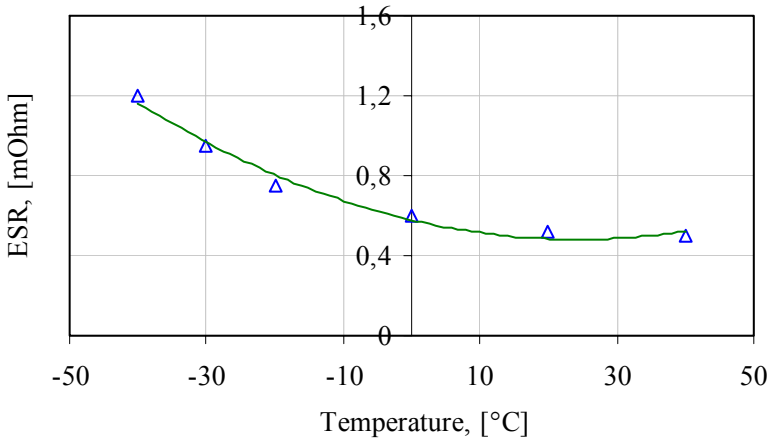

Fig. 5.14: ESR of ESMA EC104 supercapacitor versus temperature.

- ***Self-discharge rate***

The self-discharge rate describes the rate at which energy is lost within the supercapacitor as a result of parasitic losses. It is very low in ESMA capacitors. Figure 5.15 shows that the leakage discharge current increases as the temperature or the voltage of the supercapacitor increases.

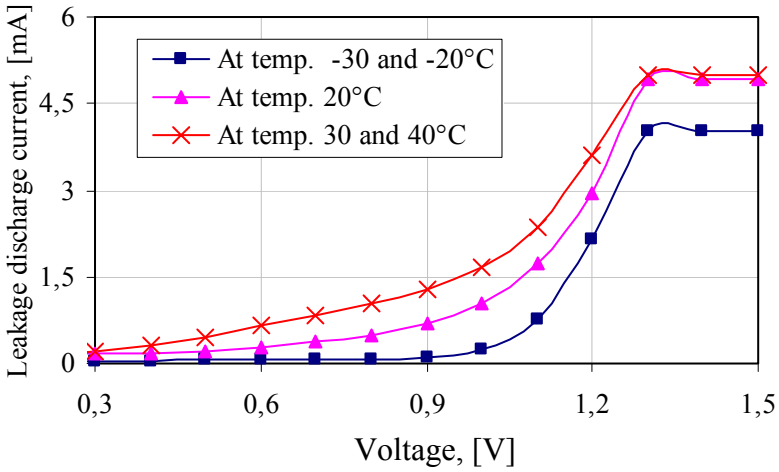

Fig. 5.15: Leakage discharge current versus temperature and voltage for ESMA EC 104 supercapacitor.

5.5 Power Conditioning Units

The purpose of this section is to select the best model, from the models represented in chapter 4, to be used in this work. All parameters required to estimate the efficiency curves are calculated from measured pairs of the input and output power of the PCU. The measured data used in this particular analysis is based on operational data from SMA Regelsysteme GmbH of the PCU Sunny Boy inverter 2.5kW. The Sunny Boy inverter is transformer-less one. Therefore, it is of high efficiency and thus ideal for large PV systems. In medium and low power ranges, the values of the efficiency are also higher than in many other inverters, since there are no losses due to the magnetization of the transformer. Simulation of this inverter with all models shows that the quadratic models and the piecewise linear model are identical and claim to agree with measured data. The worst model among these models for all output power ranges is the linear model, but it is the simplest model for its least number of parameters and simple simulation. The piecewise linear model approaches closer to the measured data for all ranges as the interval size of measuring power is decreases, i.e., as the number of measured pair of the input and output power increases. A disadvantage of the piecewise linear model is that it is very sophisticated for programming. Therefore, the quadratic model is the best model among all the models to represent all PCUs in the system study because its parameters have physical meaning of the PCU and very simple for programming. Figure 5.16 shows the efficiency curve of the measured data and simulated for one of the quadratic models (the three quadratic models are extremely coincident) of the Sunny Boy 2.5kW String inverter. The optimum values of the parameters of the quadratic models for the Sunny Boy 2.5kW inverter are given in Table 5.5., and these will be used in the system simulations in the next chapter.

The characteristic efficiency curves for all these units are obtained by curve fitting using quadratic model Q_3 and compared with measured data. Figure 5.17 shows the efficiency curves of the measured data and simulated for a DC/DC bi-directional Cuk converter and two different

DC/AC bi-directional inverters, which will be used for DC or AC coupled system with the electrochemical components. From this figure, the Sunny Island inverter is better than the SW Trace type for operation near the rated power, but the SW Trace inverter is better at low power operation. Cuk converter has the highest efficiency relative to other inverters but it used only for DC coupled. The parameters for those units which will be used in the systems simulation in the next chapter are given in Table 5.6.

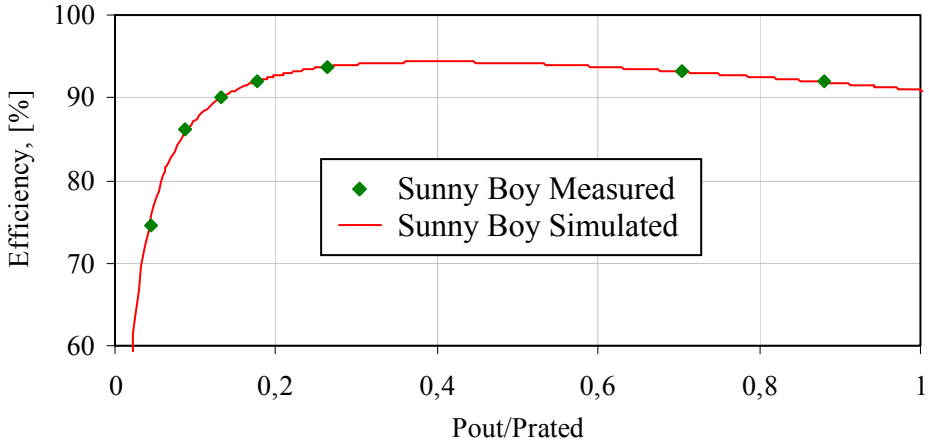

Fig. 5.16: Measured and simulated efficiency of Sunny Boy 2.5kW inverter.

Table 5.5: Optimum simulation parameters for the Sunny Boy 2500E inverter

Model 1		Model 2		Model 3	
K_0	33	η_{10}, η_{100} %	87.65, 91.37	C_0	-37.67
K_1	0.0008682	n_o	0.0132784	C_1	1.0143
K_2	0.00003213663	m	0.08117273	C_2	-0.0000333

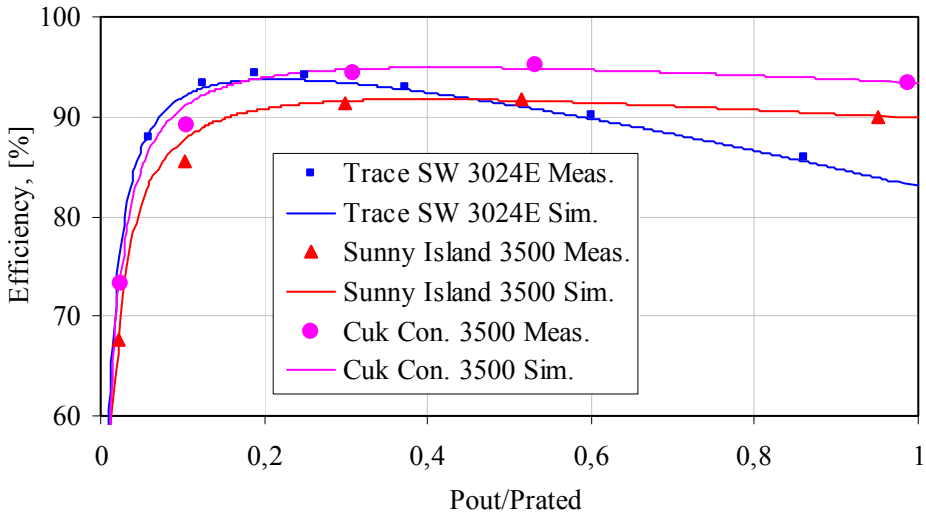

Fig. 5.17: Measured and simulated efficiencies of different PCU units by using Q_3 model.

5.6 Conclusion

- ***PV generator:*** The differences between PV generator models are found to be of no great significance and each model is good enough for the simulation purposes. The empirical model

is simpler than the one or two diode models because all its parameters could be obtained from the manufacturer's data sheet. Thus, the empirical model is recommended to represent PV generator for simulation. The thermal behaviour of PV generator models is evaluated by two methods, which are used to calculate the cell junction temperature from the ambient temperature. The simplified linear function model is found to be more accurate than the other model which uses the NOCT given by the manufacturer's data sheet. Therefore, the linear model is recommended for all simulations.

Table 5.6: Optimum simulation parameters for the Sunny Island 3.5kW; SW Trace 3kW; and 3.5kW Cuk converter

Types	Parameters		
	C_0	C_1	C_2
Sunny Island Inverter	-30.76	0.958	-0.00001338
Trace Inverter	-21.47	1.004	-0.0000456
Cuk Converter	-27.86	0.985	-0.00001173

- ***PEM Fuel Cell:*** The relationship describing the I-U characteristics of the PEM fuel cell at constant temperatures is evaluated. The evaluation concentrates only on the rated operation range for the fuel cell, because the PEM fuel cell should never operate at high current densities. Thus, the drop-off at high current densities shown in the fuel cell I-U curve has no influence on the overall accuracy of the long-term system simulations as will discussed in the next chapter.

- ***Alkaline Water Electrolyser:*** The relationship describing the I-U characteristics of the alkaline water electrolyser (Equation 4.19) is evaluated. This model is a good theoretical model that calculates precisely the major part of the electrolyser. With a set of experimental data, this relation can be easily fitted, for any kind of electrolyser. This relation is fitted in this work for a 3.6kW alkaline water electrolyser. After comparing between calculated and measured data, an excellent curve fit could be made.

- ***Supercapacitor:*** ESMA supercapacitors are highly competitive with the other supercapacitors for their good performance. Supercapacitor modules' features allow using them for high obtaining high power and energy applications. Their long service life, in addition to fast response time makes them suitable for applications requiring high power quality. Power can be quickly injected or absorbed from them to minimise voltage fluctuations in the system output.

- ***Power Conditioning Units:*** An empirical relationship describing the efficiency curve of a PCU is evaluated. The results show that the accuracy of the piecewise linear and quadratic models are good, particularly at powers above 10% of the rated power. At low powers (less than 10% of rated power), all the models give no accurate representation of the measured data.

6. SIMULATION OF STAND-ALONE HYDROGEN PVFC HYBRID SYSTEM

The investigated stand-alone hydrogen PVFC hybrid system is designed to be totally self-sufficient for generating, storing and supplying electric power to local loads. It is simulated to predict its performance before implementation. This system is often installed in rural and remote areas. Thus, it's important in the design to optimise the system configuration, component sizes and control settings. Design via simulation allows studying the different options, considering various influencing parameters and effectively fulfils the system/user requirements. Mathematical models of the system components are interconnected to form a general representation of the whole system, through a central supervisory controller that defines the way in which components interact to simulate the operation of the entire system. In this chapter, a stand-alone hydrogen PVFC hybrid system will be simulated. All the components of the system have been modelled and validated in the previous two chapters. A comparison between different system topologies, such as DC and AC coupled, with different PCU types at two different locations on the basis of the energy point of view is studied.

6.1 Description of Dynamical Simulation Tool Program

A number of hybrid system simulation packages, such as TRNSYS, INSEL, HYBRID2 etc, have been developed by different research teams during the last two decades. Most of these software tools simulate given and predefined hybrid systems based on a mathematical description of the component operation characteristics and system energy flow. A brief description of these packages can be found in [Ulleberg-98] and [Ibrahim-02]. The accuracy of the simulation reflects the accuracy with which the performance of a system can be evaluated by a simulation model. However, it must be realized that in design and analysis studies, the accuracy of the simulation model is only one of the factors that determine the accuracy of the simulation. Accurate information's about the designed system, the load, weather data, and the flexibility of the simulation tools are also factors influencing the accuracy of simulation. Hence, choosing efficient simulation tools and preparing the appropriate data can be deliver reliable and useful simulation results.

In this work, a simulation program called Simplorer is used. This program includes much technical advancements, making it a good choice for complex multi-domain simulation. In addition, advanced mathematical models not included in the standard Simplorer library can easily be added to its library. The library of this program is developed in co-operation with the Institute of Solar Energy Technology (ISET) in Kassel, Germany. A new library called "ISET Alternative Power Library" is developed that comprises all models used in PV hybrid systems technology [Caselitz-03]. Simplorer is able to simulate any time period of interest. This feature allows studying the short- as well as the long-term PVFC hybrid system performance.

6.2 Input and Output Data of the Simulation Program

A limited amount of information is usually available about the system to be designed or analysed. The user load demand may not be fully known. Resources data might not be available at the site of interest with the required resolutions or with known statistics concerning the climatologically averages. In this situation, data must be generated from daily average or monthly average values.

Two classes of input data are necessary to define the system simulation model. The first class comprises the technical characteristics, and these will be defined for the simulation model. This class was studied in detail in the previous chapters. The second class of data consists of weather data and user load demand. All these data are stored in files and are called when needed by the used components within the simulation system.

6.2.1 Weather Data and User Load Demand

Accurate analytic predictions for long-term performance of hybrid systems require, as input data, reliable information about both the renewable source such as solar radiation and the user load demand. Enough measurements or estimation procedures have to be available to provide the simulation model with the necessary weather and user load demand data.

6.2.1.1 Weather data

The important required weather data for the hydrogen PVFC hybrid system analysed in this work are the solar radiation, [W/m²] and the ambient temperature, [°C]. These data have to be supplied to the simulation model on an hourly basis. The solar radiation and ambient temperature are calculated by using the commercial database Meteonorm® 4.0, which calculates the weather data on arbitrarily oriented surfaces at any desired location on the earth [Remund-00].

6.2.1.2 User load demand data

An important step in system design is the estimation of the power requirements for the intended application. Some simulation studies use annual or seasonal load averages. However, accurate simulation studies require higher time resolution for the user load data, from minutes to hours. Hence, the load duration curve for the intended application over the study period of interest has to be available on an hourly basis. The duration curve can take any form, such as load values each hour or considering the load constant for all hours over the simulation period. In this work, the load is considered to have the basic load priority and is considered to be constant during each one hour time step.

The size of the system components, the storage and the energy transforming units are influenced by the user load demand. To find their optimum sizes, simulations over a year or years may be

needed. Besides the loads required by the user, the system itself consumes energy output. This type of energy is called a parasitic load and can be both thermal and electrical. Loads that are considered parasitic are, for example, power required by controllers, or to run fans, etc and heat required by some components or parts of the components of the system.

6.2.2 Parameters of the System Components

Each component model requires a certain number of parameters that are necessary for the execution program. The corresponding parameters of the system components are calculated and validated in chapter 5.

6.2.3 Output System Data

The developed simulation model provides sufficient information about the performance of each component and the system. During the program execution, all necessary system variables needed for a performance analysis are recorded in a simulation output file. For example, hourly values of hydrogen fuel produced by electrolyser unit, hydrogen fuel consumption by fuel cell back-up generator, generated fuel cell energy to cover the deficit energy from the PV generator to satisfy the user load demand, generated PV energy, etc are delivered. Moreover, a yearly total system energy balance is estimated. These output results can be analysed to cover all performance aspects of the overall system.

6.3 Consistency Check

An important property of any power system simulation program is that energy is balanced within each time step throughout the entire simulation run [Dumbs-99]. The total amount of produced energy (PV generator, fuel cell, and storage output) must equal the total amount of consumed energy (user load, electrolyser, storage input, and losses). Checking the energy balance at each time step assures that the model is internally consistent. The overall energy balance equation is given by:

$$P_{PV} + P_{fc} - P_{load} - P_{el} \pm P_{SCap} - \sum_i L_i = 0 \qquad 6.1$$

Where
- P_{PV} PV generator output power, [W]
- P_{fc} output power from PEM fuel cell, [W]
- P_{Load} user load power demand, [W]
- P_{el} input power to alkaline water electrolyser, [W]
- $\pm P_{SCap}$ supercapacitor discharge or charge power, [W] and
- $\sum_i L_i$ all power losses in the system, [W]

The power losses L_i in the energy balance equation for the system under study comprise only the losses in the power conditioning units during energy conversion between the different units of the system. Power line losses are neglected.

6.4 Assumptions of the System Simulations

The main assumptions made in the simulation of the hydrogen PVFC hybrid system are:

- In general, the H_2/O_2 PEM fuel cell has a better performance than the H_2/Air PEM fuel cell, but requires oxygen storage or a purification system. In this work, H_2/Air PEM fuel cell will be used in the simulated system. Thus, no oxygen purification or storage systems are required.
- Some hydrogen losses are expected such as hydrogen losses in the electrolyser or fuel cell during start-up and shutdown, hydrogen losses in the gas storage tank, and hydrogen losses in the fuel cell during operation, but these will not be included in the simulation.
- Many parasitic loads are handled by an auxiliary power supply [Ulleberg-98], such as power needed for water cooling pump for the electrolyser or fuel cell, protective current for the electrolyser during standby operation, hydrogen purification system, and data acquisition and control system. These parasitic powers are omitted from the simulation of the system. The inclusion of these losses would of course lead to different results, but will not affect on the decisions required from the simulation to operate the system optimally.

6.5 Different Topologies of Hydrogen PVFC Hybrid Systems

Two different topologies are competing for an optimal design of the hydrogen PVFC hybrid system. These topologies are DC and AC coupled systems, Fig. 6.1. The DC coupled system has two configurations which are direct and indirect coupled. A general description of the DC and AC coupled hybrid power systems is given in Chapter 2.

- Direct DC coupling of the hydrogen PVFC hybrid system implies strict conditions on the electrical characteristics of the components. The PV generator must be designed to cover the operating DC voltage range of the electrolyser. The AC inverter must be also capable of covering the operating DC voltage range of electrochemical components. To match correctly the direct coupling of the component, the maximum power point voltage of the PV generator must be equal to the maximum voltage of the fuel cell component and the rated voltage of the electrolyser component [Busquet-00].

- In the hydrogen PVFC indirect DC coupled hybrid system, the connection between the components and user demand is established through power conditioning units. The power conditioning units ensure the necessary voltage transformation and controls the individual power flows predefined by the energy management system. The PCU here keep the DC bus-bar voltage constant almost in the event of bus-bar-related power interruptions. Also, they allow increasing the efficiency of the output load inverter, thus its size is smaller, and protect the expensive electrochemical units from damage.

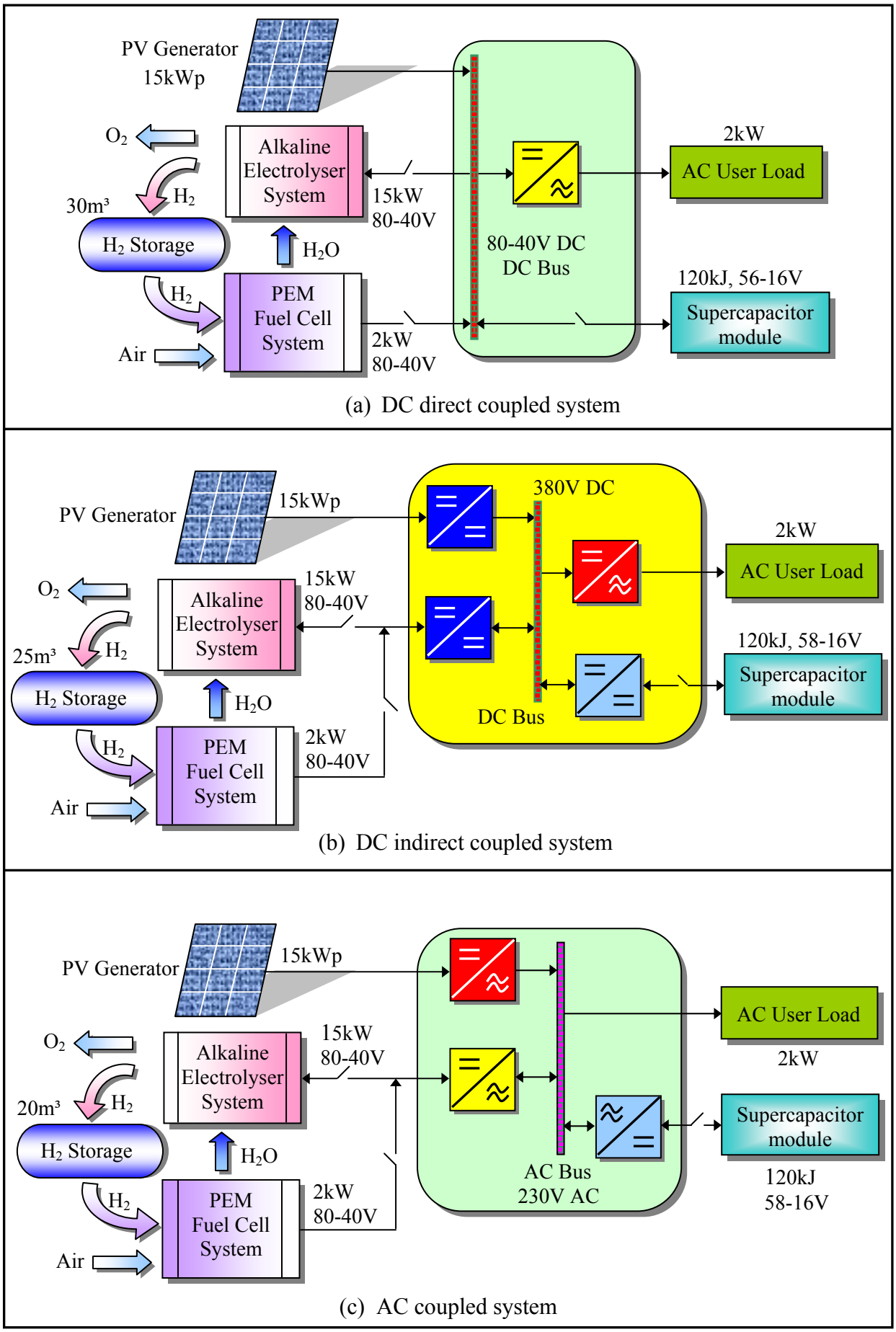

Fig. 6.1: Schematic representation of the hydrogen PVFC hybrid system different topologies.

- Components of the hydrogen PVFC hybrid system with AC coupled are connected directly to the AC side. The heart of this configuration is the inverters [Schmid-97]. These inverters can keep the output frequency and voltage stable and allow the surplus energy to flow backwards to be stored into the hydrogen sub-system. Based on this option, other power sources or loads can be connected without additional interfaces to the AC-terminal of the inverters. This system can be easily expanded to cover any further increase in the energy demand. The PV generator can be expanded simply by connecting more inverters to the AC-side. Therefore, this configuration has numerous advantages such as: expandability, utility-grid compatibility, cost reduction, and simple design and installation [Meinhardt-03]. There is no correlation between the overall system control and the size of the system components.

All these topologies are designed and simulated with the aid of the computer simulation program for one year on the basis of one hour intervals and evaluated on the basis of energy point of view in two locations with different geographical latitudes in the next subchapters.

6.6 Weather and User Load Characteristics of the System under Study

The electrical power load demand of different countries of the world depends on many factors such as climatic conditions, cultural conditions, and the relative price of electricity to other energy sources. In this work, two power load profiles for 2 projects with different climatic conditions are considered [Landau-97] and [Ibrahim-02]. The load profiles available in these projects are domestic service buildings and appliances. Summer and winter daily load curves of the hourly average electricity consumption for two different countries, Kassel/Germany and Cairo/Egypt, are shown in Figures 6.2 and 6.3 respectively.

The daily electrical load profiles vary with time, depending on the activity patterns and the type of appliances used. In cloudy weather, the electricity demand in winter is usually higher than the summer. In contrast in sunny weather, the summer and winter electricity demands are approximately identical. In two projects, the maximum load is 2kW. At project for cloudy weather, the minimum and average load is 207W and 0.7kW, respectively. Also, in project for sunny weather, the minimum and average load is 0.68kW and 1.35kW, respectively. The yearly average load energy is 11.83MWh and 6.12MWh for sunny and cloudy weather, respectively.

The monthly global solar radiation and ambient temperature in Kassel and Cairo for the system study are shown in Fig. 6.4. The yearly average solar radiation energies are 2.25MWh/m² and 1.12MWh/m² at south face modules with optimum tilt angles 35° and 25° in Kassel (cloudy weather) and Cairo (sunny weather), respectively. The optimum tilt angle is estimated according to the major share of solar radiation over the year in the northern hemisphere. The yearly average ambient temperatures are 8.56°C and 21.38°C in Kassel and Cairo, respectively.

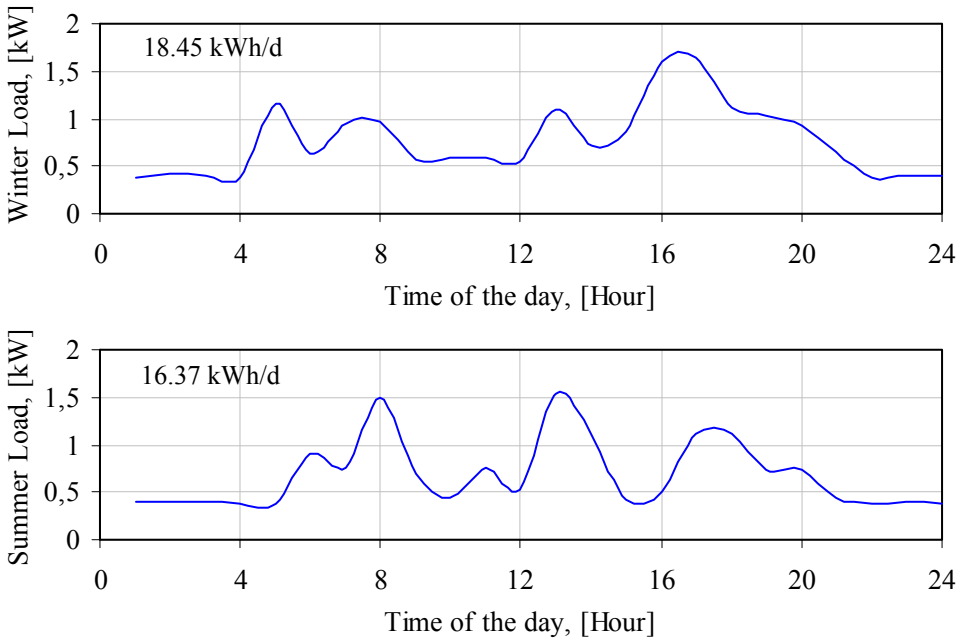

Fig. 6.2: Typical user load profile over one day operation in cloudy weather [Landau-97].

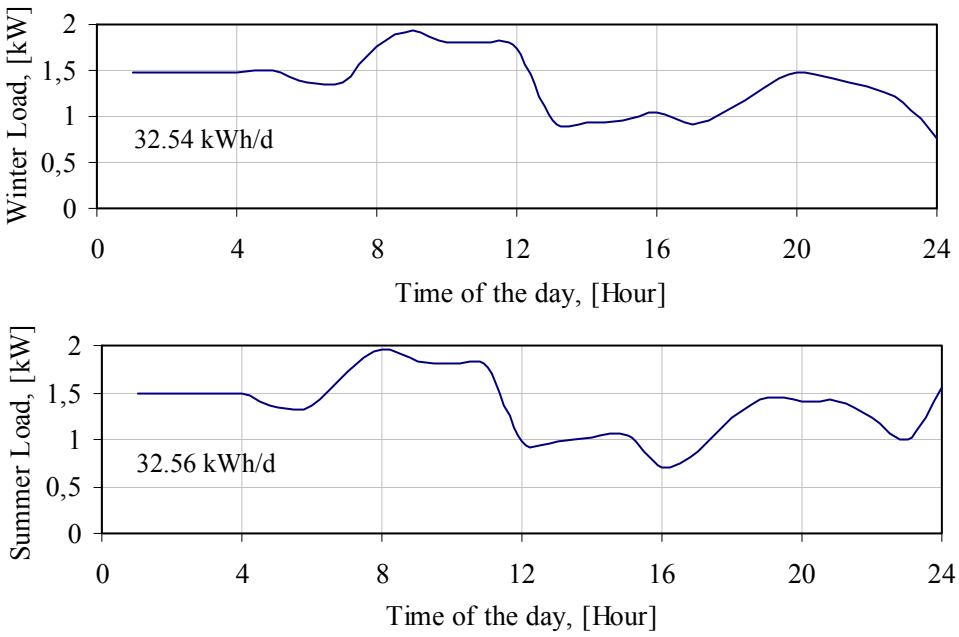

Fig. 6.3: Typical user load profile over one day operation in sunny weather [Ibrahim-02].

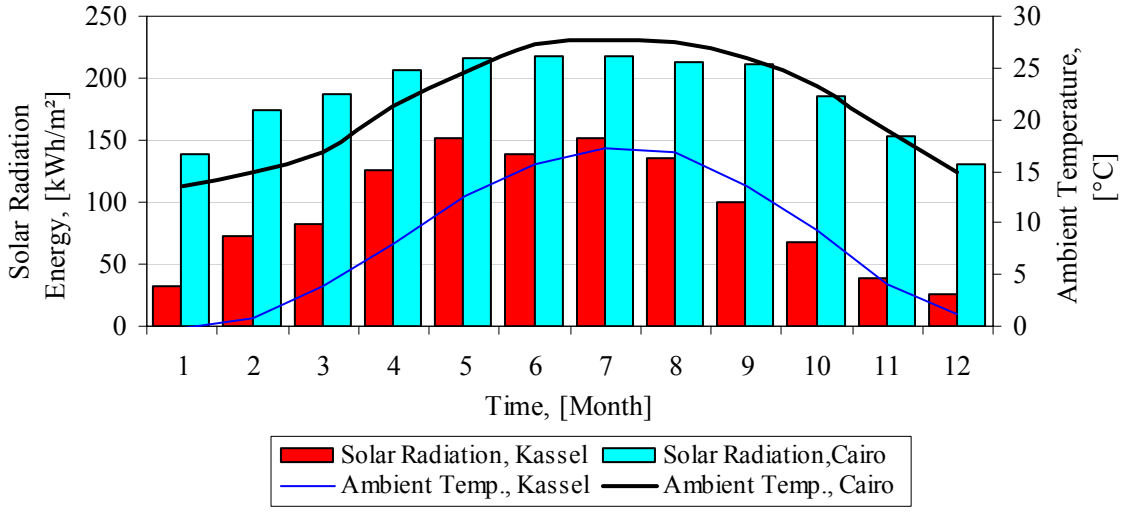

Fig. 6.4: Monthly global solar radiation energy and ambient temperature in Kassel and Cairo.

6.7 Sizing of the Hydrogen PVFC Hybrid System Components

- ***PV generator***

The essential parameters for system sizing are the average daily solar radiation energy and the load consumption energies. These parameters can be used to calculate the peak power of the PV generator and the amount of energy to store, in order to assure the autonomy of the system. To size the PV power generator, the following equation is usually used [Busquet-00]:

$$A_{PV} = \frac{E_{Ld}}{\eta_{sys} \times E_{sd}} \quad \text{and} \quad P_{PV,STC} = E_0 \times \eta_{PV,STC} \times A_{PV} \qquad 6.2$$

Where

A_{PV}	PV generator surface area, [m²]
E_{Ld}	daily mean load energy consumption, [kWh/d]
E_{sd}	daily mean solar radiation energy, [kWh/m²/d]
η_{sys}	total system efficiency taking into account the PV conversion efficiency, wires, diodes, chemical conversion, electricity regeneration, PCU, etc., [-]
$\eta_{PV,STC}$	PV generator rated efficiency (0.10-0.15), [-]
$P_{PV,STC}$	PV production power at standard test conditions, [W_p], and
E_0	Solar radiation at STC, [1kW/m²]

In Cairo, the daily average solar radiation energy is 6.2kWh/m²/d and the daily average load energy consumption is 32.4kWh/d. Assuming that the PV rated efficiency is 13.8% and the total system efficiency is 4.8%, the peak power of the PV generator is calculated from the above equation to be approximately 15kW_p. The system efficiency depends on the components efficiency and on the periods of time at which the solar energy is enough to satisfy the user load demand. In different applications around the world, the hydrogen PVFC hybrid system

efficiency varies between 20% and 40% without taking into account the PV conversion efficiency [Busquet-02].

- ***PEM fuel cell and electrolyser***

Two simple equations are used to determine the power of the electrolyser and fuel cell components.

$$P_{el,rated} = P_{PV,STC} - P_{LDI} \quad 6.3$$

$$P_{fc,rated} = P_{LDM} \quad 6.4$$

Where $P_{el,rated}$ rated power of electrolyser, [W]
$P_{fc,rated}$ rated power of fuel cell, [W]
$P_{PV,STC}$ rated PV power at standard test conditions, [W], and
P_{LDI} and P_{LDM} minimum and maximum load power, respectively, [W]

The rated power of the electrolyser equals the maximal excess power of the PV generator over the minimal load power. The fuel cell power production depends on the maximum load power. The over-sizing of these components could decrease their efficiencies.

- ***Power conditioning units***

To optimise the hydrogen PVFC hybrid system design, the energy and relative time distribution of solar radiation power at the chosen site must be taken into consideration. Figure 6.5 shows the energy distributions of solar radiation in two different geographical latitudes for one year in Kassel and Cairo. In Cairo due to clear weather, the higher power range is more dominant than in Kassel where the weather is cloudy. The curves in Fig. 6.5 are important for optimising the design of the power conditioning unit coupled with the PV generator.

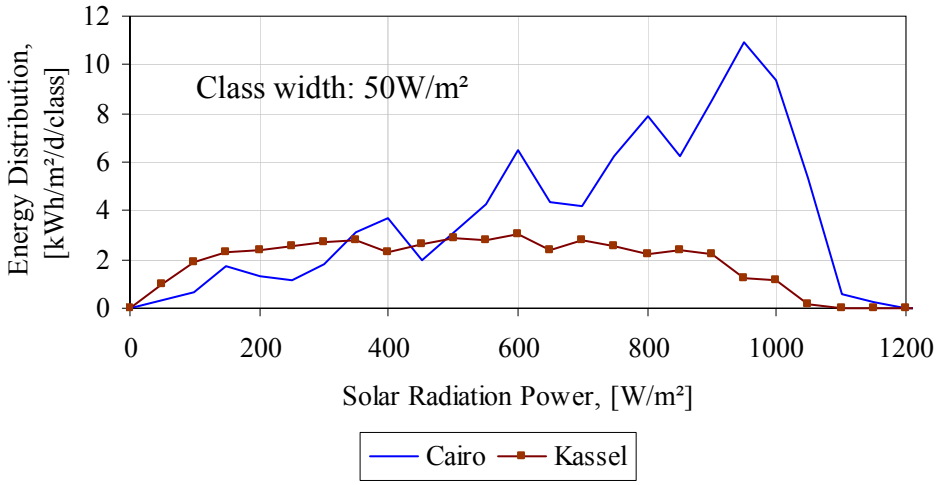

Fig. 6.5: Energy distribution of solar radiation power in Cairo and Kassel for one year.

Figure 6.6 shows the relative time distribution of solar radiation in the chosen sites. At North Africa (Cairo), this relative time distribution is nearly constant, while for middle Europe

(Kassel), it is high at low solar radiation power and decreases as solar radiation power increases. Therefore, the PCU operates a lot of time at lower power in middle Europe, which affects the annual efficiency of the power conditioning unit compared with the situation in North Africa.

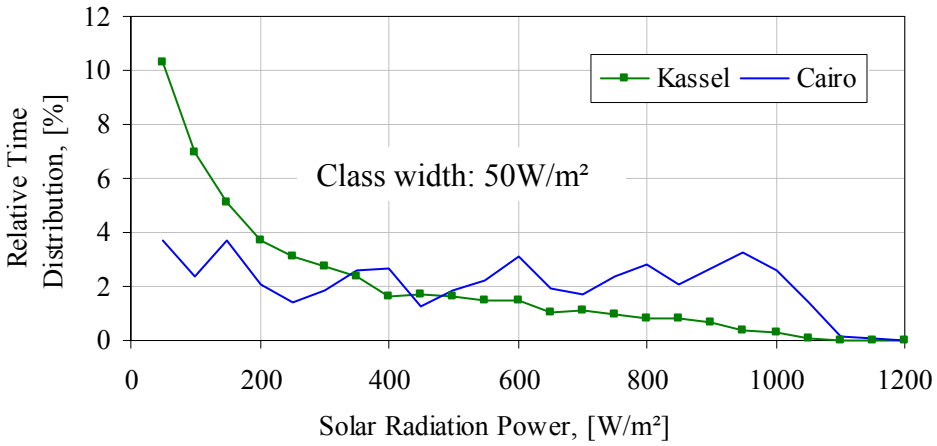

Fig. 6.6: Relative time distribution of solar radiation power in the two sites for one year.

To calculate the optimal rated power of the PCU used with the PV generator, the long-term performance of the PV generator must be analysed by studying the array yield Y_a and the final yield Y_f. Definitions of these quantities are mentioned in Appendix G. The ratio of Y_f / Y_a represents the overall PCU efficiency, which depends on the ratio $P_{rated,PCU}/P_{PV,out}$. Figures 6.7a and 6.7b show the values of Y_f and Y_f / Y_a versus the ratio $P_{rated,PCU}/P_{PV,out}$ for a Sunny Boy inverter technology at Cairo and Kassel. The outstanding conclusion is that optimum value of $P_{rated,PCU}/P_{PV,out}$ is found at around 0.75 and 1.00 for Kassel and Cairo, respectively. This study is analysed by other authors with different PCUs and they found that the optimal value of $P_{rated,PCU}/P_{PV,out}$ is independent of the type of PCU and the tracking strategies, but depends strongly on the local climate [Macagnan-92].

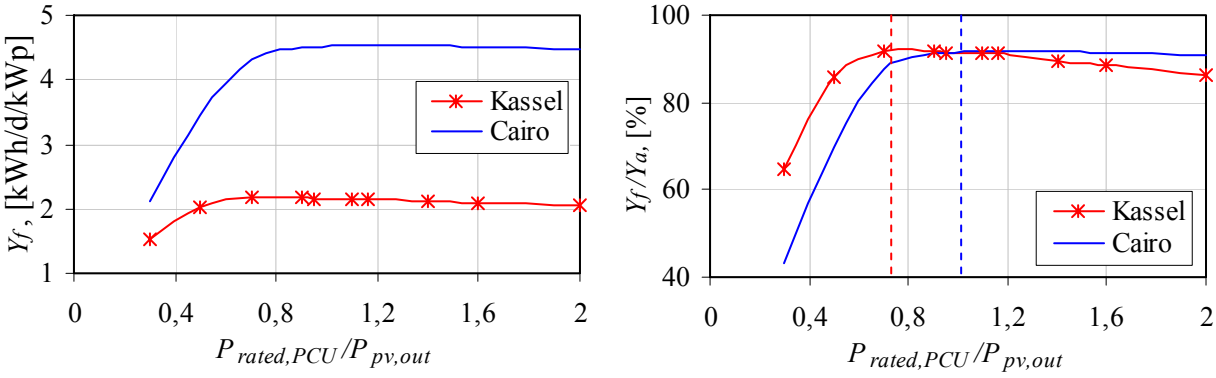

Fig. 6.7: Y_f and Y_f/Y_a versus the ratio $P_{rated,PCU}/P_{PV,out}$ for a Sunny Boy inverter at Cairo and Kassel for one day.

The selection of PCUs for the auxiliary generators (fuel cell and supercapacitor) is determined especially by the load power demand and the value of the DC voltage level at the DC side. The

PCU must be able to power all loads that might run at the same time, including any starting surges for pumps and large motors.

- ***Storage Tank Volume***

The sizing of the hydrogen PVFC hybrid system to satisfy long-term autonomy is based on the yearly average value of solar radiation energy and the load demand. Accordingly, the PV generator is sized according to the solar radiation energy and the load demand. The storage sizing method uses the PV generator sizing and the monthly solar radiation energy to determine the storage tank volume [Busquet-02]. This method can be applied to all sites and all load demands. Figure 6.8 shows the monthly average solar radiation energy with a tilt angle of 35° at Kassel/Germany. The monthly average solar radiation energy over one year is obtained by dividing the sum of the twelve monthly average values by 12, i.e., 1120kWh/m²/12month = 93.33kWh/m²/month.

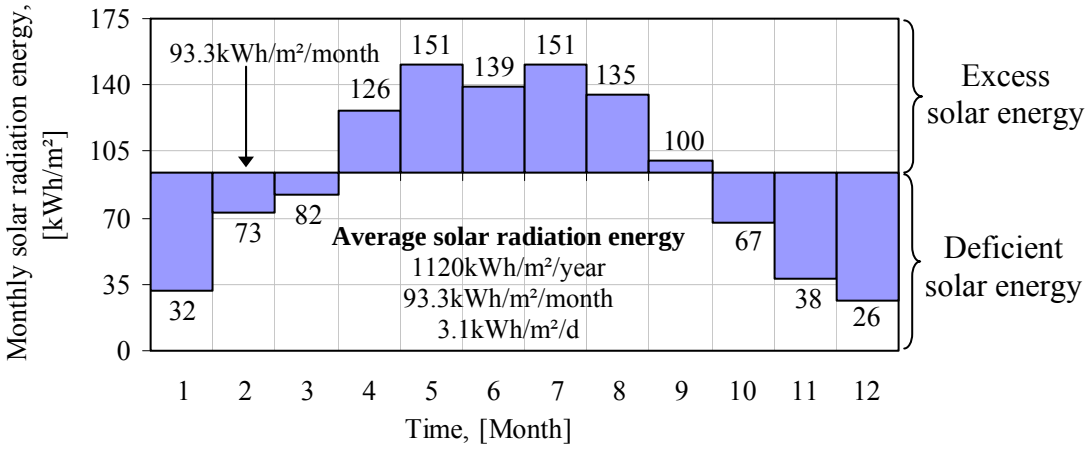

Fig. 6.8: Monthly average solar radiation energy received by a plan at Kassel/Germany.

The hydrogen amount produced by the system during each month is calculated by using the value of the PV generator surface area and assuming the efficiency of PV, PCU and electrolyser to be 10%, 90% and 70%, respectively [Busquet-00]. This method assumes also the hydrogen production is completely stored firstly before it supplied power to the user load. The monthly average value of hydrogen production over one year is calculated from the monthly average values by the same manner as for the monthly average solar radiation energy over one year. Figure 6.9 shows the monthly average hydrogen production over one year in Kassel/Germany for the system under study. From April to September, the system produces more energy than the load demand, Fig.6.8. The excess of energy can produce hydrogen which is stored into hydrogen tank during these months. From October to March, the system can't provide hydrogen energy to store, but it consumes hydrogen to cover the load demand. Hydrogen is consumed (1.72MWh) by fuel cell back-up generator. Thus, this value of hydrogen must be stored before this period in order to assure that fuel cell will provide energy to the load during the period of deficient hydrogen production. If the storage tank allows to store this excess energy 1.73MWh, the system will have an annual autonomy and thus will be completely self sufficient. Therefore,

the storage tank volume in the system under study is 577Nm³ of hydrogen, since 1Nm³ of hydrogen is equivalent to energy of approximately 3kWh. In this work, the hydrogen is stored in a tank at a pressure of up to 30bar, thus, the hydrogen tank volume is approximately 20m³. By the same manner, the storage tank volume in Cairo/Egypt can be calculated.

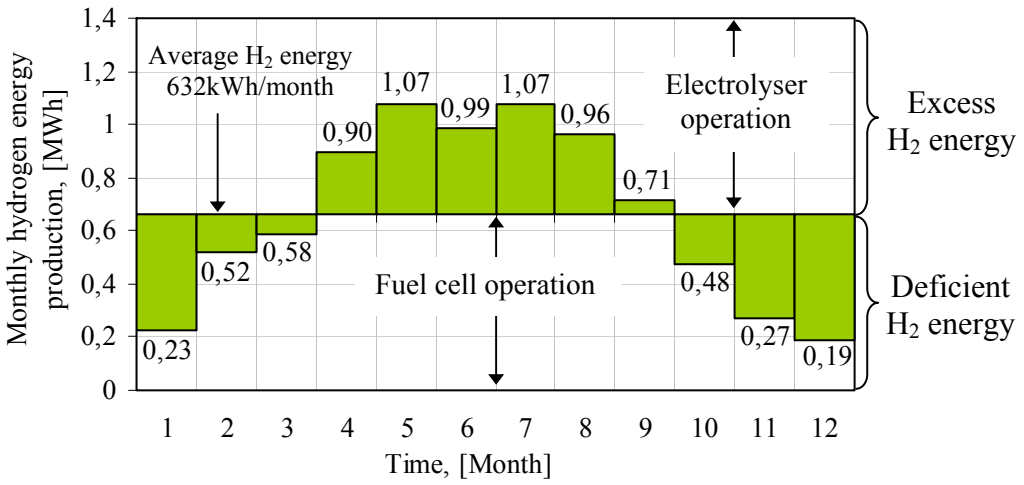

Fig. 6.9: Monthly hydrogen energy production during one year at Kassel/Germany.

6.8 Energy Flow Control Strategy

The system energy balance is checked at each time step of the simulation. The input data such as solar radiation and ambient temperature are fed in to calculate the amount of energy that can be generated by the PV generator. The value of PV energy is compared with the load demand energy to determine the distribution of energy flow between the storage unit and the load.

Surplus PV energy is stored in the form of hydrogen by the electrolyser and deficit energy can be taken from hydrogen by the fuel cell back-up generator. The PV energy that can not be used (neither delivered to the load nor stored in hydrogen) is categorized as excess energy. In real systems, this energy would be used for other purposes, such as water heating, or the PV generator has to be controlled to reduce its output power. If the totally available energy from the PV generator, fuel cell and supercapacitor is not enough to cover the load, the system must be stopped. The system under study has two controller valves to protect the hydrogen storage tank from over pressure inside the tank and to regulate the hydrogen flow supply rate to the fuel cell unit. Therefore, the system control is designed to optimise the energy utilization from the different components of the overall system and this is considered in the simulation.

The control parameters for the system under study are:

- Pressure inside the hydrogen tank p_H.
- Output power from the PV generator P_S.
- The load demand P_L.
- Minimum hydrogen tank pressure p_{off} for turn-off operation of the fuel cell.

- Hydrogen tank pressure p_{on} for turn-on operation of the fuel cell.
- The output power from fuel cell P_{fc} or the input power to electrolyser P_{el}.
- The instantaneous time and the final time of the simulation t, t_{stop} respectively.
- The time step for the simulation, Δt.
- The rated fuel cell power, $P_{fc,r}$.

A flow diagram of the control strategy for long-term steady state operation is shown in Fig. 6.10. The control strategy is based on the following three different cases:

1. If $P_S < P_L$, $P_L - P_S \leq P_{fc,r}$ and $p_H > p_{on}$ then; $P_L - P_S = P_{fc}$. This means that, the load is connected directly to the PV generator and the deficit power must be obtained from the auxiliary back-up generator system, i.e., the fuel cell.
2. If $P_S > P_L$ then; $P_{el} = P_S - P_L$. This means that, the power from the PV generator is high enough to power the load, and the excess power is stored in hydrogen by the electrolyser.
3. If $P_S < P_L$ and $P_L - P_S > P_{fc,r}$ then; $P_L = 0$, $P_{fc} = 0$ and $P_{el} = P_S$. This means that, the load and fuel cell are disconnected and the electrolyser is connected directly to the PV generator, until $p_H \geq p_{on}$ and $P_L - P_S \leq P_{fc,r}$, then the load is connected according to the conditions in 1 or 2.

According to this control strategy, if the fuel cell is switched on, then the electrolyser must be in the switched off position. The switching off of the electrolyser actually means that the electrolyser is switched to the standby mode operation, because it can never be completely switched off, as this will damage the electrodes [Ulleberg-98]. The control time step (Δt) is one hour for this long-term operation. Thus, the supercapacitor module which represents a storage unit for short-term operation, to provide a more stable power response to transient changes in load demand or to stabilize the fuel cell operation, is not considered here.

6.9 Simulation Results

Simulation results of the hydrogen PVFC hybrid system are divided into two parts; short- and long-term performance analysis. Short-term analysis concentrates only on the fuel cell and supercapacitor and illustrates how the supercapacitor can operate with the fuel cell unit to meet the transient changes in the load demand. Appendix F shows the behaviour of these components during transient changes in the load demand. In Long-term performance analysis, the simulation based on the models, which are tested and validated in the pervious chapters, investigates the energy analysis of the different hydrogen PVFC hybrid system topologies at the two different sites, Kassel (Germany) and Cairo (Egypt). An energy analysis of the system will be carried out for a period of one year, using as input the measured meteorological and the load demand data, which are described in section 6.6 for the two sites. These input data are used for all simulation topologies, i.e., the total power from the PV generator and user load demand are the same for all simulations of the two different sites.

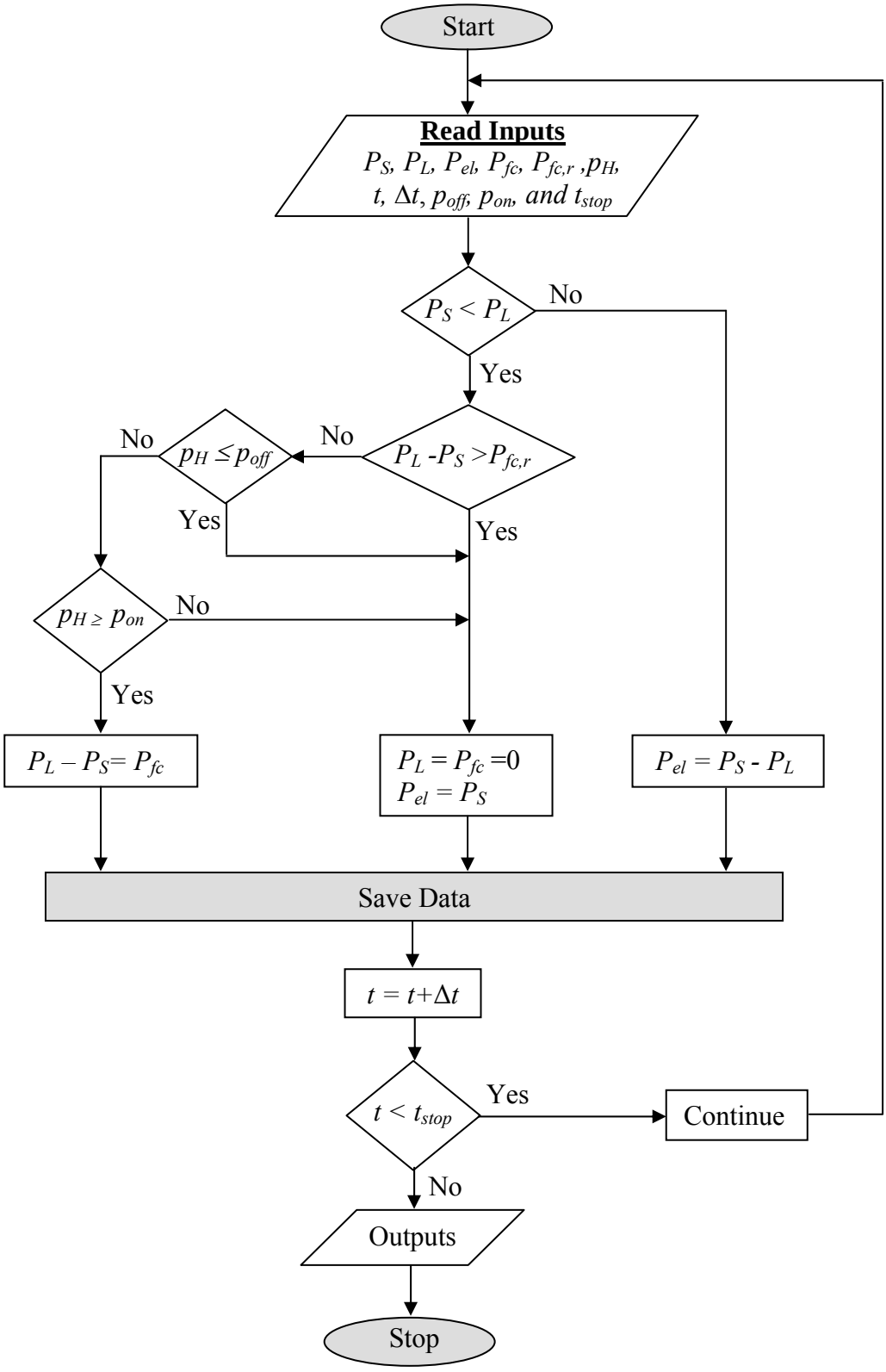

Fig. 6.10: Basic flow diagram of the control strategy for long-term operation (Δt = 1 Hour) of the system.

To well visualize the simulation of the system for long-term operation, Fig. 6.11 shows the layout of the overall AC coupled system simulation by using Simplorer program. Table 6.1 gives the summary of descriptions of the all components of the system under simulated which were analysed, programmed, and validated before implemented into the system simulation.

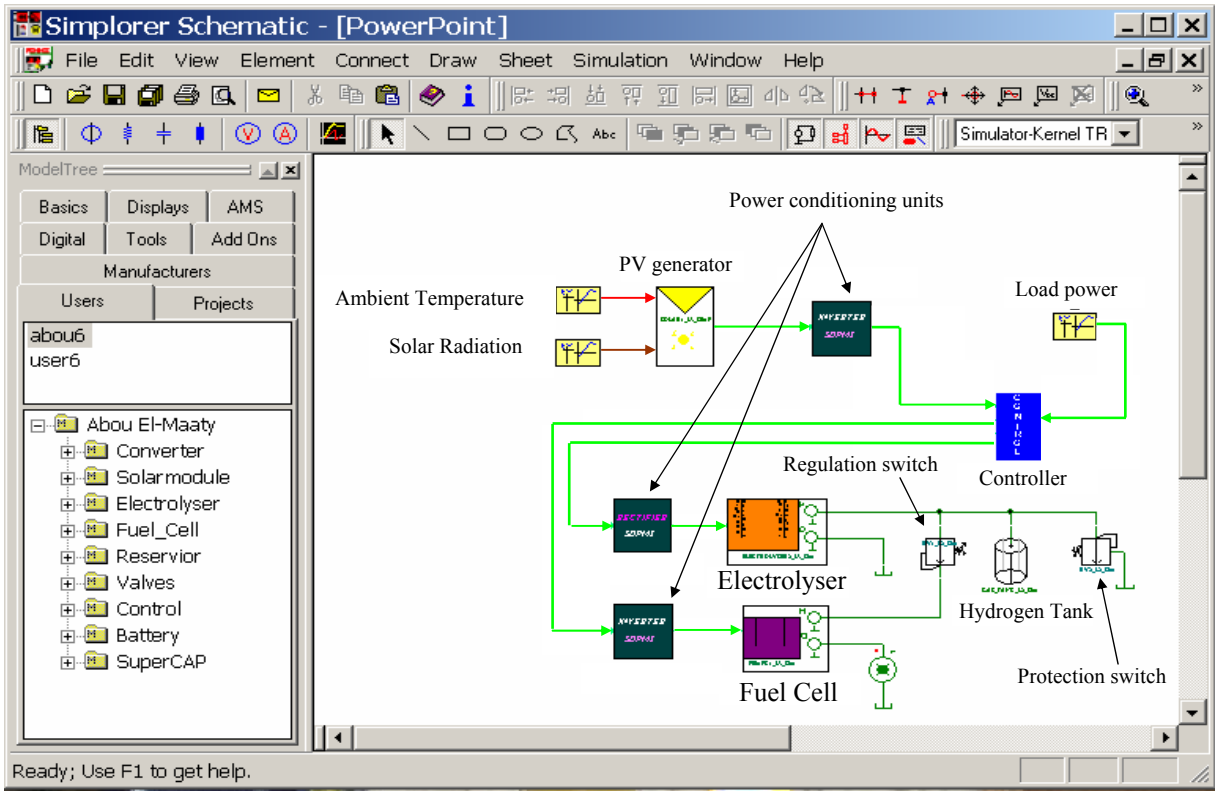

(a)

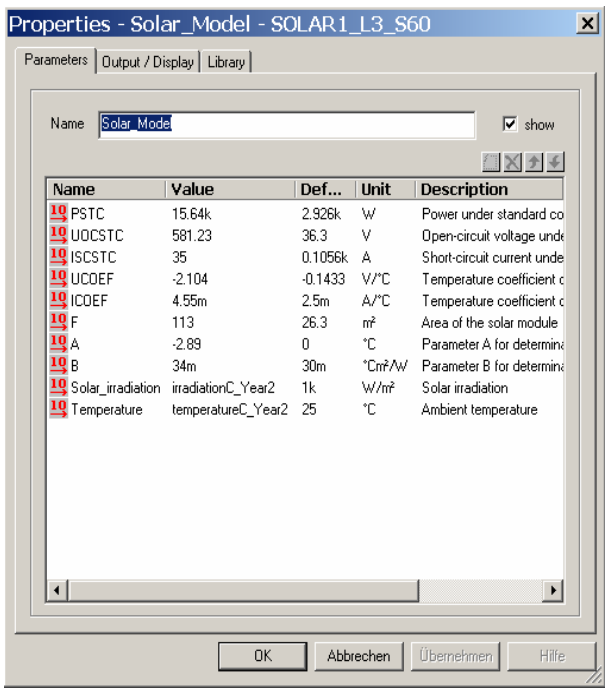

(b)

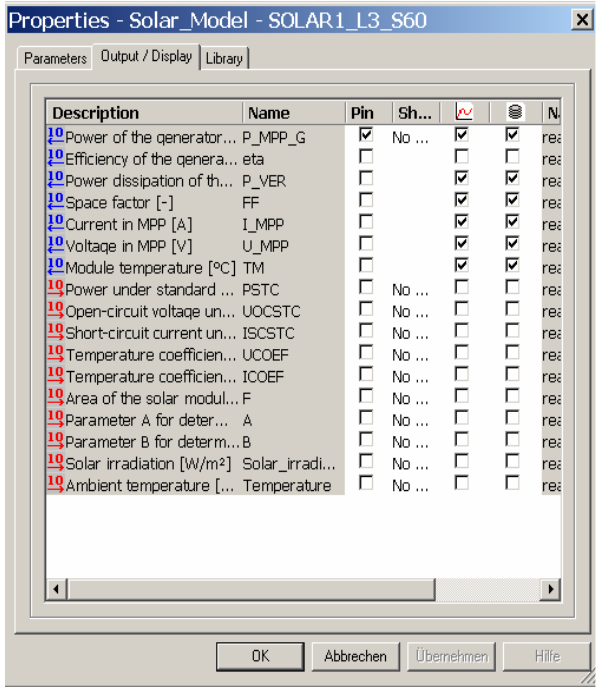

(c)

Fig. 6.11: Simplorer layout for AC coupled system simulation: (a) Overall system; (b) Parameters for PV generator; (c) Selected PV generator output results.

Table 6.1: Summary of the descriptions of main components of the system under simulation

Components	Models	Validation
PV Generator	One-diode, two-diode, and empirical models	ISET data for one day over 15sec., BP 585 module
PEM Fuel Cell	Analytical PEM model	ISET 2kW Fuel cell system
Alkaline Water Electrolyser	Analytical alkaline model	PVFC-SYS project at Agrate-Italy, 3.6kW
Power Conditioning units	Empirical energy efficiency model	- Sunny family (SMA Regelsysteme GmbH data) - SW Trace family (ISET data) - DC/DC Cuk converter (ISET data)
Supercapacitor	Empirical ISET model	ESMA Company, data from project at EPRI PEAC Corporation
Controller	Energy flow and switches	Plausibility

In the energy analysis, simulation results are used to make an energy balance check at each step of energy conversion throughout the system according to the energy control strategies mentioned in section 6.8. Table 6.2 gives the data used for all simulated system topologies. The results of the simulation are presented mainly in Tables 6.3, which give a comprehensive and clear visualization of the long-term system performance. The use of energy utilization factors has proven to be a very useful criterion for the assessment of the hydrogen PVFC hybrid system in general. All these factors are based on the Joint Research Centre (JRC) of the European Community in Ispra or the International Electro technical Commission (IEC), see Appendix G. Note that, in long-term performance analysis, the supercapacitor is neglected, because the simulation time step here is one hour while a supercapacitor operates for short-term or transient periods only, and is not considered as a power unit.

Table 6.2: Data used for all simulated system topologies

Data	Cairo/Egypt	Kassel/Germany
Altitude, [m]	16	233
Latitude	30.12°N	51.18°N
Longitude	31.24°E	9.27°E
Annual mean load energy E_L, [kWh/year]	11827	6125
Average solar radiation energy, [kWh/m²/d]	6.15	3.06
PV module	BP585	BP585
Rated power of PV generator $P_{PV,STC}$, [kWp]	15.64	15.64
PV generator surface area A_{PV}, [m²]	113	113
Solar energy on PV generator $E_{PV,in}$, [kWh]	253697	126053
Output PV generator energy $E_{PV,out}$, [kWh]	30495	15530
Fill factor FF	0.77	0.77
PV generator rated efficiency $\eta_{PV,STC}$, [%]	13.8	13.8
Mean PV generator efficiency η_{PV}, [%]	12	12.3
Maximum PV generator output power, [kW]	15.8	14.7
Rated electrolyser power $P_{el,rated}$, [kW]	15	14
Electrolyser operating temperature, [°C]	60	60
Rated Fuel cell power $P_{fc,rated}$, [kW]	2	2
Fuel cell operating temperature, [°C]	52	52

Table 6.3: Annual simulation results of the hydrogen PVFC hybrid system with different topologies, continue next page

Parameters		DC Direct Coupling		DC Indirect Coupling		AC Coupling (Mixed PCU)[1]	
		Cairo	Kassel	Cairo	Kassel	Cairo	Kassel
PV Generator	Output voltage range at MPP, [V]	67-56	70-58	67-56	70-58	440-371	462-381
	Maximum output current at MPP, [A]	246	226	246	226	37.5	34.4
Alkaline Water Electrolyser	Total input energy, [kWh]	24319	12403	21596	10874	19625	9853
	Mean efficiency[2], [%]	69.5	69	69	69	69	69
	Number of start operation, [cycles]	370	420	373	409	374	412
	Hydrogen production, [Nm³]	6223	3197	5575	2826	5092	2583
	Run time per year, [Hour]	3888	3013	3753	2915	3742	2948
	Mean run time per cycle, [Hour]	10.5	7	10	7	10	7
	Mean input power, [kW]	6.3	4.1	5.75	3.70	5.24	3.34
	Mean input voltage range, [V]	74-48	75-48	73-48	73.5-48	72-48	72-48
	Maximum input current, [A]	198	198	179	172	158	145.3
	Maximum input power, [kW]	14.4	14.5	12.8	12.5	11	10
PEM Fuel Cell	Total output energy, [kWh]	6846	3795	7197	3912	6994	3688
	Mean electrical efficiency, [%]	46	53.5	46	53	46	54
	Number of start operation, [cycles]	370	421	374	427	375	418
	Hydrogen consumption, [Nm³]	4919	2408	5198	2492	4938	2355
	Run time per year, [Hour]	4872	5747	4959	5732	4970	5734
	Mean run time per cycle, [Hour]	13	14	13	13.4	13.25	14
	Mean output power, [kW]	1.4	0.7	1.45	0.7	1.4	0.64
	Mean output voltage range, [V]	74-48	71-45	71-45.5	71-44	71-46	71-45
	Maximum output current, [A]	35	44	43.4	47	60	45.3
	Maximum output power, [kW]	1.7	2	2	2.1	2	2
Hydrogen Storage	Tank volume, [m³]	30	30	25	25	20	20
	Initial tank pressure (beginning of a year), [bar]	7	7	10	10	10	10
	Final tank pressure (end of year), [bar]	27.3	20.7	16.6	17.6	14.3	16.5
	Maximum tank pressure, [bar]	29.7	29.4	22.2	29.3	21.3	30
	Minimum tank pressure, [bar]	5.5	2.3	6.8	3.4	5.4	2.45

[1] Mixed PCU means that the AC coupled topology uses two technologies from the PCU refer to section 6.10.
[2] The overall efficiency equals the product of the Faraday's and energy efficiency.

Table 6.3: Annual simulation results of the hydrogen PVFC hybrid system with different topologies

Parameters		DC Direct Coupled		DC Indirect Coupled		AC Coupled	
		Cairo	Kassel	Cairo	Kassel	Cairo	Kassel
BOS components and system efficiencies	Net energy from H_2 subsystem E_{FCN}, [kWh]	0	0	0	0	0	0
	Net energy to H_2 subsystem E_{ELN}, [kWh]	1800	1266	494	494	198	342.4
	Total input energy E_{in}, [kWh]	30495	15530	30495	15530	30495	15530
	PV fraction $F_{in,PV}$, [-]	1	1	1	1	1	1
	Useful energy E_{use}, [kWh]	13627	7391	12321	6619	12025	6467
	PV useful energy $E_{PV,use}$, [kWh]	13627	7391	12321	6619	12025	6467
	BOS efficiency η_{BOS}, [%]	45	48	40.4	42.6	39.4	41.6
	Overall system efficiency η_{sys}, [%]	5.4	5.9	4.85	5.24	4.7	5.1
	H_2 subsystem efficiency $\eta_{sub\text{-}sys}$[3], [%]	33.6	37	28.3	32	25.4	29.4
Annual system performance indices	Reference yield Y_r, [kWh/d/kWp]	6.15	3.06	6.15	3.06	6.15	3.06
	Array yield Y_a, [kWh/d/kWp]	5.34	2.72	5.34	2.72	5.34	2.72
	Final yield Y_f, [kWh/d/kWp]	2.39	1.29	2.15	1.15	2.11	1.13
	Capture losses L_c, [kWh/d/kWp]	0.81	0.34	0.81	0.34	0.81	0.34
	System losses L_s, [kWh/d/kWp]	2.95	1.43	3.19	1.57	3.24	1.59
	Performance Ratio PR, [%]	39	42	35	38	34	37
Power Conditioning unit efficiencies	Load DC/AC inverter efficiency, [%]	91.6	90.5	93.7	93	-	-
	PV DC/DC converter efficiency, [%]	-	-	94	93	-	-
	DC/DC Cuk con. with EL efficiency, [%]	-	-	94	94	-	-
	DC/DC Cuk con. with FC efficiency, [%]	-	-	95	93	-	-
	PV DC/AC Sunny Boy inv. efficiency, [%]	-	-	-	-	93	92
	DC/AC Trace inv. with EL efficiency, [%]	-	-	-	-	86	85
	DC/AC Trace inv. with FC efficiency, [%]	-	-	-	-	92	93

[3] The efficiency of the subsystem including electrolyser, H_2 storage, fuel cell and PCU.

A summary of the simulated annual energy consumption, production, and efficiencies of the various components and subsystems of the system are given in Table 6.3. The results show that about 80% of the energy produced by the PV generator is consumed for the production of hydrogen in the electrolyser and 20% is directly consumed the user load. The overall system efficiency (η_{BOS}) varied from 39 to 45% in Cairo and from 42 to 48% in Kassel. This Table gives also an overview of the mean annual final yield, array capture and system losses, and performance ratio for all topologies. The mean annual final yield Y_f ranges from 2.06 to 2.39kWh/d/kWp in Cairo and from 1.10 to 1.29kWh/d/kWp in Kassel according to the system topology. The corresponding mean annual performance ratio *PR* ranges from 33 to 39% in Cairo and from 36 to 42% in Kassel. In the case of a stand-alone system without a back-up generator and having the same load profile, the performance ratio of the system would drop down to about 20% [Jahn-98]. The mean annual capture losses are constant for all system topologies, because the PV generator is the same for all system topologies, and equal to 0.81kWh/d/kWp and 0.34kWh/d/kWp in Cairo and Kassel, respectively.

Figure 6.12 shows the monthly values of final yield, system and array losses Y_f, L_s and L_c respectively presented in bar diagrams for the AC coupled system topology at the two selected sites. Figures 6.13-6.16 show simulation results for two days of the system at Cairo and Kassel in summer and winter seasons. The solar radiation varies according to the season. During the period of low solar radiation, in winter, the SOC of hydrogen storage drops because the hydrogen production during the daytimes is lower than the consumption during the nighttimes. In summer, the hydrogen production is higher than the hydrogen consumption, thus, the SOC of hydrogen storage increases. From these figures, the fuel cell and electrolyser operate almost all summer and winter days. Thus, the number of start operations for these components are approximately equal to the number of the days of the year. At night, the fuel cell operates to compensate the deficit in PV generator energy. During the days light, the electrolyser operates to produce hydrogen which is stored to be consumed nightly.

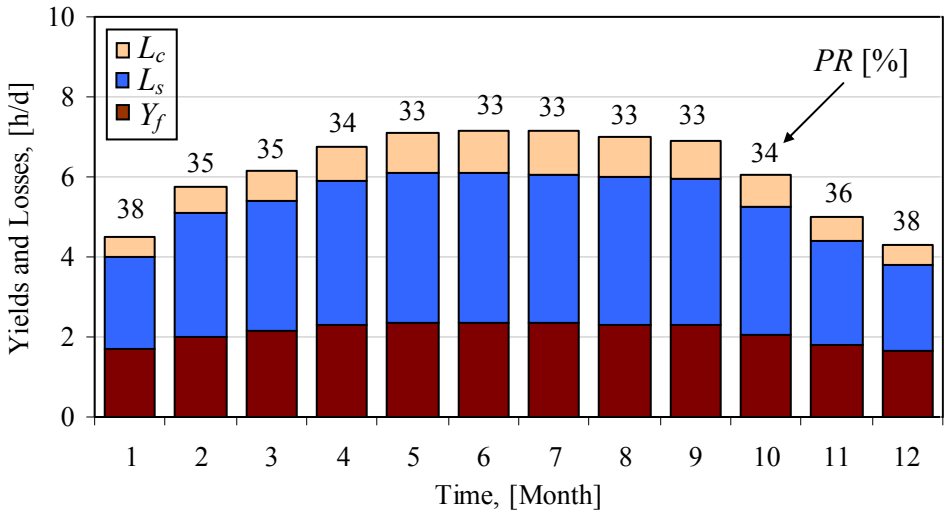

Fig. 6.12.a: Normalized yearly analysis of the AC coupled system topology (Mixed PCUs) at Cairo/Egypt and monthly values of Y_f, L_s, and L_c.

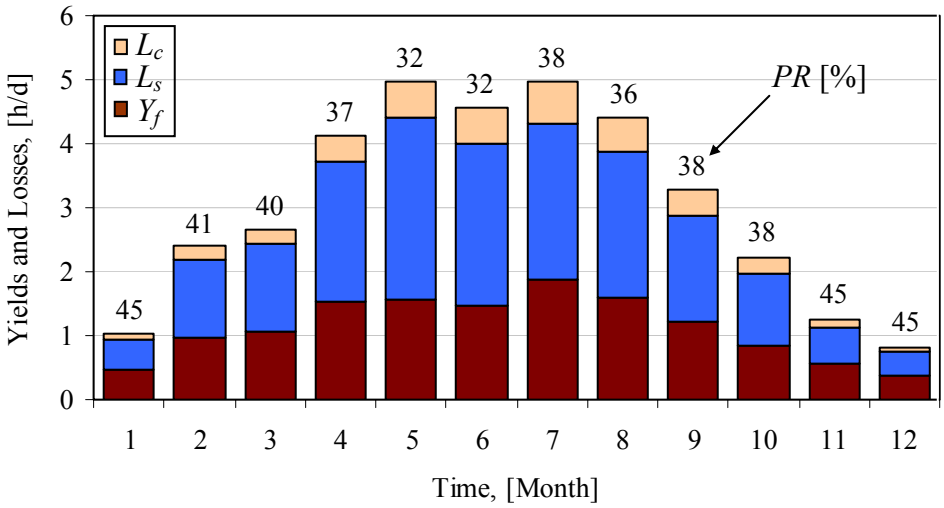

Fig. 6.12.b: Normalized yearly analysis of the AC coupled system topology (Mixed PCUs) at Kassel/Germany, and monthly values of Y_f, L_s, and L_c.

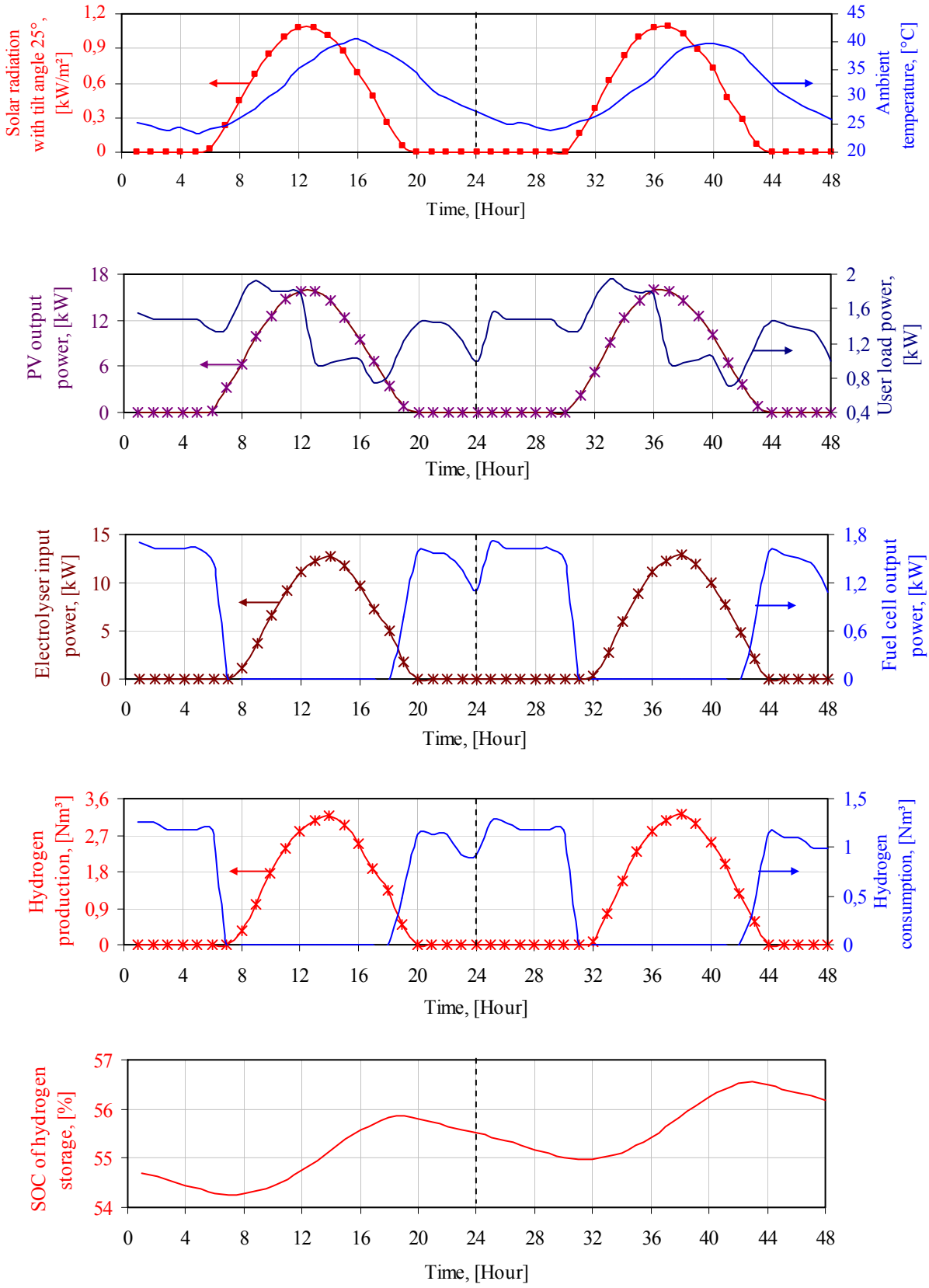

Fig. 6.13: Simulation results of the AC coupled system for two summer days in Cairo site.

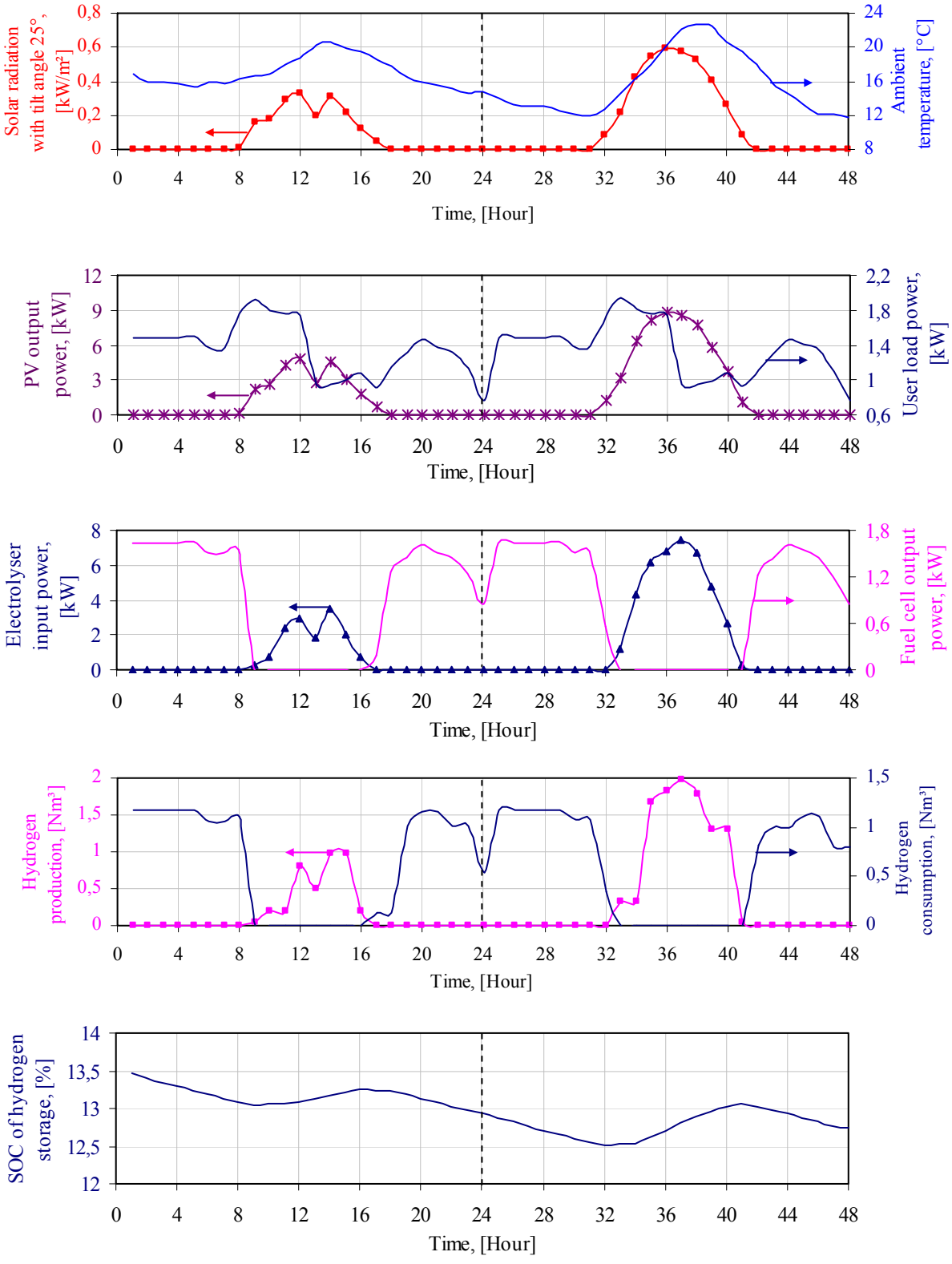

Fig. 6.14: Simulation results of the AC coupled system for two winter days in Cairo site.

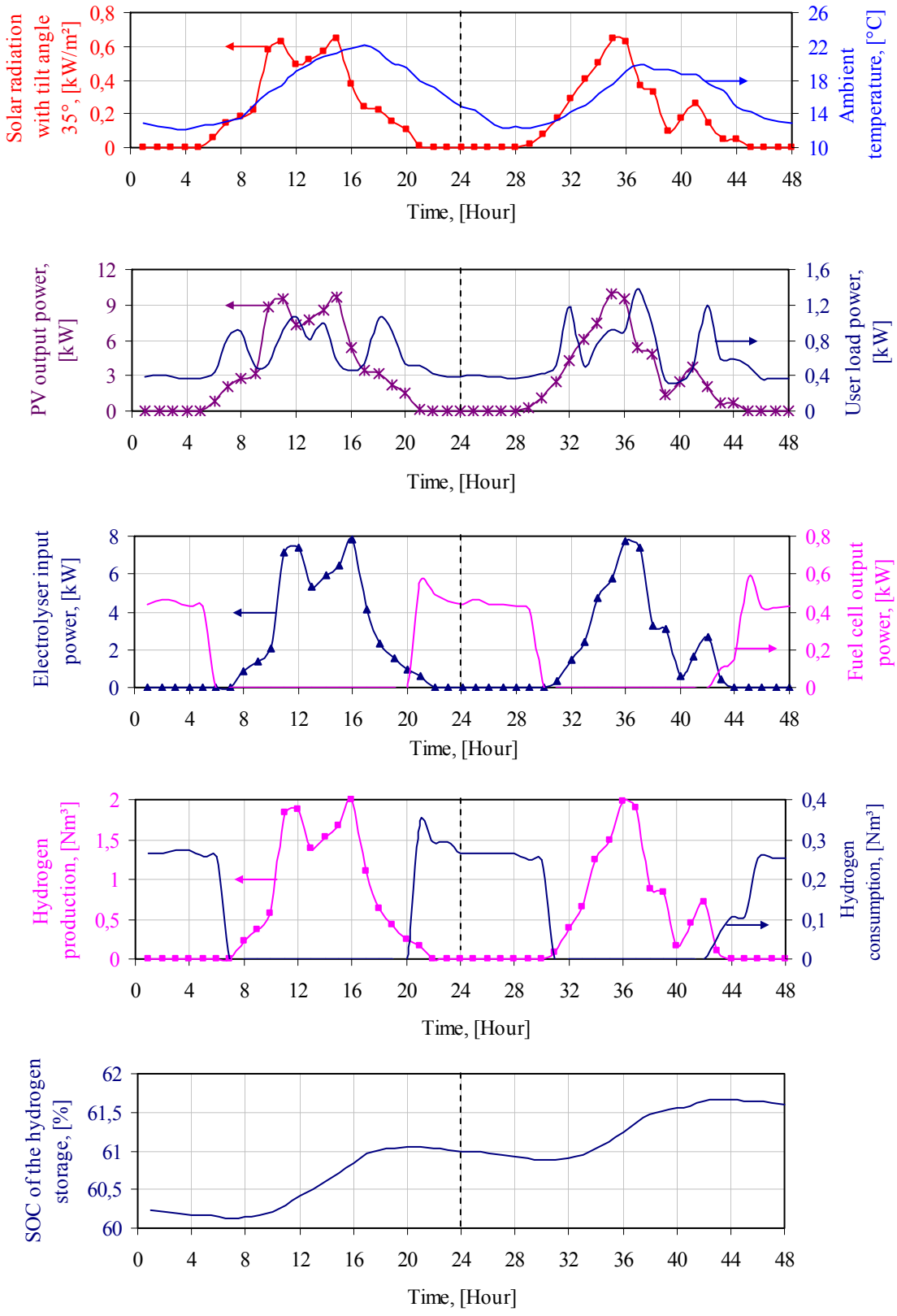

Fig. 6.15: Simulation results of the AC coupled system for two summer days in Kassel site.

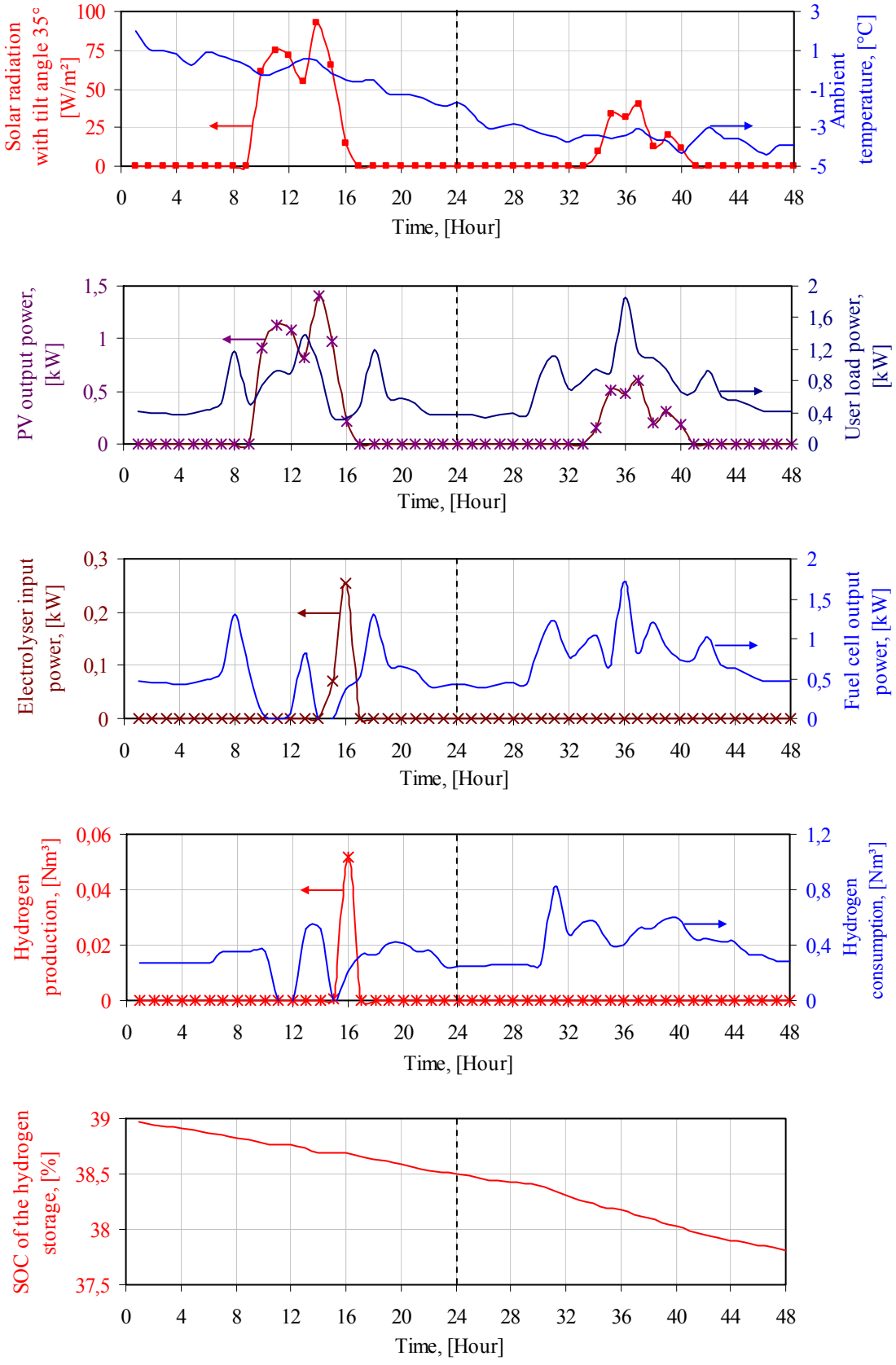

Fig. 6.16: Simulation results of the AC coupled system for two winter days in Kassel site.

6.10 Discussion of the Long-term Performance Results

In the DC direct coupled system, the efficiency of the hydrogen storage path is better than other system topologies, but the DC bus-bar voltage is lower. Therefore, a low input voltage DC/AC load inverter, which has a lower efficiency, is used and the PV generator array is arranged to give low output voltage. To connect the low input voltage to the AC consumer loads, there is an inevitable need of using a step-up DC/AC load inverter, which usually uses a step-up transformer at the input or output circuit of the inverter. In our system, Sunny Island inverter is used. Within the input circuit of this inverter, a DC/DC Cuk converter is used to increase the low input DC voltage (40 to 80V) to high DC voltage (380V) [Burger-00]. The DC direct coupled system has a lot of problems related to connecting the electrochemical components. For example, the fuel cell is not able to cope with negative currents, thus, a protective diode or any power semiconductor switch with reverse blocking capability is needed, which alone causes losses of about 2-3% [Solmecke-00]. In addition, switches are needed to regulate the working point, and these switches can cause even more losses. Also, a large cross section area of the DC bus-bar must be used to support the high DC current, which means additional losses and costs. If these factors are considered, the direct coupled hydrogen PVFC hybrid system would be economically not feasible.

On the other hand, the indirect DC coupled system has losses of about 2.9MWh/yr greater than the direct coupled one in Cairo and 1.29MWh/yr in Kassel, if the losses in the cables and switches in direct coupled are neglected. Figure 6.17 shows the annual energy losses for different topologies of the system in Cairo and Kassel, and for the main components only (PV generator, PCUs, electrolyser, and fuel cell). The losses in cables and other switches for direct coupled system are neglected.

For the AC coupled system topology, the DC/AC inverter connected to the PV generator must be able to carry the maximum current produced at the DC side and match the maximum PV generator voltage. The selection of the fuel cell inverter is determined especially by the AC power to be provided and the fuel cell DC voltage. This inverter must be able to feed all the loads that might run at the same time, including any starting surges for pumps and large motors. In this topology, two different PCU types are used: Sunny Boy inverter with a high voltage level 600V for PV generator, and Sunny Island bi-directional inverter with low voltage levels of 40 to 80V for the electrochemical components. Other used PCU type is the SW Trace inverter which has a low input voltage 48V. A simulation of the AC coupled hybrid system with these PCU types over one year is performed. Figure 6.18 shows the annual losses in these inverters of the system in the two selected sites. In Cairo site, the Sunny Boy inverter used for PV generator has lower energy losses than SW Trace inverter. In contrast, Sunny Island inverter losses are higher than SW Trace bi-directional inverter losses when used for electrochemical units. This scenario is approximately the same in Kassel site. Thus, if the AC coupled system topology is used, the

Sunny Boy inverter is suitable for the PV generator and SW Trace bi-directional inverter is suitable for the electrochemical components, to obtain lower losses in the system. As a result, the Sunny Boy and the SW Trace inverters are recommended to use for the PV generator and the electrochemical components (electrolyser and fuel cell), respectively.

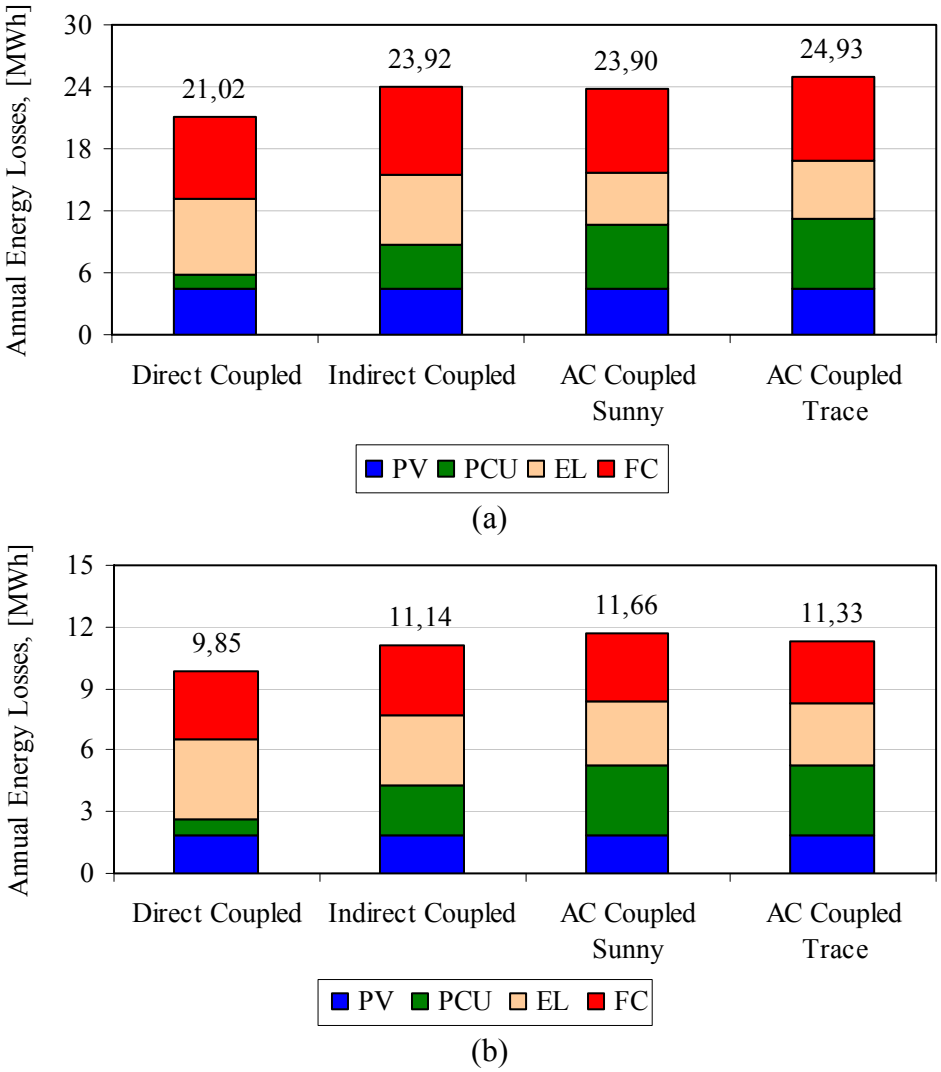

Fig. 6.17: Annual energy losses of the main components for hybrid system in (a) Cairo site; (b) Kassel site.

Figure 6.19 shows the annual storage capacity or state of charge (SOC) of the hydrogen storage during one year for the AC coupled system topology with Sunny family only, SW Trace family only, and mixed between them (Sunny Boy inverter for the PV generator and SW Trace inverter for the electrochemical components) according to the above discussion. It is clear that, the influence of the mixed PCU in the SOC of the hydrogen storage for the system at Cairo is higher than when the system is used the Sunny PCU only and the worst case when the system is used SW Trace PCU only. But, at Kassel, the influence of the mixed PCU in the SOC of the hydrogen storage for the system when compared with SW Trace PCU only is approximately identical and the worst case when the system is used the Sunny family only. A comparison

between the annual net hydrogen storage of AC coupled systems with different PCU types is shown in Fig. 6.20

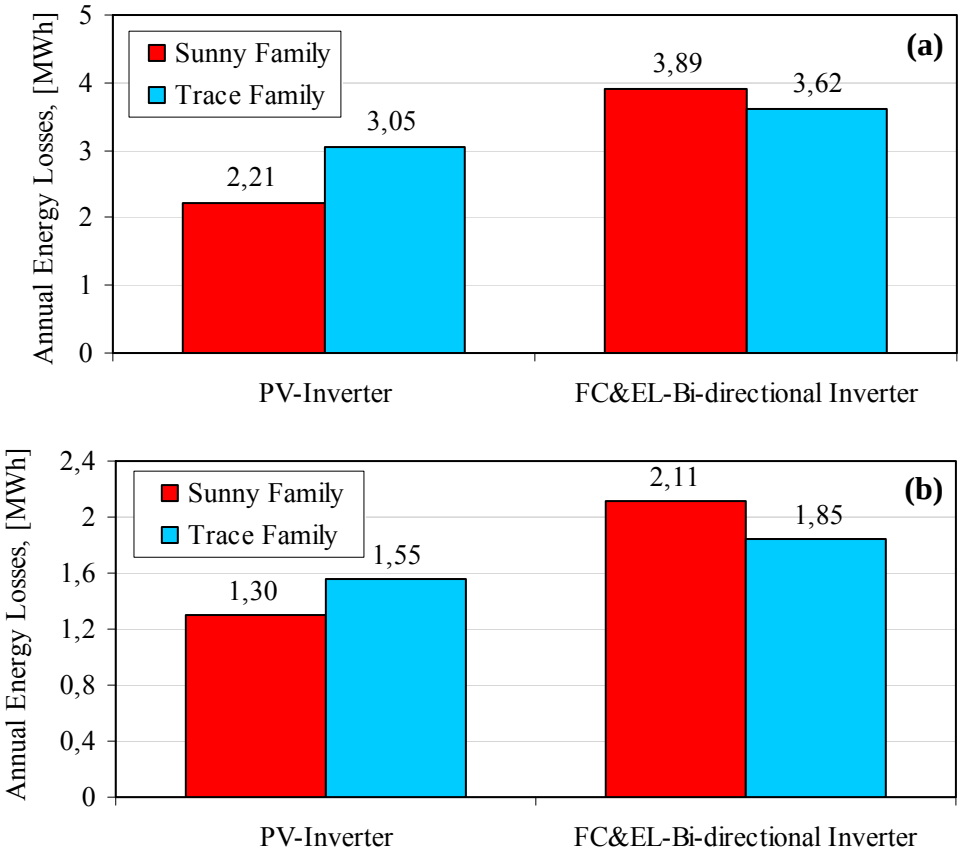

Fig. 6.18: Annual energy losses of the two different PCU types in (a) Cairo site; (b) Kassel site.

The monthly performance ratio, defined in Appendix G, for the different systems under both climatic conditions of Cairo and Kassel are shown in Fig. 6.21. From these figures, the seasonal trends in the utilization of the system can be well visualized. There are variations of the system performance ratio from month to month and more clearly from winter to summer. The trend of the curves reflects the fact that monthly solar radiation is higher in summer, leading to less system utilization in summer than in winter. In fact, the monthly performance ratios in Kassel are almost higher than in Cairo. This reflects the fact that the system works often at low temperatures and solar radiations and therefore it has low energy losses. The monthly performance ratios are more stable for the systems in Cairo than in Kassel. For example, in Cairo, the direct DC coupled system has the best performance ratio for all months and the AC coupled system with "Trace family only" has the worst performance ratio for almost all months. In Kassel, the direct DC coupled system does not give always the best performance ratio, but it is the worst in January and December.

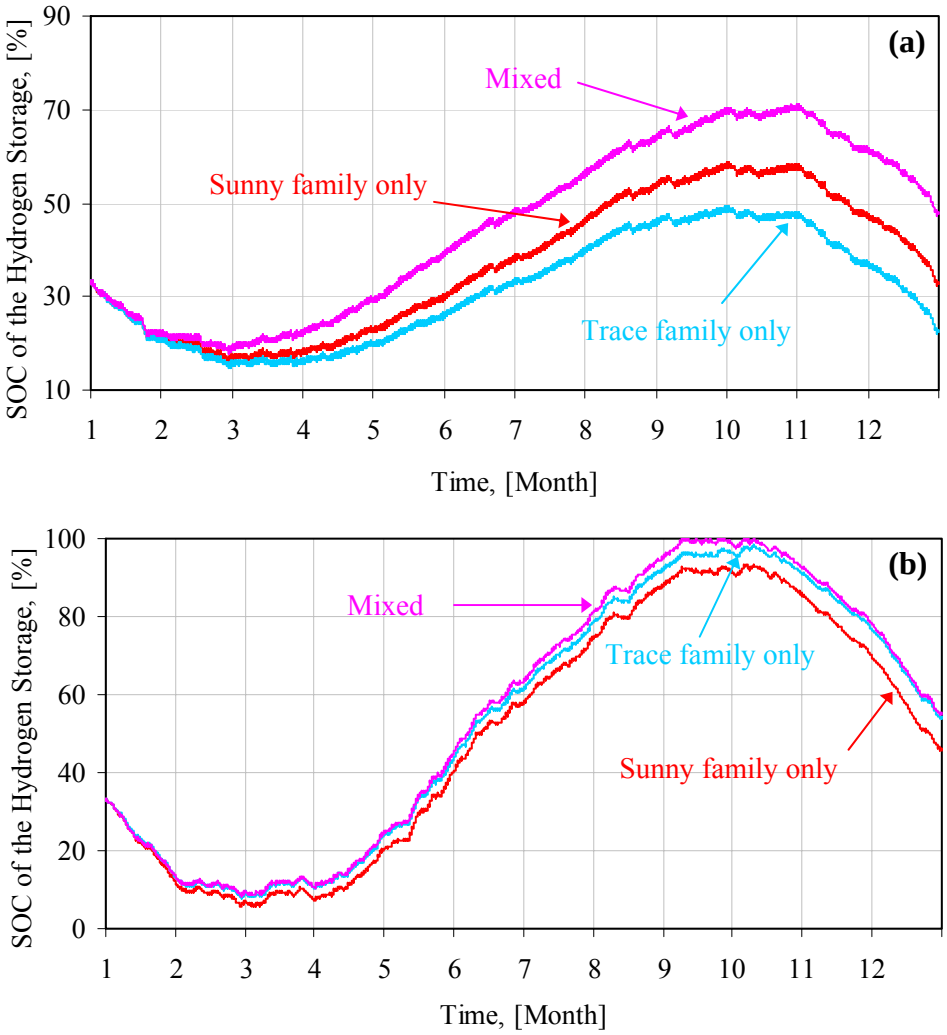

Fig. 6.19: Annual SOC of the hydrogen storage for two different PCU types in (a) Cairo site; (b) Kassel site.

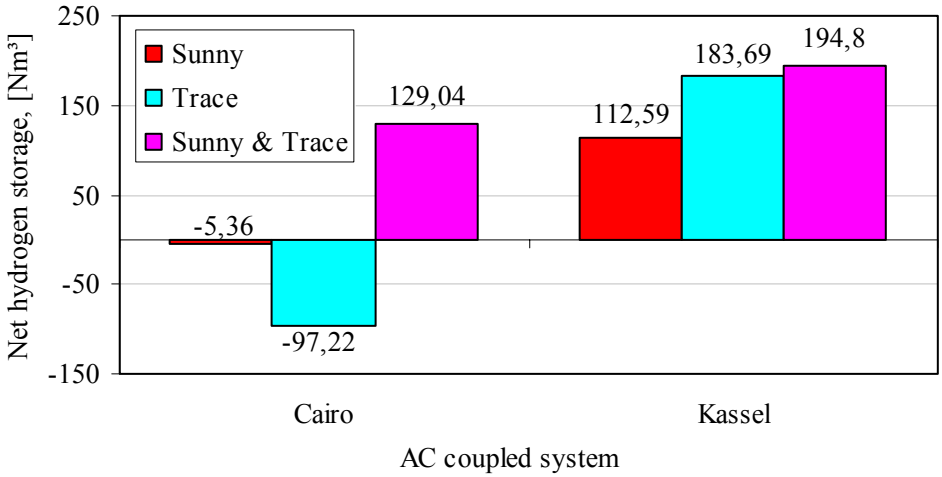

Fig. 6.20: Annual net hydrogen storage for different PCU types in the two sites.

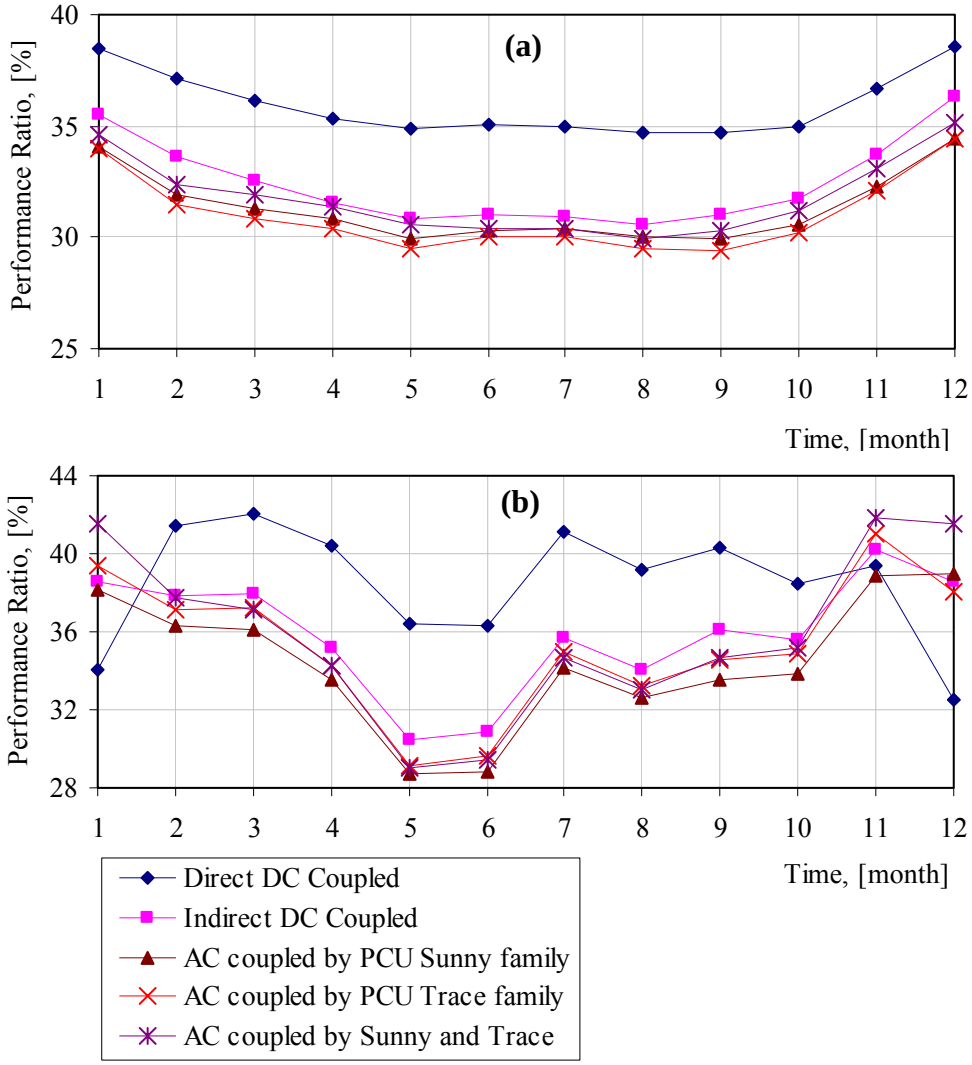

Fig. 6.21: Monthly Performance Ratio for different systems and sites: (a) Cairo; (b) Kassel.

6.11 Conclusions

The purpose of this chapter is to simulate integrated stand-alone hydrogen PVFC hybrid systems with different topologies in order to study their performance under short- and long-term operation. The simulation of these systems has enabled to perform detailed studies on the operation of the system since it uses the detailed models described in chapters 4 and 5.

The use of supercapacitors for short-term energy storage in hydrogen PVFC hybrid systems guarantees the instantaneous power balance between the components of the system and allows the voltage at the AC side to be kept very stable. The supercapacitors can also help in stabilizing the fuel cell operation within the set limits, especially under sudden load changes.

The main advantage of the direct coupled system to a DC bus-bar is that the energy losses associated with PCU are minimised. This configuration seems to be appropriate for small to

medium size systems, but it has a lot of problems associated with connecting the electrochemical components. On the other hand, using PCU is important to have a robust and flexible design. This is particularly important for large systems, where safety measures and costs for retrofitting and/or redesign are much greater than for smaller systems. However, AC coupled systems have higher losses and costs. The losses can be reduced by using advanced design concepts with higher efficiencies. The cost of the PCU can be also reduced by the use of a bi-directional DC/DC converter for DC-bus-bar or a bi-directional DC/AC inverter for AC-bus-bar to connect the electrolyser and fuel cell components, with other components of the system.

7. CONCLUSIONS AND RECOMMENDATIONS

The overall goal of this thesis is to investigate the operation of a stand-alone hydrogen PVFC hybrid system. A comparison between different system topologies such as DC direct or indirect and AC coupled in two locations with different geographical latitudes is studied. The main conclusions and recommendations drawn from this work are summarized next.

7.1 Simulation of Stand-Alone Hydrogen PVFC Hybrid System

In this work, a complete model for hydrogen PVFC hybrid system has been implemented in computer codes and utilized to predict its operational performance through numerical simulation. The Simplorer simulation environment has been selected for this work because it includes an advanced library for the system components called ISET-APL "ISET **A**lternative **P**ower **L**ibrary". This library has been compiled by the **I**nstitute of **S**olar **E**nergy supply **T**echnology in Kassel/Germany and comprises a number of models, which are used in PV hybrid systems technology. In this work, the ISET-APL has been used to simulate different system topologies at two completely different sites.

7.1.1 Modelling of Hydrogen PVFC Hybrid System Components

Detailed descriptions of the individual component models required to simulate a hydrogen PVFC hybrid system are presented. These models are mainly based on electrical and electrochemical relations. However, a number of empirical relationships for some models are also used. The models of PV generator, PEM fuel cell, alkaline water electrolyser, and power conditioning units are discussed in details, while supercapacitor and storage tank are presented by simple models.

The modelling, identification and validation of the component models show that the agreement between simulated and measured data is very good. Several short-term simulations are performed, such that the I-U characteristics, hydrogen production and consumption rates, and other physical processes of the individual component models are properly evaluated. The main conclusions that could be drawn from the evaluation of the individual component models of the hydrogen PVFC hybrid system are given in the following subsections.

7.1.1.1 PV generator

- Three PV generator models are studied in this work: one-, two-diode analytical model, and empirical model. The differences between them when evaluated by short-term simulations for one day at a location in Kassel/Germany with a time step of 15 seconds are found to be insignificant, thus each model is accurate enough for simulation purposes. The empirical

- model is recommended because it is very simple and all parameters can be found in the manufacturer's data sheet.
- The thermal behaviour of the PV generator is also studied using two models, a linear model and an empirical model which use the NOCT given by the manufacturer's data sheet. These models are evaluated by short-term simulations for one day in Kassel/Germany. The inclusion of wind speed in the calculations was not considered. The percentage deviations from the measured values are 0.014% for the linear model and 0.96% for the empirical model. Thus, the linear model is used in this work.

7.1.1.2 Hydrogen energy system

- The PEM fuel cell and alkaline water electrolyser are modelled by using analytical equations and including empirical aspects, when the theoretical analysis is either too complicated or the parameters are not accessible. The parameters of these models are determined for practical units. A 2.5kW PEM fuel cell is originally integrated into laboratory of the ISET in Kassel/Germany and a 3.6kW alkaline water electrolyser is installed at Agrate in Italy. The comparison between measured and simulated data for the PEM fuel cell shows that there is an good agreement between them; the mean RMS voltage error is about 14mV/cell and the percentage error in energy is less than 2% with 176 data measured points. The electrolyser model is also good, the maximum voltage difference between simulated and measured data saved every one minute over one day operation is about ±1.5V and the voltage percentage mean error is 0.94%.
- The comparison between simulated and measured data for hydrogen consumption in the PEM fuel cell is also positive. Calculations of the RMS error in hydrogen consumption for 152 samples show that the mean RMS error is 0.12 Nm^3/h and the percentage absolute error is not more than 1.8%. However, a comparison between simulated and measured hydrogen production was not done because no measured data are available.

7.1.1.3 Power conditioning units

In this work, three empirical PCU models, which are linear, quadratic, and piecewise linear, are studied. From the evaluation of these models, it is found that the accuracy of each of the quadratic and piecewise linear models is particularly good at powers above 10% of the rated power. At low powers, less than 10% of rated power, all the models do not accurate represent the measured data. The quadratic model is used to represent all the PCUs in this work. Two different inverter types, Sunny and Trace, are used in the hydrogen PVFC hybrid system.

7.1.2 Overall Operation of the Hydrogen PVFC Hybrid System

The main conclusions about the overall operation of the hydrogen PVFC hybrid system at two sites with different topologies that could be drawn from the integrated system simulation are:

- Using supercapacitor in the PV hybrid systems guarantees the power balance between the components and allows the voltage at the AC side to be kept very stable. It can also stabilize the fuel cell operation within the set limits especially when sudden load variations occur. This is better than to oversize the power sources, which is an expensive solution.
- The inclusion of a power conditioning unit with each component in the PV hybrid systems and using AC coupled gives the overall system a robust and flexible design, particularly for large systems, where the safety measures and costs for retrofitting and/or redesigning are usually much greater than for smaller systems. However, coupling PV generator, fuel cell, and/or electrolyser directly to the DC bus-bar may be a good alternative for small systems. The energy losses in this system associated with the power conditioning units are minimised.
- For long-term operation, the results of the simulation have been used for a detailed energy analysis, in which the energy conversion steps and losses for each individual component are analyzed and quantified, and their influence on the system overall efficiency is investigated. The mean annual performance ratios *PR* and final yields Y_f are utilized as two measures of the system performance to compare different system configurations at different sites with different PCU types, as given in Table 7.1.

Table 7.1: Mean annual performance ratio *PR* [%] and final yields Y_f [kWh/d/kWp] of hydrogen PVFC hybrid system with different topologies, sites, and PCU types

System configuration	Cairo/Egypt		Kassel/Germany	
	PR	Y_f	*PR*	Y_f
Direct DC coupled	39	2.39	42	1.29
Indirect DC coupled	35	2.15	38	1.15
AC coupled with PCU Sunny family	34	2.08	36	1.10
AC coupled with PCU Trace family	33	2.06	37	1.13
AC coupled with PCU Sunny &Trace families	34	2.11	37	1.13

- The results of the energy analysis have shown that the operational performance of the system does not depend only on component efficiencies but also on system design and consumption behaviour. The efficiency of the storage subsystem made of the electrolyser, the gas storage unit, and the fuel cell is still low, around 25-34% in Cairo and 29-37% in Kassel. This fact points out that the search for performance improvement of hydrogen PVFC hybrid system should be concentrated on development of subsystem components, especially the fuel cell and electrolyser.
- The results obtained from the analysis have shown that the performance of hydrogen PVFC hybrid system can be optimised in different ways: by understanding the system behaviour better, by improving component's efficiency, by utilizing new systems concepts, and by helping people to use their systems as efficiently as possible.

7.2 Recommendation for Future Work

To enhance the performance of hydrogen PVFC hybrid systems, the following recommendations for future work are proposed:

- Designing a new high pressure electrolyser that can operate at pressures over 200bar. This electrolyser could eliminate the need for a compressor to compress hydrogen into high pressure and, thus the volume of the gas storage tank is decreased. Other concept is to store the hydrogen in metal hydride (MH) storage, i.e., replacing the compressed hydrogen gas storage with low pressure ambient temperature metal hydride storage. The greatest advantage of the MH-storage is that it can be coupled directly to a low pressure electrolyser, thus eliminating the need for a compressor. The choice of the suitable concept should be based on the type of application.
- Adding other renewable sources, such as a wind turbine, to the system. A wind energy conversion would reduce the required PV generator area, and reduce the hydrogen storage volume. A trade-off between PV generator area and wind generator size is an interesting challenge for systems located at sites with high average wind speeds.
- A practical limitation on the system design is the voltage operating range of the available power conditioning units, which are designed mainly for lead-acid batteries rather than fuel cells or supercapacitors. As a result, an optimum energy utilization of the supercapacitors and fuel cells could not be achieved. Thus, designing a new power conditioning units that can match the characteristics of these components is recommended.
- In hydrogen PVFC hybrid system without battery energy storage, such as in this work, the annual numbers of the on and off switching of the electrochemical components and also the annual operating times of these components are large, see simulation results in Table 6.3, leading to large hydrogen losses. This would probably affect in the overall simulation results, if the hydrogen losses are not included in the simulation. These losses must be calculated to make the simulation more accurate.
- The H_2/O_2 PEM fuel cell has a better performance than the Air/H_2 PEM fuel cell which is used in this work, but requires a storage tank for oxygen and a purification system. Thus, it is recommended to study using H_2/O_2 PEM fuel cell with the PVFC hybrid system and evaluate the system according to the cost point of view.

8. REFERENCES

[**Ahmad-97**] G. E. Ahmad, M. A. Mohamad, S. A. Kandil, and R. Hanitsch: *Fault Detection in PV Generators Using an Improved Electronic Load*, 14th EPVSEC, Barcelona, Spain, 1997, pp. 199-202.

[**Almonacid-98**] M. Almonacid and J. Aguilera: *Fuzzy Logic Charge Regulator*, 2nd World Conference And Exhibition on PV Solar Energy Conversion, Vienna, Austria, 1998, pp. 3273-3275.

[**Amphlett-95**] J. C. Amphlett, R. M. Baumert, R. F. Mann, B. A. Peppley, and P. R. Roberge: *Performance Modelling of the Ballard Mark IV Solid Polymer Electrolyte Fuel Cell: II. Empirical Model Development*, Journal of the Electrochemical Society, Vol. 142, No. 1, 1995, pp. 9-15.

[**Bafna-02**] R. Bafna, J. Beulow, and et al: *Transition to a Hydrogen-Based Energy Systems: The next Ten Years*, Conferences-Reinforcement Papers, Toronto, Canada, 2002. http://www.epp.cmu.edu/undergraduate/summaries/HydrogenEnergy/final-paper.pdf

[**Balkin-02**] A. R. Balkin: *Modelling A 500W Polymer Electrolyte Membrane Fuel Cell*, Bs. D., University of Technology, Faculty of Engineering, Sydney, 2002.

[**Barbir-97**] F. Barbir and T. Gomez: *Efficiency and Economics of Proton Exchange Membrane (PEM) Fuel Cells*, Int. J. Hydrogen Energy, Vol. 22, No. 10/11, 1997, pp. 1027-1037.

[**Barbir-03**] F. Barbir: *Review of Hydrogen Conversion Technologies*, Clean Energy Research Institute, University of Miami, Coral Gables, FL 33124, U.S.A, Visit 2003. http://www.iahi.org/H2Convrt.doc

[**Barrade-00**] P. Barrade, S. Pittet, and A. Rufer: *Series connection of supercapacitors, with an active device for equalizing the voltages*, PCIM 2000: International Conference on Power Electronics, Intelligent Motion and Power Quality, Nürnberg, Germany, 2000.

[**Barrade-02**] P. Barrade and A. Rufer: *Considerations on the energy efficiency of a supercapacitive tank*, MAGLEV 2002: International Conference on Magnetically Levitated Systems and Linear Drives, Lausanne, Switzerland, 2002.

[**Barrade-03**] P. Barrade: *Energy storage and applications with supercapacitors*, ANAE: Associazione Nazionale Azionamenti Elettrici, 14o Seminario Interattivo, A Zionamenti elettrici: Evoluzione Tecnologicae Problematiche Emergenti, Bressanone, Italy, 2003.

[**Bendel-03**] C. Bendel and A. Wagner: *Photovoltaic Measurement Relevant to the Energy Yield*, WCPEC-3 World Conference on Photovoltaic Energy Conversion, Osaka, Japan, Pr. No. 7P-B3-09, 2003, pp. 1-4.

[**Benz-03**] J. Benz, B. Ortiz, W. Roth, and et al: *Fuel Cells in Photovoltaic Hybrid Systems for Stand-Alone Power Supplies*, 2nd European PV-Hybrid and Mini-Grid Conference, Kassel, Germany, 2003, pp. 232-239.

[**Bernardi-92**] D. M. Bernardi and M. W. Verbrugge: *A Mathematical Model of the Solid-Polymer-Electrolyte Fuel Cell*, Journal of the Electrochemical Society, Vol. 139, No. 9, 1992, pp. 2477-2491.

[**Bocklisch-03**] Thilo Bocklisch: *Modellbildung und dynamische Simulation eines 2.5kW PEM-Brennstoffzellen-Systems*, Diplomingenieur, Fakultät für Elektrotechnik und Informationstechnik der Technischen Universität Chemnitz, Deuchland, 2003.

[**Braun-00**] A. Braun and E. Krause: *A study on oxidized Glassy carbon sheets for Bipolar Supercapacitor Electrodes*, Mat. Res. Soc. Symp. Proc., Vol. 575, 2000, pp. 369-380.

[**Burke-00**] A. Burke: *Ultracapacitors: why, how, and where is the technology*, Journal of power sources 91, 2000, pp. 37-50. http://www.elsevier.com/locate/jpowsour

[**Burger-00**] B. Burger and P. Zacharias: *Hybrid Systems-Easy in Configuration and Application*, Proc. of 16th EPVSEC, Glasgow, UK, 2000, pp. 2195-2197.

[**Busquet-00**] S. Busquet, R. Metkemeyer and D. Mayer : *Development of a Clean Stand-alone Power System Integrating PV, Fuel Cell and Electrolyser*, Proc. of the Photovoltaic Hybrid Power Systems Conference, Aix en Provence, Session I, Oral n° 5, 2000.

[**Busquet-02**] S. Busquet, F. Domain, R. Metkemeijer, and D. Mayer: *Stand Alone Power System Coupling a PV Field and a Fuel cell Description of the Selected System and Advantages*, Proc. of the Photovoltaic Hybrid Power Systems Conference, Rome, Italy, 2002, pp. 667-670.

[**Busquet-03**] Severine Busquet: *Study of a Stand Alone Power System Based on a Photovoltaic Field, an Electrolyseur and a Fuel Cell: Test bench and Modelisation*, PhD, Centre d'Energetique, Ecole des Mines de Paris, France, 2003.

[**Caamano-95**] E. Caamano and E. Lorenzo: *Inverters in PV grid connected systems: an assessment on the proper selection*, Proc. 13th EPVSEC, 1995, pp. 1900–1903.

[**Caselitz-03**] P. Caselitz, D. Lehmkuhl, and B. Panahandeh: *ISET Alternative Power Library-Universal Model Library for Simulation of Decentralised Power Supply Systems*, 2nd European PV-Hybrid and Mini-Grid Conference, Kassel University, Germany, 2003, pp. 456-461.

[**Cotrell-03**] J, Cotrell and W. Pratt: *Modelling the Feasibility of Using Fuel Cells and Hydrogen Internal Combustion Engines in Remote Renewable Energy Systems*, WINDPOWER Conference, NREL/CP-500-34043, Austin, Texas, 2003.

[**Dumbs-99**] Christian DUMBS: *Development of analysis tools for photovoltaic-diesel hybrid systems*, PhD, Paris, 1999.

[**Duzat-00**] Rejane Moraes-Duzat: *Analytical and Experimental Investigation of Photovoltaic Pumping Systems*, Ph.D. dissertation, University Oldenbury, Germany, 2000.

[**Edelmoser-97**] K.H. Edelmoser and F. A. Himmelstoss: *High Efficiency DC-AC Inverter for Solar Application*, Proceeding of the 14th EPVSEC, Barcelona, Spain, 1997, pp. 2180-2283.

[**Engler-97**] A. Engler, O. Haas, F. Raptis, J. Sachau, and P. Zacharias: *Standard Interface for PV and Hybrid Systems*, 14th EPVSEC, Barcelona, Spain, 1997, pp. 1074-1077.

[**Engler-01**] A. Engler, C. Hardt, P. Strauss, and et al: *Parallel Operation of Generators for Stand-Alone Sinle-phase Hybrid Systems – First Implementation of a New Control Technology*, 17th EPVSEC, Munich, Germany, 2001, pp. 2690-2693.

[**Fry-98**] Bryan Fry: *Simulation of Grid-Tied Building Integrated Photovoltaic Systems*, M.Sc., University of Wisconsin, Madison, 1998.

[**Gomatom-03**] P. Gomatom and W. Jewell: *Fuel Parameter and Quality Constraints for Fuel Cell Distributed Generators*, proceedings of the IEEE Transmission and Distribution Conference, Wichita State University, Wichita, KS, 2003.
http://www.pserc.wisc.edu/ecow/get/publicatio/2003public/

[**HIL*Tech*-01**] HIL*Tech* Developments Limited: *Super Capacitors calculation Data*, 2001. http://www.hiltechdevelopments.com/downloads/supercap-01.pdf

[**Hirschenhofer-99**] J.H. Hirschenhofer, D.B. Stauffer, R.R. Engleman, and M.G. Klett: *Fuel Cell Handbook*, Fourth Edition, Federal Energy Technology Centre, P.O. Box 880,3610 Collins Ferry Road, Morgantown, WV 26507-0880, 1999.

[**Hoffmann-01**] Winfried Hoffmann: *PV Solar Electricity: One Among the New Millennium Industries*, 17th EPVSEC, Paper No. PB 2.1, Munich, Germany, 2001, pp. 851-861.

[**Hollmuller-00**] P. Hollmuller, J. Joubert, B. Lachal, and K. Yvon: *Evaluation of a 5 kWp Photovoltaic Hydrogen Production and Storage Installation for a Residential Home in Switzerland*, International Journal of Hydrogen Energy 25, 2000, pp. 97-109.

[**Hoogers-03**] G. Hoogers: *Fuel Cell Technology handbook*, CRC press LLC, 2003.

[**Hottinen-01**] T. Hottinen: *Technical Review and Economic Aspects of Hydrogen Storage Technologies*, MSc, Helsinki University of Technology, Department of Engineering Physics and Mathematics, Espoo, 2001.

[**Ibrahim-02**] M. Ibrahim: *Decentralized Hybrid Renewable Energy Systems Control Optimization and Battery Ageing Estimation Based on Fuzzy Logic*, Ph.D. dissertation, Kassel University, Germany, 2002.

[**Jahn-98**] U. Jahn, and et al: *International Energy Agency Task II Database on Photovoltaic Power Systems: Statistical and Analytical Evaluation of PV Operational Data*, Proc. 14th EPVSEC, Vienna, Austria, 1998.

[**Jahn-00**] U. Jahn, B. Grimmig, and W. Nasse: *Analysis of Photovoltaic Systems*, Report IEA-PVPS T2-01, 2000.

[**Jahn-01**] U. Jahn, and W. Nasse: *Operational Performance, Reliability and Promotion of Photovoltaic Systems*, Report IEA-PVPS Task2, 2001.

[**Jantsch-92**] M. Jantsch, H. Schmidt, and J. Schmid: *Results of the concerted action on power conditioning and control*, Proc. 11th EPVSEC, 1992, pp. 1589 – 1593.

[**Jantsch-97**] M. Jantsch, M. Real, H. Häberlin, C. Whitaker, K. Kurokawa, G. Blässer, P. Kremer, and C. W. G. Verhoeve: *Measurement of PV Maximum Power Point Tracking Performance*, 14th EPVSEC, Barcelona, Spain, 1997, pp. 2188-2193.

[**Jaouen-03**] F. Jaouen: *Electrochemical Characterisation of Porous Cathodes in the Polymer Electrolyte Fuel Cell*, Ph.D., Department of Chemical Engineering and Technology, Kungl Tekniska högskolan, Stockholm, 2003.

[**Jeong-02**] J. Jeong, H. Lee, C. Kim, H. Choi, and B. Cho: *A Development of an Energy storage System for hybrid Electric Vehicles using Supercapacitor*, Proceedings of the 19th

International battery, Hybrid and Fuel Cell Electric Vehicle Symposium and Exhibition, BEXCO, Busan, Korea, 2002, pp. 1379-1389.

[**Kansteiner-98**] B. Kansteiner, Ph. Strauß, K. Preiser, P. Schweizer, and H. Aulich: *Rural Electrification Project with Photovoltaic-Hybrid Systems and Solar Home Systems for Vietnam*, 2th World Conference and Exhibition on Photovoltaic Solar Energy Conversion, Vienna, Austria, 1998, pp. 3010-3013.

[**Kato-03**] T. Kato, M. Kubota, N. Kobayashi, and Y.Suzuoki: *Effective Utilization of By-Product Oxygen of Electrolysis Hydrogen Production*, Annual Meeting of the International Energy Workshop (IEW), Laxenburg, Austria, 2003.
http://www.iiasa.ac.at/Research/ECS/IEW2003/Papers/2003P_kato.pdf

[**Key-03**] T. S. Key, H. E. Sitzlar, and T. D. Geist: *Fast Response, Load-Matching Hybrid Fuel Cell*, EPRI PEAC Corp., NREL/SR-560-32743, Knoxville, Tennessee, 2003.

[**Kim-03**] Y. H. Kim (NESSCAP Company): *Ultracapacitor Technology: Powers Electronic Circuits*, Power Electronics Technology, 2003, pp. 34-39.

[**Kininger-03**] Franz Kininger: *Photovoltaic Systems Technology*, Rationelle Energiewandlung, Universistät Kassel, Deutchland, 2003.

[**Kleinkauf-94**] W. Kleinkauf and J. Sachau: *Components for modular Expandable and Adaptable PV systems*, 12th EPVSEC, Amsterdam, the Netherlands, 1994, pp. 1711-1713.

[**Kleinkauf-95**] W. Kleinkauf, F. Raptis, J. Sachau, P. Zacharias, and et al: *Modular Systems Technology for Decentral Electrification – Components for Modular Expandable and Adaptable PV systems*, 13th EPVSEC, Nice, France, 1995, pp. 1006-1010.

[**Kleinkauf-03**] W. Kleinkauf, M. Ibrahim, O. Haas, and B. Gruß: *Basics of Hybrid Technology for Grid Compatible Stand-Alone Plants*, 2nd European PV-Hybrid and Mini-Grid Conference, Kassel, Germany, 2003, pp. 61-67.

[**Klementov-01**] A. D. Klementov, S.V. Litvinenko, A.B. Stepanov, and I.N. Varakin: *Internal Losses and Features of Asymmetric Capacitor Operation*, 11th International Seminar on Double Layer Capacitors, Deerfield Beach, Florida, 2001.

[**Kordesch-96**] K. Kordesch, and G. Simader: *Fuel Cells and Their Applications*, VCH, 1996.

[**Krauter-00**] S. Krauter and R. Araujo: *New Power Conditioning Unit Incorporating Charge Controller, Energy Flow Monitor, Data Logger, DC/AC Converter for Stand Alone and Combined PV-Diesel Operation*, Proc. 16th EPVSEC, Glasgow, UK, 2000, pp. 2575-2577.

[**Kuo-01**] Yeong-Chau Kuo and Tsorng-Juu Liang: *Novel Maximum-Power-Point-Tracking Controller for Photovoltaic Energy Conversion System*, IEEE transactions on industrial electronics, Vol. 48, No. 3, 2001, pp. 594-601.

[**Lai-95**] R. Lai and K. Ngo: *A PWM Method for Reduction of Switching Loss in a Full-Bridge Inverter*, IEEE Transactions on Power Electronics, Vol. 10, No. 3, 1995, pp. 326-332.

[**Landau-97**] M. Landau, T. Krieger, C. Schmitz, M. Schröder, and P. Zacharias: *Pilot Plant Starkenburger Hütte*, FhG-ISE and Uni. Kassel, 1996-2005.

[**Louche-94**] A. Louche, G. Notton, P. Poggi, and G. Peri: *Global approach for an Optimal Grid Connection PV System Sizing*, Proc. 12th EPVSEC, 1994, pp. 1638–1641.

[**Macagnan-92**] M.H. Macagnan and E. Lorenzo: *On the Optimal Size of Inverters for Grid Connected PV Systems*, Proc. 11th EPVSEC, 1992, pp. 1167–1170.

[**Mayer-01**] D. Mayer, R. Metkemeijer, S. Busquet, P. Caselitz, J. Bard, and et al: *Photovoltaic/Electrolyser/Fuel cell Hybrid System the Tomorrow Power Station for Remote Areas*, 17th EPVSEC, Munich, Germany, 2001, pp. 2529-2530.

[**Meinhardt-03**] Mike Meinhardt: *New V/f-Static's controlled Battery Inverter: Sunny Island – the key component for AC-coupled Hybrid Systems and Mini Grids*, 2nd European PV-Hybrid and Mini-Grid Conference, University Kassel, Germany, 2003, pp. 245-250.

[**Mikkola-01**] M. Mikkola: *Experimental Studies on Polymer Electrolyte Membrane Fuel Cell Stacks*, MSc, Helsinki University of Technology, Department of Engineering Physics and Mathematics, Espoo, 2001.

[**Miller-00**] E. Miller and R. Rocheleau: *Photo-electrochemical hydrogen production*, Proceedings of the Hydrogen Program Review, 2000.
http://www.hnei.hawaii.edu/PEC/HNEI_PEC_00.pdf

[**Möller-00**] C. Möller and R. Lucks: *Seminar: Fuel Cells*, Technical faculty, University of Kiel, Germany, 2000. http://www.texnic.de/FC/

[**Müller-97**] Christof Müller: *Interakives Modell für den Betrieb von Photovoltaikanlagen mit Energiespeicherpfaden*, Ph.D., Gerhard-Mercator-Universität Duisburg, Germany, 1997.

[**Myrzik-97**] J. Myrzik and P. Zacharias: *New inverter technology and harmonic distortion problems in modular PV systems*, Proceeding of the 14th EPVSEC, Barcelona, Spain, 1997, pp. 2207-2210.

[**Namisnyk-03**] A. M. Namisnyk: *A survey of Electrochemical Supercapacitor Technology*, B.Sc., faculty of Engineering, University of Technology, Sydney, 2003.

[**Noponen-00**] M. Noponen: *Experimental Studies and Simulations on Proton Exchange Membrane Fuel Cell Based Energy Storage Systems*, MSc, Helsinki University of Technology, Department of Engineering Physics and Mathematics, Espoo, 2000.

[**Ogden-02**] Dr. Joan M. Ogden: *Review of Small Stationary Reformers for Hydrogen Production*, a report for International Energy Agency (IEA) agreement on the production and utilization of Hydrogen, Princeton University, 2002.

[**Preiser-97**] K. Preiser, L. Anton, G. Bopp, K. V. Dohlen: *Photovoltaics, Hydropower and Gas generator The Hybrid Energy System in Kaysersberg (France)*, 14th EPVSEC, Barcelona, Spain, 1997, pp. 1106-1109.

[**Prophet-03**] G. Prophet (gpropbet@reedbusiness.com): *Supercaps for Supercaches*, END magazine, 2003, pp. 53-58.
http://www.e-insite.net/endmag/contents/images/268379.pdf

[**Protogeropoulos-97**] C. Protogeropoulos and M. Soursos: *Ecological Tourism: An Innovative Stand-Alone PV/Hybrid Commercial Installation in Greece for the Electrification of a Complex of Twelve Bungalows*, 14th EPVSEC, Barcelona, Spain, 1997, pp. 1671-1676.

[**Pyle-94**] W. Pyle, J. Healy, and R. Cortez: *Solar Hydrogen Production by Electrolysis*, Home Power (HP) #39, 1994, pp. 32-38.

[**Redi-01**] P. Redi, J. Soler, J. Esteban, A. Simmons, and M. Ruzinsky: *High Efficiency Converter*, Proceeding of the 17th EPVSEC, Munich, Germany, 2001, pp. 2791-2793.

[**Remund-00**] J. Remund, S. Kunz, and R. Lang: *METEONORM® 4.0: Global meteorological database for solar energy and applied climatology*, Solar Engineering Handbook, 2000.

[**Rufer-02**] A. Rufer and P. Barrade: *A Supercapacitor-Based Energy-Storage System for Elevators With Soft Commutated Interface*, IEEE Transactions on Industry Applications, Vol. 38, Issue 5, 2002, pp. 1151-1159.

[**Sayigh-97**] A. A. M. Sayigh: *Photovoltaic Applications in the Arab World*, 14th EPVSEC, Barcelona, Spain, 1997, pp. 452-456.

[**Schmid-97**] J. Schmid and W. Kleinkauf: *New Trends in Photovoltaic Systems Technology*, 14th EPVSEC, Barcelona, Spain, 1997, pp. 1337-1339.

[**Schneuwly-02**] A. Schneuwly, M. Bärtchschi, V. Hermann, G. Sartorelli, R. Gallay, and R. Kotz: *BOOSTCAP Double-layer capacitors for peak power automotive applications*, Proceedings of the 2nd International Advanced Automotive Battery Conference (AABC), Las Vegas, Nevada, USA, 2002.

[**Singer-84**] S. Singer, B. Rozenshtein, and S. Surazi: *Characterization of PV array output using a small number of measured parameters*, Solar Energy, Vol. 32, No. 5, 1984, pp. 603-607.

[**Solmecke-94**] H. Solmecke, G. Scheible, and D. Hackstein: *System Engineering of the Solar Hydrogen Plant in Jülich (FRG)*, Proc. 12th EPVSEC, 1994, pp. 444-447.

[**Solmecke-97**] H. Solmecke and D. Hackstein: *Simple bi-directional DC-DC converter with high efficiency for use with fuel-cell and electrolyzer in solar hydrogen storage systems*, Proc. 14th EPVSEC, 1997, pp. 2280–2283.

[**Solmecke-00**] H. Solmecke, O. Just, and D. Hackstein: *Comparison of solar hydrogen storage systems with and without power-electronic DC-DC-converters*, Renewable Energy 19, 2000, pp. 333-338.

[**Strauss-00**] P. Strauss, R.P. Wurtz, O. Haas, M. Ibrahim, and et al: *Stand-alone AC PV Systems and Micro Grids with New Standard Power Components – First Results of Two European Joule Projects PV – MODE and MORE*, 16th EPVSEC, Glasgow, UK, 2000, pp. 2613-2617.

[**Ulleberg-98**] Oystein Ulleberg: *Stand-alone power systems for the future: optimal design, operation & control of Solar-Hydrogen energy systems*, Ph.D. dissertation, Norwegian University, Trondheim, 1998.

[**Taylor-03**] H. Taylor: *Fuel Cell Report to Congress*, 2003.
http://www.eere.energy.gov/hydrogenandfuelcells/pdfs/fc_report_congress_feb2003.pdf

[**Varakin-99**] I. N. Varakin, A. D. Klementov, and S. V. Litvinenko: *Power Characteristics of "ESMA" Capacitors*, 9th International Seminar on Double Layer Capacitors and Similar Storage Devices, Deerfield Beach, Florida, 1999.

[**Veziroglu-04**] T. Veziroglu: *Hydrogen Energy System: A Permanent Solution to Global Problems*, Clean Energy Research Institute, USA, Web Site, visit 2004.
http://www.iahe.org/Hydrogen_energy_system.htm

[**VLEEM-02**] VLEEM: Final report: *Very Long Term Energy Environment Modelling*, 2002. http://www.vleem.org/PDF/annex8-monograph-distribution.pdf

[**Vosen-99**] S.R. Vosen and J. O. Keller: *Hybrid energy storage systems for stand-alone electric power systems: optimisation of system performance and cost through control strategies*, International Journal of Hydrogen Energy, 24, 1999, pp. 1139–1156.

[**Wagner-00**] A. Wagner: *Peak-Power and Internal Series Resistance Measurement under Natural Ambient Conditions*, Proc. (CD-ROM) EuroSun, Copenhagen, 2000.

[**Wang-92**] J. T. Wang and R. F. Savinell: *Simulation studies on the fuel electrode of a H_2-O_2 polymer electrolyte fuel cell*, *Electrochimia Acta*, vol. 37, No. 15, Great Britain, 1992, pp. 2737-2745.

[**Wedler-87**] Gerd Wedler: *Lehrbuch der Physikalischen Chemie*, Third Edition, VCH Verlagsgesellschaft mbH, D-6940 Weinheim (Federal Republic of Germany), 1987.

[**Wendt-90**] Hartmut Wendt: *Electrochemical Hydrogen Technologies, Electrochemical Production and Combustion of Hydrogen*, ELSEVIER, 1990.

[**WS-esma-04**] Web Site, ESMA Company, Visit 2004. http://www.esma-cap.com

[**WS-pvfcsys-04**] Web Site, visit 2004. http://pvfcsys.cma.fr/pilot_system/index.html

[**WS-qtww-03**] Web Site, Quantum Technologies, Inc., Visit 2003. http://www.qtww.com

[**WS-water-04**] Web Site, Water Resources- Office Water Quality: *National Field Manual for the collection of Water-Quality Data*, visit 2004. http://water.usgs.gov/owq/FieldManual/

[**Wurster-99**] Reinhold Wurster: *PEM Fuel Cells in Stationary and Mobile Applications-Commercialisation*, Ludwig-Bölkow-Systemtechnik GmbH, Daimlerstrasse 15, D-85521 Ottobrunn, 1999. http://www.lbst.de

[**ZSW-02**] *Reference Manual 2.5kW Fuel Cell System*, Centre of Solar Energy and Hydrogen Research (ZSW), Baden-Württemberg, Germany, 2002.

9. APPENDIXES

Appendix A: Photovoltaic Cell Model

➢ ***One-diode model*** [Dumbs-99]

The characteristic equation of the PV cell model $I_s=f(U_s, I_s)$ is obtained by applying Kirchoff's current law to the equivalent circuit Fig. A.1, where I_s [A] and U_s [V] are the terminal current and voltage of the model respectively:

$$I_s = I_{ph} - I_d - I_{sh} \qquad \text{A.1}$$

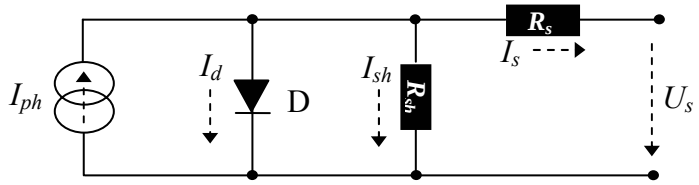

Fig. A.1: Equivalent circuit of the PV cell one-diode model.

The photocurrent I_{ph} [A] is directly dependent on the solar radiation E_s and the ambient temperature T_a and is modelled by:

$$I_{ph} = P_1 E_s \left[1 + P_2 (E_s - E_0) + P_3 (T_j - T_0)\right] \qquad \text{A.2}$$

Where E_0 =1000W/m² and T_0 =298.15K correspond to a reference solar radiation and a reference ambient temperature, respectively. P_1 [Am²/W], P_2 [m²/W] and P_3 [1/K] are constant parameters.

The I-U characteristic of a PV cell is also influenced by the temperature of the cell. The cell temperature is a simple linear function of the cell junction temperature T_j [K] and the global solar radiation E_s [W/m²]. Equation A.3 below describes the junction temperature, where the ambient temperature T_a [°C] determines the crossing point of the function on the vertical axis:

$$T_j = (T_a + 273.15) + \frac{E_s}{800 W/m^2}(NOCT - 20) \qquad \text{A.3}$$

Where, *NOCT* is a parameter and called "*Normal Operating Cell Temperature*". It is given by the PV cell module manufacturer, mostly between 45 and 49°C.

The diode loss current I_d [A] due to charge carrier recombination is given by:

$$I_d = I_{sat}.\left[\exp(\frac{e_0}{a_f N_s k}\frac{U_s + R_s I_s}{T_j}) - 1\right] \quad \text{A.4}$$

Where $I_{sat} = P_4 T_j^3 \exp(-\frac{E_g}{kT_j})$ saturation current, [A]

e_0 electron charge, [C]

a_f ideality factor of the photovoltaic array, [-]

N_s number of cells in series, [-]

k Boltzmann's constant, [J/K]

R_s series resistance, [Ω]

E_g gap energy, [eV] and

P_4 correction parameter, [A/K^3]

Finally, the shunt current I_{sh} [A] is calculated from:

$$I_{sh} = \frac{U_s + R_s I_s}{R_{sh}} \quad \text{A.5}$$

Where R_{sh} [Ω] is shunt resistance.

➢ ***Two-diode model*** [Duzat-00]

The characteristic equation of this model is obtained by the same manner as for the one-diode model. Figure A.2 shows the equivalent circuit of the two-diode model. The terminal current I_s [A] is given by:

$$I_s = I_{ph} - (I_{d1} + I_{d2}) - I_{sh} \quad \text{A.6}$$

Where

$$I_{d1} + I_{d2} = I_{sat1}\left[\exp(\frac{e_0}{\alpha.a_f N_s k}\frac{U_s + R_s I_s}{T_j}) - 1\right] + I_{sat2}\left[\exp(\frac{e_0}{\beta.a_f N_s k}\frac{U_s + R_s I_s}{T_j}) - 1\right] \quad \text{A.7}$$

α and β are fit parameters that are set to 1 and 2 respectively in the two-diode model. The dependence of the saturation currents on temperature is given by:

$$I_{sat1} = P_{01} T_j^3 \exp(-\frac{E_g}{kT_j}) \quad \text{A.8}$$

$$I_{sat2} = P_{02} T_j^{\frac{5}{2}} \exp(-\frac{E_g}{2kT_j}) \quad \text{A.9}$$

Where P_{01} [A/K³] and P_{02} [A/K$^{5/2}$] are constant parameters.

Furthermore, the photocurrent I_{ph} [A] is proportional to the solar radiation E_s and is assumed to be linearly dependent on the cell temperature T_j:

$$I_{ph} = (P_1 + P_2 T_j) \times E_s \qquad \text{A.10}$$

Where P_1 [Am²/W] and P_2 [Am²/WK] are constant parameters.

The shunt-current I_{sh} is expressed in the same way as for the one-diode model.

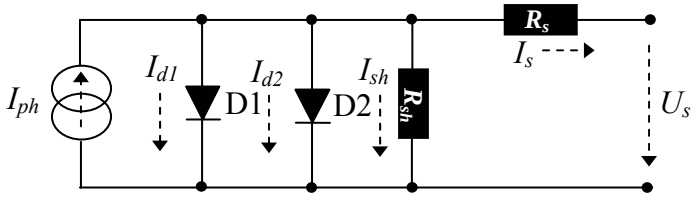

Fig. A.2: Equivalent circuit of the PV cell two-diode model.

➢ ***Empirical model*** [Singer-84]

This model describes the behaviour of a PV cell via the equivalent electrical circuit shown in Fig. A.3., which consists of a current source I_{ph}, a parallel-connected diode D and a series resistor R_s. The main advantage of this model is the limited number of parameters, which can be found in manufacturer's data sheet. The equation describing the I-U curve of the PV cell is:

$$I_s = I_{ph} - I_d \qquad \text{A.11}$$

The photocurrent and diode loss current cannot be measured by a simple manner. Therefore, a few number of parameters which can be measured easily such as open-circuit voltage (U_{oc}); short-circuit current (I_{sc}); and maximum power (P_{max}) are used to represent this model.

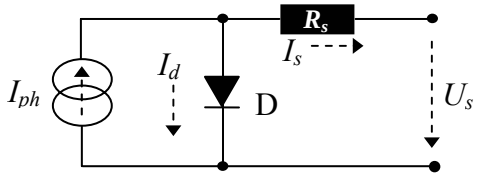

Fig. A.3: Equivalent circuit of the PV cell empirical model.

In Equation A.11, the following simplification is used: $I_{ph} \approx I_{sc}$ and substituting $\delta = e_0/a_f k T_j$ (see I_d in Equation A.4), the I-U curve can be expressed as:

$$I_s = I_{sc}\left[1 - \left(\frac{I_{sat}}{I_{sc}}\right)\exp\delta(U_s + I_s R_s)\right] \qquad \text{A.12}$$

Since δ and R_s are unknown, two conditions are required to find them:

1. At $I_s = 0$, then $U_s = U_{oc}$
2. At the maximum power point $U_s(I_{s,max}) = P_{max}/I_{s,max}$

From condition 1: $$U_{oc} = U_s\big|_{I_s=0} = \frac{1}{\delta}\ln\left(\frac{I_{sc}}{I_{sat}}\right) \text{ or } \delta = \frac{1}{U_{oc}}\ln\left(\frac{I_{sc}}{I_{sat}}\right) \quad \text{A.13}$$

It was found that a typical value of the ratio I_{sat}/I_{sc} for a silicon cell at standard test conditions (T_0=25°C, E_0=1000 W/m²) ranges approximately from 10^{-8} to 10^{-10}. The accuracy of calculations of the fit is affected only slightly when this ratio varies within that range. Thus, in order to reduce the number of measurements, it is assumed that $I_{sat}/I_{sc} = 10^{-9}$. Substituting this value into Equations A.12 and A.13 then:

$$U_s = U_{oc}\left[1 + \frac{1}{20.7}\ln\frac{I_{sc} - I_s}{I_{sc}}\right] - R_s I_s \quad \text{A.14}$$

From condition 2: $$U_s\big|_{I_s=I_{s,\max}} = \frac{P_{\max}}{I_{s,\max}} \quad \text{A.15}$$

$$\left.\frac{\partial U_s}{\partial I_s}\right|_{I_s=I_{s,\max}} = \left.\frac{\partial}{\partial I_s}\left(\frac{P_{\max}}{I_s}\right)\right|_{I_s=I_{s,\max}} = \frac{-P_{\max}}{I_{s,\max}^2} \quad \text{A.16}$$

The current at the maximum power point $I_{s,max}$ is unknown. Therefore, substituting Equation A.15 into Equation A.14:

$$\frac{P_{\max}}{I_{s,\max}} = U_{oc}\left[1 + \frac{1}{20.7}\ln\left(\frac{I_{sc} - I_{s,\max}}{I_{sc}}\right)\right] - R_s I_{s,\max} \quad \text{A.17}$$

Differentiating Equation A.14 according to Equation A.16; we get

$$\frac{P_{\max}}{I_{s,\max}^2} = \frac{U_{oc}}{20.7}\left(\frac{1}{I_{sc} - I_{s,\max}}\right) + R_s \quad \text{A.18}$$

Combining Equations A.17 and A.18:

$$I_{s,\max}\left[1 + \frac{1}{20.7}\left(\frac{I_{s,\max}}{I_{sc} - I_{s,\max}} + \ln\frac{I_{sc} - I_{s,\max}}{I_{sc}}\right)\right] - \frac{2P_{\max}}{U_{oc}} = 0 \quad \text{A.19}$$

This equation has to be solved numerically in order to determine the value of $I_{s,max}$. Then R_s is calculated using Equation A.18, and this value is substituted into Equation A.14 to find the I-U curve of the PV cell.

A PV cell module consists of a matrix of PV cells arranged in series and parallel connections. If all the cells are identical, the I-U curve of the module could be determined by scaling the I-U curves of each individual cell (i.e. by multiplying the voltage by the number of rows and the current by the number of columns). Because the I-U curves of the module and the single PV cell have a similar shape, the same model is suitable for both. Thus, the same parameters should be measured, and no additional parameters are required such as the number of cells in series and parallel connection. The I-U curve of the PV cell array is approximated according to the model used for a single cell, so that the influence of the blocking diodes, interconnections and wiring resistance is included in the model and affects the parameters, especially R_s. The shape of the resulting I-U curve of the array should, again, be similar to that of a single cell.

- ***Effect of solar radiation E_s and junction temperature T_j***

The I-U curves of the PV generator vary with solar radiation E_s [W/m²] and junction cell temperature T_j [°C]. Therefore, the values of U_{oc}, I_{sc}, and P_{max} at any combination of E_s and T_j are needed. The parameters of the model at standard test conditions are known from manufacturer's data sheet. Now, the parameters at any other E_s, T_j combinations must be calculated. T_j is the junction cell temperature, which is related to the ambient temperature T_a by the linear relation.

$$T_j = T_a + \left(A + B \times E_s\right) \qquad \text{A.20}$$

Where A [°C] and B [°C.m²/W] are constants.

Defining $I_{sc,STC}$, $U_{oc,STC}$, $P_{max,STC}$ as the short-circuit current, open-circuit voltage and maximum power at standard test conditions respectively, these parameters (I_{sc}, U_{oc}, and P_{max}) can be computed, to a good degree of accuracy, at any ambient temperature and solar radiation by the following equations:

$$I_{sc} = \frac{I_{sc,STC}.E_s}{E_0}\left(1 + \frac{i_{coef}(T_j - T_0)}{I_{sc,STC}}\right) \qquad \text{A.21}$$

$$U_{oc} = U_{oc,STC}\left(1 + \frac{u_{coef}(T_j - T_0)}{U_{oc,STC}}\right)\ln\left(2.72 + \theta(E_s - E_0)\right) \qquad \text{A.22}$$

$$P_{\max} = P_{\max,STC}\left(\frac{I_{sc}.U_{oc}}{I_{sc,STC}.U_{oc,STC}}\right) \qquad \text{A.23}$$

Where

i_{coef}	temperature coefficient of short-circuit current, [A/°C]
u_{coef}	temperature coefficient of open-circuit voltage, [V/°C] and
θ	constant equal to 0.0005, [m²/W]

The serial resistor R_s is now calculated by substituting these parameters into Equations A.18 and A.19. By substituting the resulting value of R_s into Equation A.14, the I-U curve of the PV generator is determined.

Appendix B: PEM Fuel Cell Model

Analytical models focus on the theoretical voltage of the fuel cell and the major losses. The major losses are the activation, ohmic and concentration losses. PEMFC models are much simpler when water management is not taken into consideration. These models combine an analytical background with empirical techniques.

- ***Reversible PEM Fuel Cell Model***

The theoretical cell voltage U_{th} of the PEM fuel cell is given by the change in Gibbs free energy ΔG of the electrochemical reaction [Hirschenhofer-99].

$$U_{th} = -\frac{\Delta G}{nF} \qquad \text{B.1}$$

Where n is the number of electrons participating in the reaction, and F is Faraday's constant.

If the reactants and products are in the standard conditions (T_0=298.15K, p_0=100kPa), then the theoretical (reversible) standard voltage U_0 is

$$U_0 = -\frac{\Delta G_0}{nF} \qquad \text{B.2}$$

From the overall reaction of H_2/O_2 PEM fuel cell, given by Nernst equation (Equation 4.7), both electrical energy and heat could be produced. The maximum theoretical cell voltage available from a fuel source is related to the change Gibbs free energy, which depends on change in enthalpy, entropy, and on absolute cell temperature, as follows:

$$\Delta G = \Delta H - T\Delta S \qquad \text{B.3}$$

Where ΔG change in Gibbs energy, [J/mol]
ΔH change in enthalpy, [J/mol]
ΔS change in entropy, [J/K/mol]
T cell temperature, [K]

The difference between ΔG and ΔH is proportional to the change in entropy ΔS. The amount of heat that is produced by a fuel cell operating reversibly is $T\Delta S$. Both enthalpy and entropy are also dependent on the temperature. The values of ΔH and ΔS are required to calculate ΔG. The magnitudes of the ΔH and ΔS for a reaction are relatively insensitive to the temperature. This is because the enthalpies and entropies of both the reactants and products increase about equally with increasing temperature, so their difference, ΔH and ΔS, remain nearly the same. As a result, ΔH_0 and ΔS_0 could be used as reasonable approximations of ΔH and ΔS [Balkin-02]. This means that ΔG can be written as:

$$\Delta G \cong \Delta H_0 - T\Delta S_0 \qquad \text{B.4}$$

Therefore, the theoretical voltage U_{th} of an electrochemical reaction of an H_2/O_2 PEM fuel cell at standard conditions can be calculated from:

$$U_{th}\big|_{T=T_0} = -\frac{\Delta H_0 - T\Delta S_0}{nF}\Big|_{T=T_0} = -\frac{-237.3 kJ/mol}{2 \times 96485.309 C/mol} = 1.2297 \text{ V} \qquad \text{B.5}$$

Where ΔH_0 = -286 kJ/mol, ΔS_0 = -0.1634kJ/K/mol, and T_0 = 298.15K.

Thus, the theoretical thermal voltage $= -\frac{\Delta H_0}{nF}$ = 1.482 V.

The change in Gibbs free energy ΔG increases as cell temperature decreases and accordingly the theoretical cell voltage U_{th} increases. U_{th} can be calculated at any temperature T by using the expression:

$$U_{th} = U_0 + \left(\frac{\partial U_{th}}{\partial T}\right)_p (T - 298.15K) \qquad \text{B.6}$$

Where, $\left(\frac{\partial U_{th}}{\partial T}\right)_p = \frac{\Delta S_0}{nF}$, by differentiating Equation B.1 with respect to temperature.

For the general cell reaction and the Nernst equation, the free energy change can be expressed as:

$$\Delta G = \Delta G_0 + RT \ln\left[\frac{a_{H_2O}}{a_{H_2} \times a_{O_2}^{1/2}}\right] \qquad \text{B.7}$$

When Equations B.1 and B.2 are substituted in Equation B.7, which is the general form of the Nernst equation; we get

$$U_{th} = U_0 - \frac{RT}{nF} \ln\left[\frac{a_{H_2O}}{a_{H_2} \times a_{O_2}^{1/2}}\right] \qquad \text{B.8}$$

Where U_{th} reversible cell voltage, [V]

U_0 reversible cell voltage at standard operating conditions, [V]

R universal gas constant (8.31451), [J/K/mol]

T cell operating temperature, [K]

n number of electrons per mole, i.e., $n = 2$

F Faraday's constant (96485.309), [C/mol]

a_{H_2O} activity of species H_2O, nearly equals one, since the standard potential corresponds to a dilute aqueous solution; $a_{H_2O} \approx 1$

a_{H_2} activity of species H_2, according to pressure, $a_{H_2} = \frac{p_{H_2}}{p_0}$, where p_{H_2} is the partial pressure of species H_2, and

a_{O_2} activity of species O_2, according to pressure, $a_{O_2} = \frac{p_{O_2}}{p_0}$, where p_{O_2} is the partial pressure of species O_2.

From this relationship, once the cell voltage at standard conditions is known, the cell voltage can be determined at other temperatures and pressures. The theoretical equilibrium cell voltage can be expressed also as a change in Gibbs free energy for the reaction of hydrogen and oxygen. Therefore, this voltage at conditions different from the standard conditions is given by:

$$U_{th} = 1.2297 + (T - 298.15)\frac{\Delta S_0}{nF} + \frac{RT}{nF} \ln\left[\frac{p_{H_2} \times p_{O_2}^{1/2}}{p_0^{3/2}}\right] \qquad \text{B.9}$$

- ***Actual PEM Fuel Cell Model***

The actual voltage of the PEM fuel cell is lower than the theoretical voltage due to various irreversible loss mechanisms, which are often called over-voltages or losses. These losses are:

- *Activation over-voltage* (U_{act}), which arises from the kinetics of charge transfer reactions.
- *Concentration over-voltage* (U_{conc}), which arises from the limited rate of mass transfer.
- *Resistive or ohmic over-voltage* (U_{ohm}), which arises from component resistances.
- *Internal current loss* (I_n), which it is due to wasted fuel and oxidant that passes through the membrane.

Activation over-voltage (U_{act})

The activation over-voltage of the fuel cell is related to the slowness of the reactions that take place on the surface of the electrodes. A proportion of the voltage generated is lost in driving the chemical reaction at the electrodes. It is called an activation loss because it is related to the activation energy required at both the anode and cathode of the fuel cell. In a PEM fuel cell the activation loss at the hydrogen-anode is much smaller than at the oxygen-cathode, so it is often neglected. This activation is described by the **Butler-Volmer-Equation** [Kordesch-96] and [Hoogers-03]:

$$j = j_0 \left(e^{\frac{\alpha n F}{RT} U_{act}} - e^{-\frac{(1-\alpha) n F}{RT} U_{act}} \right) \qquad \text{B.10}$$

Where
j current density, [A/cm²]
j_0 exchange current density, [A/cm²]
α transfer coefficient, [-]
U_{act} activation over-voltage, [V]
n number of electrons participating, [-]
R universal gas constant, [J/K/mol]
T cell operating temperature, [K] and
F Faraday's constant, [C/mol]

This equation gives a general description of a heterogeneous electrochemical reaction, including both reduction and oxidation components.

The analytical relationships of the exchange current density of the anode $j_{0,a(fc)}$ and cathode $j_{0,c(fc)}$ in terms of the temperature and the concentration of hydrogen and oxygen are [Balkin-02], [Bernardi-92], and [Amphlett-95]:

$$j_{0,\ a(fc)} = j_0^{ref} z_a \left(C_{H_2}\right)^{1-\alpha_a} \left(C_{H^+}\right)^{\alpha_a} e^{\frac{-\Delta F_{e,a}}{R}\left(\frac{1}{T}-\frac{1}{298.15}\right)} \qquad \text{B.11}$$

$$j_{0,\ c(fc)} = j_0^{ref} z_c \left(C_{O_2}\right)^{\alpha_c} \left(C_{H_2O}\right)^{1-\alpha_c} e^{\frac{-\Delta F_{e,c}}{R}\left(\frac{1}{T}-\frac{1}{298.15}\right)} \qquad \text{B.12}$$

Where

j_0^{ref}	anodic or cathodic standard exchange current density, [A/cm²]
z	ionic valence of cations or anions, [-]
α	anodic or cathodic transfer coefficient, [-]
ΔF_e	standard free energy of activation for anode or cathode, [J/mol]
R	universal gas constant (8.31451), [J/K/mol]
T	cell operating temperature, [K]
$C_{H_2} = \gamma_{H_2} \frac{p_{H_2}}{p_{H_2}^O}$	concentration of the hydrogen reduced at the anode, [-]
C_{H^+}	concentration of hydrogen protons in the membrane, [-]
$C_{O_2} = \gamma_{O_2} \frac{p_{O_2}}{p_{O_2}^O}$	concentration of the oxygen oxidized at the cathode, [-]
C_{H_2O}	concentration of pure water, [-]
$p_{H_2} = p_{H_2}^O - p_{H_2O,\,r}$	partial pressure of hydrogen, [Pa]
$p_{O_2} = p_{O_2}^O - p_{H_2O,\,r}$	partial pressure of oxygen, [Pa]
$p_{H_2}^O$	operating pressure of hydrogen, [Pa]
$p_{O_2}^O$	operating pressure of oxygen, [Pa]
$p_{H_2O,\,r} = 610.7 \times 10^{\frac{7.5(T-273.15)}{237+(T-273.15)}}$	Saturated vapour pressure of pure water, [Pa]
γ_{H_2}	fugacity coefficient of hydrogen, [-] and
γ_{O_2}	fugacity coefficient of oxygen, [-]

According the Equation B.10, the total current density (j) of an electrochemical reaction consists of two parts, one part at the cathode (j_c) and the other at the anode (j_a).

$$j = j_a + j_c \qquad \text{B.13}$$

At the anode, the current density is anodic j_a and it is used to calculate the activation over-voltage at the anode from Butler-Volmer-Equation after substituting j_0, α, and U_{act} by $j_{0,a}$, α_a, and $U_{act,a}$ respectively. Similarly, at the cathode, the current density is cathodic j_c and it is used to calculate the activation over-voltage at the cathode from Butler-Volmer-Equation after substituting j_0, α, and U_{act} by $j_{0,c}$, α_c, and $U_{act,c}$ respectively. These equations have to be solved numerically in order to determine the values of $U_{act,a}$ and $U_{act,c}$.

***Concentration over-voltage* (U_{conc})**

The concentration loss is related to the reduction of the reactant's concentration in the gas channels. The fuel and oxidant are used at the surface of the electrodes. The incoming gas must then take the place of the used reactant. The concentration of the fuel and oxidant is reduced at the various points in the fuel cell gas channels and is less than the concentration at the inlet valve of the stack. This loss becomes significant at higher currents when the fuel and oxidant are used at higher rates and the concentration in the gas channel is at its minimum.

$$U_{conc,\ a} = \frac{2.303RT}{nF}\log_{10}(1-\frac{j_a}{j_L}), \text{ at the anode} \qquad \text{B.14}$$

$$U_{conc,\ c} = \frac{2.303RT}{nF}\log_{10}(1-\frac{j_c}{j_L}), \text{ at the cathode} \qquad \text{B.15}$$

Where j_L [A/cm²] is the limiting current density.

Ohmic over-voltage (U_{ohm})

Ohmic losses occur due to resistance to the flow of ions (protons) in the electrolyte membrane and resistance to flow of electrons through the electrode substrates and the two catalyst layers. Therefore, the total ohmic resistance R_i is the combination of the electronic and ionic resistances of various fuel cell components; i.e. ohmic losses occur during transport of electrons and ions, and because both obey Ohm's law, the ohmic over-voltage can be expressed by:

$$U_{ohm} = j \times R_i \qquad \text{B.16}$$

Where j [A/cm²] is the total current density flowing through the cell and R_i [Ω.cm²] is the total cell resistance. The total resistance of the fuel cell stacks can be estimated using *numerical fitting* to the data recorded of the fuel cell current/voltage curves, using *impedance spectroscopy*, or using the *current interrupt technique* [Balkin-02], [Hoogers-03], and [Jaouen-03].

Another method may be used to calculate the ohmic losses of the fuel cell due to flow of ions in the membrane. In this method, it is assumed that the water content has been kept at a reasonable level. This means that the water content in the membrane is saturated without flooding the reactant gas flow. Therefore, ohmic over-voltage (U_{ohm}) can be also calculated by:

$$U_{ohm} = I \times R_{fc} \qquad \text{B.17}$$

Where, I [A] is the fuel cell terminal current and R_{fc} [Ω] is the internal resistance of the fuel cell, which is calculated from:

$$R_{fc} = \frac{d_e}{\sigma \times A_c} \qquad \text{B.18}$$

Where R_{fc} internal fuel cell resistance, [Ω]
d_e electrode gap width, [cm]
A_c cross section area of the electrolyte body, [cm²] and
σ electrical conductivity of the electrolyte membrane, [1/ Ω/cm]

The electrical conductivity of the electrolyte membrane is calculated by [Bocklisch-03] and [Wang-92]:

$$\sigma = (0.005139\,\lambda - 0.00326) \times e^{1268(\frac{1}{303}-\frac{1}{T})} \qquad \text{B.19}$$

Where $\lambda = 0.043 + 17.81\phi - 39.85\phi^2 + 36.0\phi^3$ water content, [-]

$\phi = \frac{p_{H_2O,\,v}}{p_{H_2O,\,r}}$ water vapour activity, [-]

$p_{H_2O,\,v} = p_{H_2O,\,r}\Big|_T - p_{H_2O,\,r}\Big|_{T_0}$ partial vapour pressure of pure water, [Pa] and

T cell operating temperature, [K]

Internal Current Loss (I_n)

The internal current loss is due to the wasted fuel and oxidant that passes through the membrane and does not produce any useful energy. This loss affects the fuel cell's performance clearly at open circuit and insignificantly at higher currents. It is mathematically represented in each of the other losses and often absent from PEM fuel cell models. Since the activation loss is the most pronounced loss at low currents, the internal current affects the activation loss significantly. Generally, the currents for all the loss mechanisms are increased because of the internal current. Effectively this means that the current used in the voltage loss equations is equal to the external current I plus the internal current I_n. Thus, the losses are:

Activation loss $$j + j_n = j_0\left(e^{\frac{\alpha nF}{RT}U_{act}} - e^{-\frac{(1-\alpha)nF}{RT}U_{act}}\right)$$ B.20

Where j_n is the internal current density, [A/cm²].

Ohmic loss $U_{ohm} = (j + j_n) \times R_i$, and B.21

Concentration loss $$U_{conc} = \frac{2.303RT}{nF}\log_{10}(1 - \frac{j + j_n}{j_L})$$ B.22

The internal current greatly affects the activation loss, since this loss occurs at low currents. At higher currents j_n has only a minor effect on the other losses. In the case of the ohmic loss, the loss will be j_nR_i, since both j_n and R_i are small, so this loss is insignificant. For the concentration loss, the current at which this loss becomes significant is very high so that $j+j_n$ will be approximately equal to j. Therefore, if the internal current is omitted from the model, this would mean that the model is not accurate near the open circuit condition.

Finally, activation and concentration losses can exist at both the cathode and anode electrodes in fuel cell. The total losses at these electrodes are the sum of U_{act} and U_{conc}.

$$U_{anode}=U_{act,a}+U_{conc,a}$$ B.23

$$U_{cathode}=U_{act,c}+U_{conc,c}$$ B.24

Therefore, the actual PEM fuel cell voltage is:

$$U_{actual} = U_{th}\text{-}U_{anode}\text{-}U_{cathode}\text{-}U_{ohm}$$ B.25

Appendix C: Alkaline Water Electrolyser Model

The theoretical equilibrium cell voltage U_{th} of the alkaline water electrolyser under the effective working conditions, such as temperature and pressure, may be given by the form [Wendt-90]:

$$U_{th} = U_0 + \frac{RT}{2F}\ln\left[\left(\frac{p^O_{H_2} - p_{H_2O}}{p_0}\right)^{1.5}\left(\frac{p_{H_2O,\ r_0}}{p_{H_2O}}\right)\right] \qquad \text{C.1}$$

Where the reversible cell voltage at standard operating conditions is:

$U_0 = 1.5184 - 1.5421\times10^{-3}T + 9.523\times10^{-5}T\ln T + 9.84\times10^{-8}T^2$, and

R universal gas constant (8.31451), [J/K/mol]

T cell operating temperature, [K]

F Faraday's constant, [C/mol]

p_0 reference pressure, [Pa]

$p_{H_2O,\ r_0}$ saturated vapour pressure of pure water at standard operating conditions, [Pa]

$p^O_{H_2}$ operating pressure of hydrogen, [Pa] and

p_{H_2O} the vapour partial pressure of water, [Pa]

The value of p_{H_2O} calculated over broad concentration of potassium hydroxide M_{KOH} and temperature T ranges between 0-18 [mol/kg] and 273.15-573.15[K] respectively is given by:

$$p_{H_2O} = 10^{f_4(M_{KOH},\ T)}\ p_0 \qquad \text{C.2}$$

Where $f_4 = f_1 + f_2 \times f_3$,

$f_1 = -0.0151\times M_{KOH} - 1.679\times10^{-3}M^2_{KOH} + 2.26\times10^{-5}M^{-5}_{KOH}$,

$f_2 = 1.0 - 1.206\times10^{-3}M_{KOH} + 5.60\times10^{-4}M^2_{KOH} - 7.82\times10^{-6}M^3_{KOH}$, and

$f_3 = 35.446 - \frac{3343.9}{T} - 10.9\log T + 4.16\times10^{-3}T$

The ohmic over-voltage $U_{ohm} = I\times R_{el}$, where R_{el} is the internal resistance of the electrolyser, and given by [Müller-97] and [Wedler-87]:

$$R_{el} = \frac{d_e}{\sigma_k \times A_c} \qquad \text{C.3}$$

Where R_{el} internal electrolyser resistance, [Ω]

d_e distance between electrodes, [cm] and

A_c cross section area of the electrolyte body, [cm²]

The electrical conductivity σ_k [1/Ω/cm] of the electrolyte KOH is given by

$$\sigma_k = 2.62\times Cm_{KOH} + 0.067\times Cm_{KOH}(T - 273.15) - 4.8\times Cm^2_{KOH} - 0.088\times Cm^2_{KOH}(T - 273.15)$$

Where Cm_{KOH} [g/100g solution] is the weighted concentration of potassium hydroxide.

According to the partial reactions during the electrolysis of an alkaline (KOH) solution at the cathode and the anode, the total current density *j* consists of two parts, the cathodic and anodic parts.

$$j = j_a + j_c \tag{C.4}$$

The **Butler-Volmer-Equation,** as shown in Equation B.10, can calculate the activation over-voltage at the cathode $U_{cathode}$ and the anode U_{anode} in the electrolyser. The analytical relationships of the exchange current densities of the anode $j_{0,a(el)}$ and the cathode $j_{0,c(el)}$ in terms of the temperature and the concentration of reactions are [WS-Water-04] and [Balkin-02]:

$$j_{0,\ a(el)} = j_{0,a}^{ref} z_a \left(C_{O_2}\right)^{\alpha_a} \left(C_{OH^-}\right)^{1-\alpha_a} e^{\frac{-\Delta F_{e,a}}{R}\left(\frac{1}{T}-\frac{1}{298.15}\right)} \tag{C.5}$$

$$j_{0,\ c(el)} = j_{0,c}^{ref} z_c \left(C_{H_2O}\right)^{\alpha_c} \left(C_{H_2}\right)^{1-\alpha_c} e^{\frac{-\Delta F_{e,c}}{R}\left(\frac{1}{T}-\frac{1}{298.15}\right)} \tag{C.6}$$

Where

$C_{H_2} = \gamma_{H_2}\left(p_{H_2} / p_{H_2}^O\right)$	concentration of the hydrogen reduced at the cathode, [-]
$C_{O_2} = \gamma_{O_2}\left(p_{o_2} / p_{O_2}^O\right)$	concentration of the oxygen oxidized at the anode, [-]
$p_{H_2} = p_{H_2}^O - p_{H_2O}$	partial pressure of hydrogen, [Pa]
$p_{O_2} = p_{O_2}^O - p_{H_2O}$	partial pressure of oxygen, [Pa]
$C_{H_2O} = \gamma_{H_2O} Mf_{H_2O}$	concentration of the water at the cathode, [-]
$C_{OH^-} = \gamma_{OH^-} M_{KOH}$	concentration of the OH^- at the anode, [-]
$\gamma_{H_2O} = p_{H_2O} \big/ p_{H_2O,\ r}$	fugacity coefficient of water, [-]
$Mf_{H_2O} = 1 \Big/ \left(1 + \frac{Cm_{KOH} Mm_{H_2O}}{(1 - Cm_{KOH}) Mm_{KOH}}\right)$	molar fraction of water, [-]
Mm_{H_2O}, Mm_{KOH}	molar mass of the H_2O and KOH, [g/mol] and

γ_{OH^-} [-] is the fugacity coefficient of OH^- ions, and calculated from the next equation:

$$\begin{aligned}\gamma_{OH^-} &= 4.0628 - 1.5793 \times 10^{-2}(T - 273.15) - 4.5946 \times 10^{-4}(T - 273.15)^2 \\ &\quad + 9.2092 \times 10^{-6}(T - 273.15)^3 - 6.3966 \times 10^{-8}(T - 273.15)^4\end{aligned} \tag{C.7}$$

The actual cell voltage U_{actual} is composed of the theoretical cell voltage U_{th}, ohmic voltage losses U_{ohm}, caused by the internal resistance R_{el} of the electrolyser and the cathodic and anodic over-voltages $U_{cathode}$ and U_{anode}. Therefore, U_{actual} can be written as:

$$U_{actual} = U_{th} + U_{anode} + U_{cathode} + U_{ohm} \tag{C.8}$$

Appendix D: Constants and Some Standard Formulas

Constants of models

- ***Photovoltaic Models***

Standard Test Conditions:

Reference junction temperature	T_0	= 298.15	[K]
Reference solar radiation	E_0	= 1000	[W/m²]
Electron charge	e_0	= 1.602×10^{-19}	[C]
Boltzmann's constant	k	= 1.3854×10^{-23}	[J/K]
Gap energy voltage for Silicon	$E_{g[Si]}$	= 1.12	[eV]
Ideality factor of the PV generator	a_f	= 1	
Fit diode parameters	α, β	= 1, 2 respectively	

- ***Electrochemical Models***

Standard Test Conditions:

Reference cell temperature	T_0	= 298.15	[K]
Reference pressure	p_0	= 0.1×10^6	[Pa]
Faraday's constant	F	= 96485.309	[C/mol]
Universal gas constant	R	= 8.31451	[J/K/mol]
Reaction entropy change of liquid water at standard test conditions	ΔS_0	= -0.1634	[kJ/K/mol]
Reaction enthalpy change of liquid water at standard test conditions	ΔH_0	= -286	[kJ/mol]
Ionic valence of anions or cations	Z_i	= 1 (i = a or c)	
Fugacity coefficients of hydrogen or oxygen	γ_i	= 1 (i = H_2 or O_2)	
Concentration of the electrolyte solution (KOH)	M_{KOH}	= 7.638	[mol/kg solution]
Molar mass of the electrolyte solution (KOH)	Mm_{KOH}	= 56.108	[g/mol]
Molar mass of the water	Mm_{H_2O}	= 18.016	[g/mol]
Weighted concentration of potassium hydroxide (KOH)	Cm_{KOH}	= 0.3	[g/100g solution]

Standard Formulas

Root mean square error (RMS) $= \sqrt{\sum_{i=1}^{N}(S_i - M_i)^2 \Big/ (N-1)}$

Percentage absolute error, % $= \left|(S_i - M_i)/M_i\right| \times 100$

Percentage mean error, % $= \dfrac{Percentage \quad absolute \quad error}{N}$

Where S_i simulated value of sample i
M_i measured value of sample i
N total number of samples

Appendix E: Manufacturer's data sheet of the system components

This appendix contains manufacturer specifications and data sheets for the system components of the hydrogen PVFC hybrid system under study.

Appendix E.1: The 85-Watt High-Efficiency Mono-crystalline Photovoltaic Module
Appendix E.2: The technical data for 2.5kW PEM fuel cell system
Appendix E.3: 3.6kW alkaline Electrolyser
Appendix E.4: The ESMA 20EC104S (24V) supercapacitor module

Appendix E.1: 85-Watt High-Efficiency Mono-crystalline Photovoltaic Module

- ***Electrical Characteristics***

Maximum power, P_{max}	85W
Voltage at P_{max}, U_{mpp}	18.0V
Current at P_{max}, I_{mpp}	4.72A
Warranted minimum P_{max}	80.8W
Short-circuit current, I_{sc}	5.0A
Open-circuit voltage, U_{oc}	22.1V
Temperature coefficient of I_{sc}	(0.065±0.015)%/°C
Temperature coefficient of voltage	-(80±10)mV/°C
Temperature coefficient of power	-(0.5±0.05)%/°C
NOCT	47±2°C

Appendix E.2: Technical data for 2.5kW PEM fuel cell system

Power Data	
Electrical rated power	2kW (2 × 1kW)
Maximum electric power	3kW (2 × 1.5kW)
Open circuit voltage	2 × ca. 48V
Rated electric current	34A
Rated electric voltage	30V
Maximum electric current per stack	60A
Hydrogen consumption at rated electric power	Ca. 1.6Nm³/h (every stack 0.8Nm³/h)
CHP coefficient at operating point	0.92
Power peripheral supply	Max. 10A at $24V_{DC}$
Fuel Gas Supply	
Operating pressure of hydrogen	20 – 40kPa
Maximum operating pressure of hydrogen	50kPa
Connection pressure of hydrogen	500kPa
Tube/flexible tube diameter for hydrogen supply	High-grate steel, outside diameter 10mm
Hydrogen loss through sink cycle	40kPa per purge (0.3s) ca. 570ml
Dimensions	
Width × depth × high	110cm × 70cm × 172cm
Environmental Conditions	
Permissible ambient temperature	15 to 25°C
Permissible relative humidity	30 to 70%

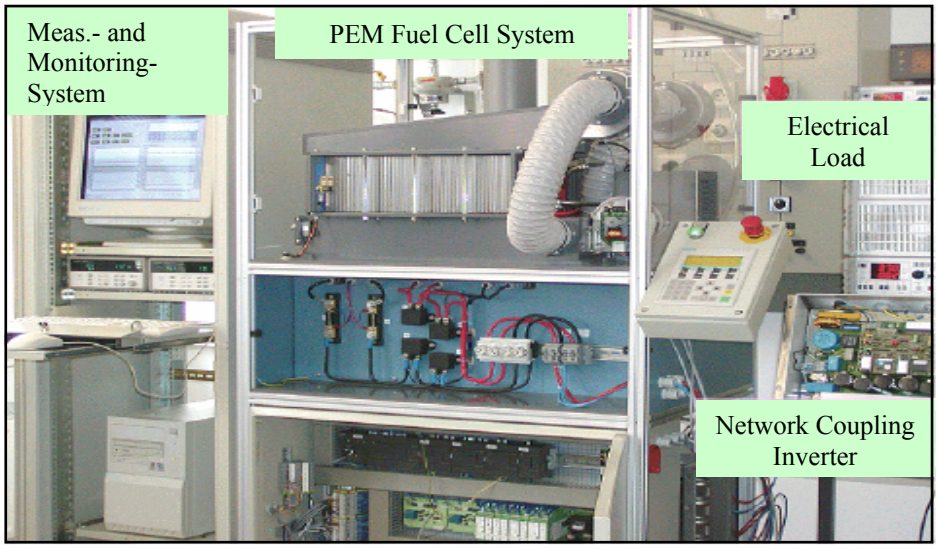

2kW PEM fuel cell system in ISET (KASSEL, Germany)

Appendix E.3: 3.6kW alkaline Electrolyser

- **Technical Specification**

Supplier:	Hydrogen Systems
Model:	30 Cells of 150cm², Zero gap Alkaline Technology
Operating Pressure:	30bar
Nominal Voltage and Intensity:	60V- 60A
Ambient Temperature:	2 to 40°C
Electrolyte Temperature:	85°C (max)
Electrolyte:	KOH (30 wt. %)
Maximum Power:	3.6kW
Module Conversion Efficiency:	3.9kWh/Nm³
Current Density:	400mA/cm² (max)
Hydrogen Production:	0.8Nm³/h at 30bar
Purity of the Hydrogen:	99.8%
Oxygen Production:	0.4Nm³/h
Purity of the Oxygen:	99.5%
Water Cooling of Cells:	0.40L/h at 15°C

The alkaline Electrolyser 3.6kW (Hydrogen Systems) and the PLC Box from Hydrogen Systems, www.hydrogensystems.be

Appendix E.4: ESMA 20EC104S (24V) supercapacitor module (http://www.esma-cap.com)

Operating Voltage [V]	29-8
Maximum Voltage [(1)] [V]	32
Minimum Voltage [(2)] [V]	8
Internal Ohmic resistance (ESR) at +25°C (-30°C) [m. Ω]	12 (18)
Capacitance [F]	150
Energy stored within operating voltage window [kJ]	60
Energy stored within 26-13V voltage window [kJ]	40
Maximum power [kW]	17.5
Leakage current at 28V [mA]	5
Overall dimensions (L×W×H) [mm]	265×125×163
Weight [kg]	9
Operating temperature [(3)] [°C]	-50/+50
Storage temperature [°C]	-60/+70
Life cycles [(3)] [cycles]	300000

[(1)] Module can be kept at this voltage for a short period;

[(2)] Short-term discharge of the module down to zero voltage is possible. However, it should be stored at voltage not less than the minimum voltage specified in the above data;

[(3)] Operating temperature depends not only on the ambient temperature, but also on the module operating mode. High charge/discharge cycle frequency and high charge/discharge currents produce higher internal temperatures. To insure guaranteed life cycles of the capacitor module, internal cell temperatures should not exceed 55 °C. Module operation at temperatures above 55 °C may result in a reduction of the module's capacitance and delivered energy. Capacitance and delivered energy values of a module can be fully restored by charging the capacitor at room temperature.

Appendix F: Simulation results for short-term analysis (fuel cell and supercapacitor)

The stand-alone PVFC hybrid system must include some form of short-term stored energy in order to supply the AC load without interruption. The supercapacitor is used in the system under study for this purpose. The stored energy in this unit is used to meet the transient load demand during sudden increase, while the fuel cell output slowly increases to meet the steady state load demand up-till the normal rated power. This energy in the supercapacitor must be replenished by the fuel cell when the load is low or drops to values less than the rated power of the fuel cell. The control scheme ensures that the supercapacitor possesses sufficient energy to start the fuel cell system at any time or to compensate the deficit of the fuel cell when the load increases to values over the rated power of the fuel cell for several seconds. Therefore, the supercapacitor is important in the hybrid system to stabilize the fuel cell response under power system variations.

In this appendix, the partial system consisting of the fuel cell and supercapacitor is discussed. The connection of the supercapacitor unit in the system under study differs according to the system topology, see Fig. 6.1. The 2kW PEM fuel cell stack used in the hybrid system operates between 40 to 70V and can deliver up to 50A at full load. The fuel cell stack consists of 75 cells connected in series and each of the fuel cells has an electrode area 168cm². To avoid irreparable damage to the fuel cell stack, a maximum current ramp rate is specified as approximately 20% of the maximum rated current per second. Therefore, the output current of the stack could safely increase or decrease with a rate of at most 10A per second. If the load power suddenly changes, the fuel cell power must be controlled to slowly ramp up or down to meet the load demand.

The supercapacitor set used in the system under study consists of two ESMA 20EC104S supercapacitor modules connected in series. Thus, it is able to deliver a peak power of 6kW for about 20 seconds within the operating voltage window, since a single module can store energy of 60kJ (see Appendix E.4). The energy available from the supercapacitor depends on the discharge time and on the start and end voltage. The supercapacitor set can store approximately 120kJ within operating voltage window, but in our system only 50% from this energy is used because the system is controlled by the allowable voltage variation range at the input of the associated power conditioning unit (Sunny or Trace family). The supercapacitor operates also to clamp the input voltage to the PCU to be within the operation range values whenever the slowly changing fuel cell power is greater or less than the load demand. This is achieved by charging power to the supercapacitor system from the fuel cell when the fuel cell operates at power greater than the power of the load or discharging power from the supercapacitor system to the load when the fuel cell operates at power less than the power of the load. Since the energy stored in the supercapacitor may be required at any given moment, the control system

must assume that the supercapacitor is charged at all time. A supervisory controller monitors the state of charge of the supercapacitor system to ensure that it is within set limits.

Figure F.1 illustrates the operation of the system throughout a load transient. When the load power is suddenly increased from 10% to 90% at t = 20 seconds, the fuel cell power slowly adjusts to the new load level. During this time, power flows out of the supercapacitor by discharging to the AC bus to maintain the output voltage level in the normal value. When the fuel cell output power is sufficient to raise the AC bus voltage, the power flow from supercapacitor is shut off and the fuel cell supplies the load independently with the nominal AC bus voltage. At t = 60 seconds, the load power is suddenly reduced from 90% to 10% and the fuel cell is providing more power than the required load power. The supercapacitor responds to the surplus fuel cell power by recharging, while the fuel cell decreases slowly its output power to the new level of the load demand power. When the fuel cell power has reduced to the level of the load demand power, the supercapacitor is shut off.

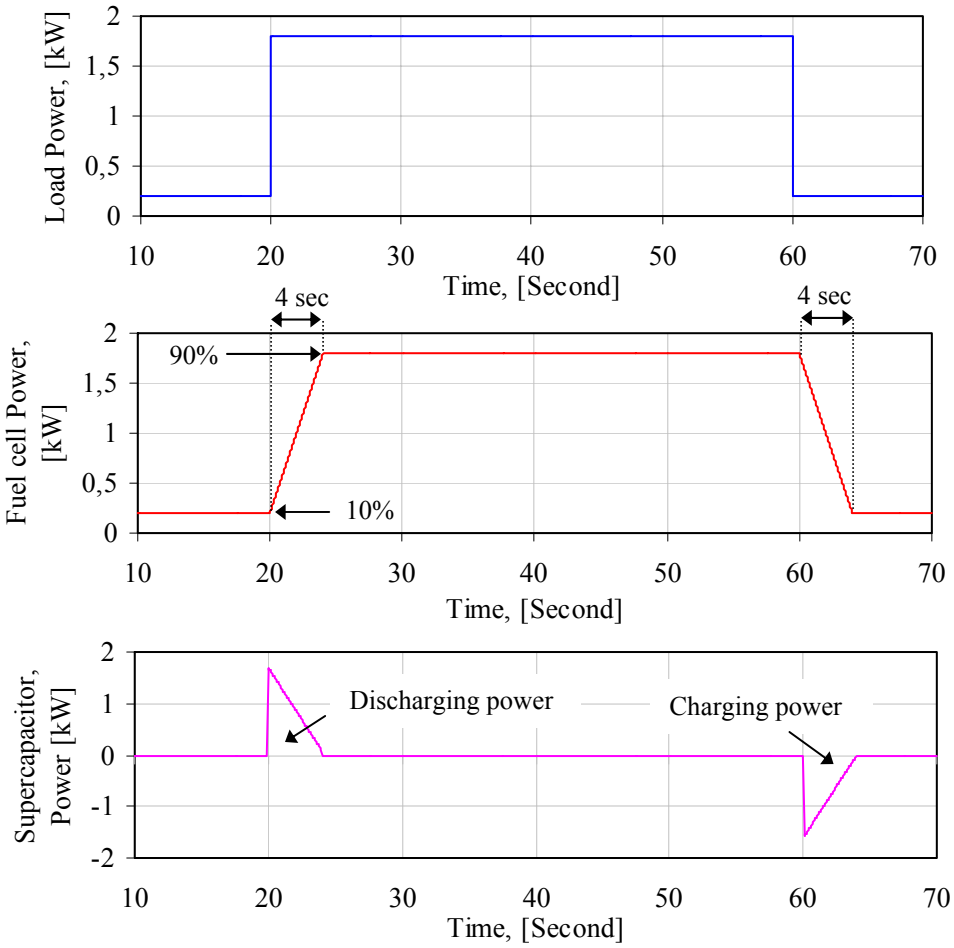

Fig. F.1: System behaviour during transient increase/decrease of load power.

Figure F.2 shows the system behaviour during a transient increase in the load over the rated power of the fuel cell and a sudden decrease of the load to zero. The system control ensures that the supercapacitor will have sufficient energy to start the fuel cell or to compensate the deficit of the fuel cell when the load power increases to a level over the rated power of the fuel cell. When the load power has been turned off, the fuel cell must continue operation until the supercapacitor has been full charged. The fuel cell voltage changes from 46V at rated power to 70V at off operation, while the supercapacitor voltage decreases from 60V at full charge to 48V. Thus, the voltage ranges of the fuel cell and supercapacitor components are in the allowed voltage range of the input DC voltage of the PCU.

These results demonstrate that the transient as well as the steady state load demand could be met. Also, this control mode of operation guarantees the power balance between the components and allows the voltage of the AC side to be kept very stable. The supercapacitor helps in stabilizing the fuel cell operation within the set limits as it adjusts itself slowly to a step load change.

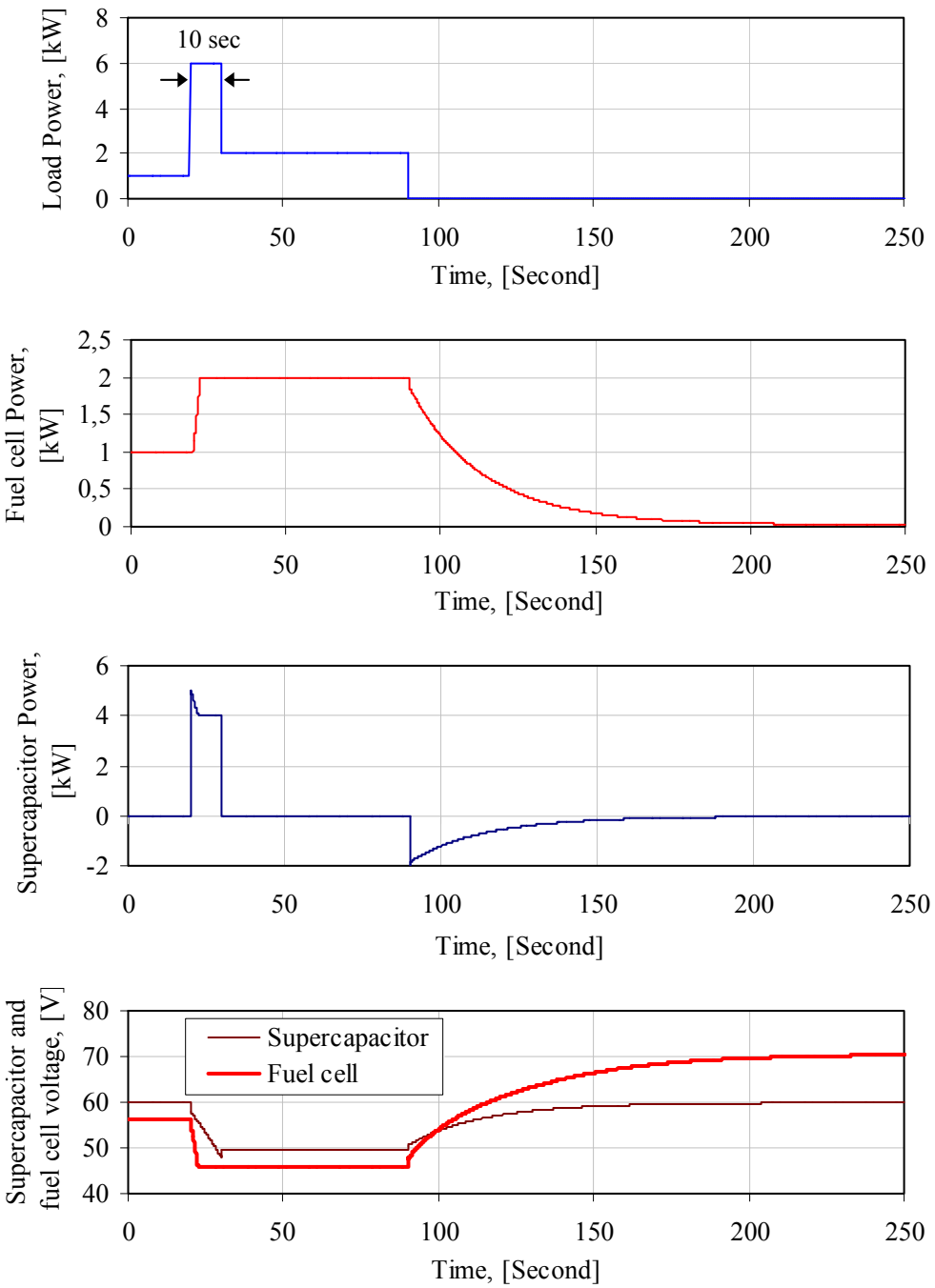

Fig. F.2: System behaviour during transient load power.

Appendix G: Definitions of system performance indices

The long-term performance analysis of a hybrid system is important in order to understand its operation and to compare systems of different sizes and architectures. The analysis is done in two steps, accounting for two different aspects of the overall performance: ***energy system balances*** are established in order to determine mean operating efficiencies for each component and describe the performance of the hybrid system; then ***indices of system performance*** are calculated to be able to compare between the different topologies of the hybrid system. The so-called yields are normalised performance indicators obtained by dividing the relevant energy balances by a nominal reference value. More analysis methods have been published by different organisations such as the Joint Research Centre (JRC) of the European Community in Ispra or the International Electro-technical Commission (IEC) [Dumbs-99], [Jahn-00] and [Jahn-01]. Brief definitions of all parameters are described hereunder.

- ***ENERGY SYSTEM BALANCES***

Simulation results of the hybrid system are used to calculate a certain number of parameters that characterize the system operation.

* ***Total input energy*** $E_{in} = E_{PV,out} + E_{FCN}$ of a stand-alone PVFC hybrid system is defined as the sum of all contributions from the different energy sources, where $E_{PV,out}$ [kWh] is the total output energy of the PV generator, and $E_{FCN} = 3 \times (H_{2,cons} - H_{2,prod}) \times \eta_{fc} \times \eta_{PCU,FC}$ is the integral amount of energy that is drawn from the hydrogen storage by the fuel cell unit during the entire simulation duration. E_{FCN} [kWh] is a net quantity; as it is positive when $H_{2,cons} > H_{2,prod}$ or zero when $H_{2,cons} \leq H_{2,prod}$. $H_{2,cons}$ and $H_{2,prod}$ [Nm³] are the hydrogen consumption from the hydrogen tank by the fuel cell and the hydrogen production supplied by the electrolyser to the hydrogen tank, respectively. η_{fc} and $\eta_{PCU,FC}$ are efficiencies of the fuel cell and associated PCU, respectively. The number 3 in the equation means that 1Nm³ from hydrogen corresponds to approximately 3kWh. The total input energy E_{in} [kWh] serves as a reference value for the PV fraction of the total input energy $F_{in,PV}$.

* ***PV generator fraction of the total input energy*** $F_{in,PV} = E_{PV,out} / E_{in}$ is the fraction of the total input energy that is produced by the PV generator.

* ***Useful energy*** $E_{use} = E_L + E_{ELN}$ of a stand-alone PVFC hybrid system is the total output energy of the system which is supplied to a user load. E_L [kWh] is the energy consumed by the user load and $E_{ELN} = 3 \times (H_{2,prod} - H_{2,cons}) \times \eta_{fc} \times \eta_{PCU,FC}$ is the net stored energy in the hydrogen storage during the entire simulation duration. E_{ELN} [kWh] is also a net quantity; as it is positive when $H_{2,prod} > H_{2,cons}$ or zero when $H_{2,prod} \leq H_{2,cons}$.

* ***PV generator part of the useful energy*** $E_{PV,use} = F_{in,PV} \times E_{use}$ is obtained from multiplying the PV generator fraction of the total input energy by the useful energy.

* ***PV generator nominal energy*** $E_{PV,STC} = \int E_s \times A_{PV} \times \eta_{PV,STC}$, where E_s is the solar radiation [W/m²], A_{PV} is the PV generator area [m²], and $\eta_{PV,STC}$ is the PV generator efficiency at Standard Test Conditions.

* ***Mean operating efficiencies*** of all components are the quotient of energy output over energy input. These efficiencies can be easy calculated by knowing the input and output energy from all components. The overall balance of system BOS component performance can be calculated by $\eta_{BOS} = (E_L + E_{ELN} - E_{FCN}) / E_{PV,out}$.

- ***INDICES OF SYSTEM PERFORMANCE***

In order to be able to compare hydrogen PVFC hybrid systems of different topologies and at different sites, normalised performance indices have to be evaluated. A common set of yields, losses and efficiencies have been proposed. Energy yields are normalized to the rated power P_{rated} of the PV generator and they reflect the actual PV operating performance with respect to the rated capacity. They have units of [kWh/d/kWp] and sometimes written as [h/d]. Normalized energy losses could be obtained by subtracting between different energy yields and therefore they have the same units as yields. The efficiencies are normalized to the PV generator energy and the performance ratio *PR* is normalized to the solar radiation energy of the system.

* ***Array yield*** $Y_a = E_{PV,out} / P_{PV,STC}$ is the daily energy output of the PV generator per kWp of the installed PV generator power. Therefore, it represents the number of hours per day that the PV generator would have to generate electricity at its rated output power.

* ***Final yield*** $Y_f = E_{PV,use} / P_{PV,STC} = Y_a \times \eta_{BOS}$ is defined as the part of the daily energy production that was provided by the PV generator power.

* ***Reference yield*** $Y_r = (\Delta t \times \sum E_s) / E_0$ is the number of hours that the solar radiation E_s would have to be at the reference solar radiation E_0 = 1kW/m² to produce the amount of energy. Δt is a distinct recording time, or time step, of the simulation, i.e., 1 hour.

* ***Array capture losses*** $L_c = Y_r - Y_a$ are defined by the difference between reference and array yield and comprise losses related to the operation of the PV generator, such as wiring, string diodes, spectral losses, partial shading, contamination, snow covering, spectral losses, etc.

* ***System losses*** $L_s = Y_a - Y_f = Y_a \times (1 - \eta_{BOS})$ are defined by the overall system losses, and are summed from the PCU conversion losses in the system.

* ***Performance Ratio*** $PR = Y_f / Y_r$ is the ratio of the actually used PV generator energy to the theoretical energy available (rated energy at STC). It is independent of location and system size, and indicates the overall losses from the array's rated output power due to module temperature, incomplete utilization of solar radiation and system component inefficiencies or failures. In other words, it depends on the components efficiency and on the time overlaps between the periods of solar production and the user load demand.

In fact, the above quantities are very good indicators for system problems. If the system fails completely, the values of Y_a, Y_f and PR will drop to zero, while capture losses will rise towards Y_r and system losses become negligible.

* ***Mean PV generator efficiency*** $\eta_{PV} = E_{PV,out} / (\Delta t \times \sum E_s \times A_{PV})$ represents the mean energy conversion efficiency of the PV generator, which is used for comparing with the rated PV generator $\eta_{PV,STC} = P_{PV,STC} / (E_0 \times A_{PV})$. Where E_s [kW/m²] and A_{PV} [m²] are solar radiation and the PV generator area, respectively.

* ***Overall system efficiency*** is $\eta_{sys} = \eta_{PV} \times \eta_{BOS} = E_{PV,use} / (E_s \times A_{PV})$.

GLOSSARY

AM (Air Mass): It is defined as the ratio of the mass of atmosphere through which the solar radiation passes to the mass it would pass through if the sun were at the zenith.
Array: It is a group of photovoltaic modules wired together in series or parallel.
BOS (Balance Of System): It refers to components that are used with PV generator source to make a full system. Power conditioning units and energy storage system have the largest reliability and cost concerns in the balance of system.
FF (Fill Factor): The fill factor is the ratio of the maximum power output of a photovoltaic module to the product of its open circuit voltage and short circuit current.
Grid Connected: It is a situation where the renewable energy is fed to the local utility grid.
Heating Value: The heating value of a fuel is defined as the amount of energy released when a fuel is burned completely at standard test conditions (T_0=25°C & p_0=100kPa). Also, it depends on the phase of water in the products of the reaction. The heating value is called the higher heating value HHV when the water in the products is in the liquid form, and is called the lower heating value LHV when the water in the products is in the vapour form.
Hybrid System: It is a system designed for the generation of electrical power, typically in remote areas away from major electric grids. The word "hybrid" refers to the use of multiple power sources, such as renewable energy sources (Photovoltaic, Wind turbine, Hydroelectric, Biomass generators, etc), fossil fuel generators (diesel or gas fuelled generators) or any other electrical power generator. However, the term "Hybrid Power System" is must often used in remote or rural areas where the system comprises at least two different power sources and may

typically include energy storage, power conditioning units, load management options, a supervisory control system, etc. Also, the term "Autonomous System" is commonly used for the same meaning.

Module: A module or panel is the smallest detachable PV unit sold on the market. Several modules wired together in a series or parallel connection to form an array.

MPPT (Maximum Power Point Tracker): A PV operating control strategy where the PV array's voltage is electronically adjusted to be at or sufficiently close to the PV array maximum power point. MPPT requires the presence of a load capable of accepting the full available power.

NOCT (Normal Operating Cell Temperature): The NOCT is used to describe one of the thermal properties of PV modules. Its value is usually given by the manufacturer and corresponds to the junction cell temperature T_j which is found at a solar radiation of 800W/m², an ambient temperature of 20°C and an average wind speed of 1m/s.

Off Grid: An electrical system that is not connected to a utility network.

Peak Watt (Wp): A unit used to describe the performance rating of PV modules, arrays or subsystems. A system rated at 1Wp will deliver 1W at reference temperature and solar radiation (T_0 = 25°C, E_0 = 1000W/m² & AM=1.5).

PV system: The components that form a solar electric generating system, usually consisting of PV modules, charge controller, circuit protectors (fuses or breakers) and batteries.

RMS (Root Mean Square) or Effective Value: It is a measure used for any time varying signal's effective value. It is not an average value and its value varies depends on the shape of the waveform of the time varying signal.

Stand-alone Systems: A power system that operates independently of any controlled energy distribution network such as the utility grid.

STC (Standard Test Conditions): Reference conditions defined by: solar radiation 1000W/m²; Air mass 1.5; junction cell temperature for PV generator or reference temperature for electrochemical components 25°C; wind speed 1m/s; and reference pressure 100kPa.

User Load: Any electrical device that consumes electricity in order to operate. Appliances, tools, and lights are examples of electrical loads; often referred to as the consumer.